

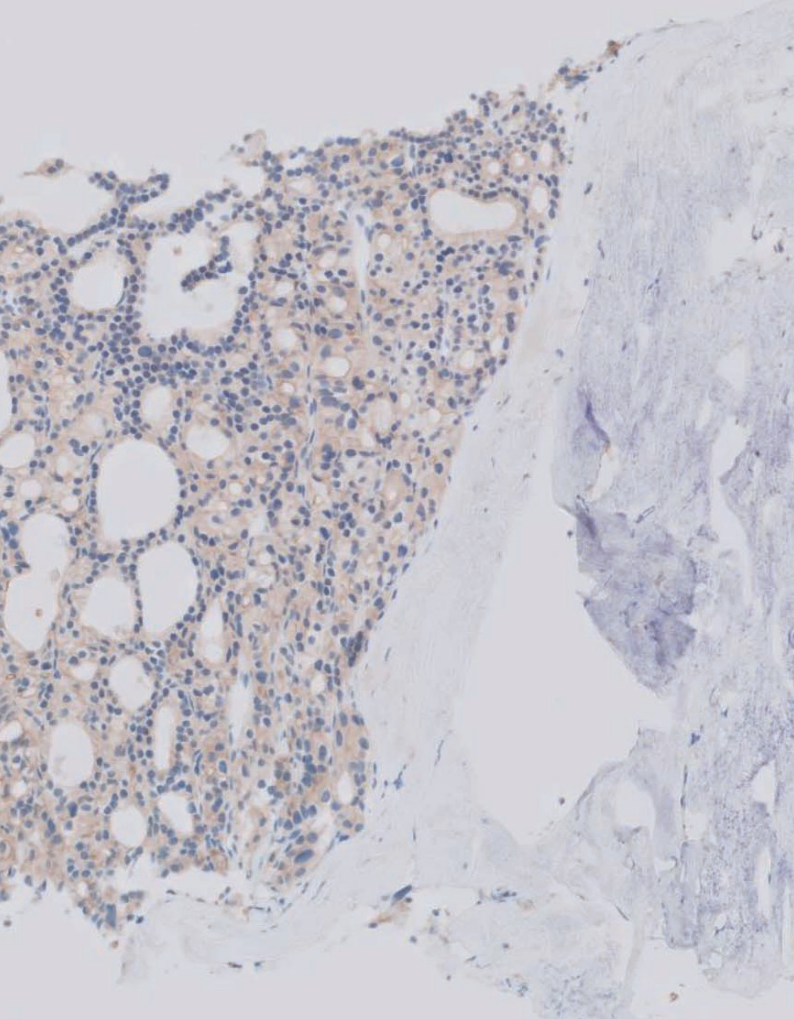
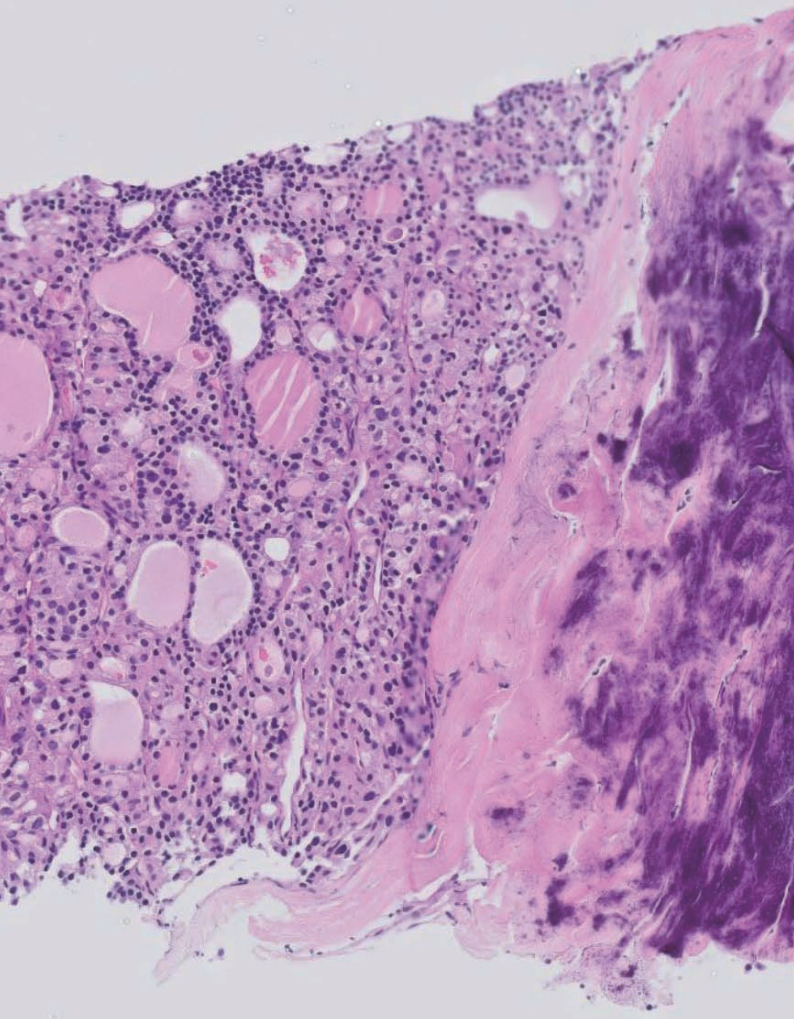
JPTM

Journal of Pathology
and Translational Medicine

July 2023
Vol. 57 / No.4
jpatholtm.org
pISSN: 2383-7837
eISSN: 2383-7845



*Updates on Thyroid
Core Needle Biopsy*



Aims & Scope

The *Journal of Pathology and Translational Medicine* is an open venue for the rapid publication of major achievements in various fields of pathology, cytopathology, and biomedical and translational research. The Journal aims to share new insights into the molecular and cellular mechanisms of human diseases and to report major advances in both experimental and clinical medicine, with a particular emphasis on translational research. The investigations of human cells and tissues using high-dimensional biology techniques such as genomics and proteomics will be given a high priority. Articles on stem cell biology are also welcome. The categories of manuscript include original articles, review and perspective articles, case studies, brief case reports, and letters to the editor.

Subscription Information

To subscribe to this journal, please contact the Korean Society of Pathologists/the Korean Society for Cytopathology. Full text PDF files are also available at the official website (<https://jpatholtm.org>). *Journal of Pathology and Translational Medicine* is indexed by Emerging Sources Citation Index (ESCI), PubMed, PubMed Central, Scopus, KoreaMed, KoMCI, WPRIM, Directory of Open Access Journals (DOAJ), and CrossRef. Circulation number per issue is 50.

Editors-in-Chief

Jung, Chan Kwon, MD (*The Catholic University of Korea, Korea*) <https://orcid.org/0000-0001-6843-3708>

Park, So Yeon, MD (*Seoul National University, Korea*) <https://orcid.org/0000-0002-0299-7268>

Associate Editors

Bychkov, Andrey, MD (*Kameda Medical Center, Japan; Nagasaki University Hospital, Japan*) <https://orcid.org/0000-0002-4203-5696>

Kim, Haeryoung, MD (*Seoul National University, Korea*) <https://orcid.org/0000-0002-4205-9081>

Lee, Hee Eun, MD (*Mayo Clinic, USA*) <https://orcid.org/0000-0001-6335-7312>

Shin, Eunah, MD (*Yongin Severance Hospital, Yonsei University, Korea*) <https://orcid.org/0000-0001-5961-3563>

Editorial Board

Avila-Casado, Maria del Carmen, MD (*University of Toronto, Toronto General Hospital UHN, Canada*)

Bae, Jeong Mo, MD (*Seoul National University, Korea*)

Bae, Young Kyung, MD (*Yeungnam University, Korea*)

Bongiovanni, Massimo, MD (*Lausanne University Hospital, Switzerland*)

Bova, G. Steven, MD (*University of Tampere, Finland*)

Choi, Joon Hyuk (*Yeungnam University, Korea*)

Chong, Yo Sep, MD (*The Catholic University of Korea, Korea*)

Chung, Jin-Haeng, MD (*Seoul National University, Korea*)

Fadda, Guido, MD (*Catholic University of Rome-Foundation Agostino Gemelli University Hospital, Italy*)

Fukushima, Noriyoshi, MD (*Jichi Medical University, Japan*)

Go, Heounjeong (*University of Ulsan, Korea*)

Hong, Soon Won, MD (*Yonsei University, Korea*)

Jain, Deepali, MD (*All India Institute of Medical Sciences, India*)

Kakudo, Kennichi, MD (*Izumi City General Hospital, Japan*)

Kim, Jang-Hee, MD (*Ajou University, Korea*)

Kim, Jung Ho, MD (*Seoul National University, Korea*)

Kim, Se Hoon, MD (*Yonsei University, Korea*)

Komuta, Mina, MD (*Keio University, Tokyo, Japan*)

Kwon, Ji Eun (*Ajou University, Korea*)

Lai, Chiung-Ru, MD (*Taipei Veterans General Hospital, Taiwan*)

Lee, C. Soon, MD (*University of Western Sydney, Australia*)

Lee, Hwajeong, MD (*Albany Medical College, USA*)

Lee, Sung Hak, MD (*The Catholic University, Korea*)

Liu, Zhiyan, MD (*Shanghai Jiao Tong University, China*)

Lkhagvadorj, Sayamaa, MD (*Mongolian National University of Medical Sciences, Mongolia*)

Moran, Cesar, MD (*MD Anderson Cancer Center, U.S.A.*)

Paik, Jin Ho, MD (*Seoul National University, Korea*)

Park, Jeong Hwan (*Seoul National University, Korea*)

Sakhuja, Puja, MD (*Govind Ballabh Pant Hospital, India*)

Shahid, Pervez, MD (*Aga Khan University, Pakistan*)

Song, Joon Seon, MD (*University of Ulsan, Korea*)

Tan, Puay Hoon, MD (*National University of Singapore, Singapore*)

Than, Nandor Gabor, MD (*Semmelweis University, Hungary*)

Tse, Gary M., MD (*The Chinese University of Hong Kong, Hong Kong*)

Yatabe, Yasushi, MD (*Aichi Cancer Center, Japan*)

Zhu, Yun, MD (*Jiangsu Institution of Nuclear Medicine, China*)

Ethic Editor

Choi, In-Hong, MD (*Yonsei University, Korea*)

Huh, Sun, MD (*Hallym University, Korea*)

Statistics Editors

Kim, Dong Wook (*National Health Insurance Service Ilsan Hospital, Korea*)

Lee, Hye Sun (*Yonsei University, Korea*)

Manuscript Editor

Chang, Soo-Hee (*InfoLumi Co., Korea*)

Layout Editor

Kim, Haeja (*iMiS Company Co., Ltd., Korea*)

Website and JATS XML File Producers

Cho, Yoonsang (*M2Community Co., Korea*)

Im, Jeonghee (*M2Community Co., Korea*)

Administrative Assistants

Kim, Da Jeong (*The Korean Society of Pathologists*)

Jeon, Anmi (*The Korean Society for Cytopathology*)

Contact the Korean Society of Pathologists/the Korean Society for Cytopathology

Publishers: Choe, Gheeyoung, MD, Lee, Seung-Sook, MD

Editors-in-Chief: Jung, Chan Kwon, MD, Park, So Yeon, MD

Published by the Korean Society of Pathologists/the Korean Society for Cytopathology

Editorial Office

Room 1209 Gwanghwamun Officia, 92 Saemunan-ro, Jongno-gu, Seoul 03186, Korea

Tel: +82-2-795-3094 Fax: +82-2-790-6635 E-mail: office@jpatholtm.org

#1508 Renaissancetower, 14 Mallijae-ro, Mapo-gu, Seoul 04195, Korea

Tel: +82-2-593-6943 Fax: +82-2-593-6944 E-mail: office@jpatholtm.org

Printed by iMiS Company Co., Ltd. (JMC)

Jungang Bldg. 18-8 Wonhyo-ro 89-gil, Yongsan-gu, Seoul 04314, Korea

Tel: +82-2-717-5511 Fax: +82-2-717-5515 E-mail: ml@smileml.com

Manuscript Editing by InfoLumi Co.

210-202, 421 Pangyo-ro, Bundang-gu, Seongnam 13522, Korea

Tel: +82-70-8839-8800 E-mail: infolumi.chang@gmail.com

Front cover image: Histological and immunohistochemical features of thyroid nodules in core needle biopsy samples (p213).

© Copyright 2023 by the Korean Society of Pathologists/the Korean Society for Cytopathology

© Journal of Pathology and Translational Medicine is an Open Access journal under the terms of the Creative Commons Attribution Non-Commercial License (<https://creativecommons.org/licenses/by-nc/4.0>).

© This paper meets the requirements of KS X ISO 9706, ISO 9706-1994 and ANSI/NISO Z.39.48-1992 (Permanence of Paper).

CONTENTS

REVIEWS

- 189 A review of liver fibrosis and cirrhosis regression
Michael J. Lee
- 196 A stepwise approach to fine needle aspiration cytology of lymph nodes
Yosep Chong, Gyeongsin Park, Hee Jeong Cha, Hyun-Jung Kim, Chang Suk Kang, Jamshid Abdul-Ghafar, Seung-Sook Lee
- 208 Reevaluating diagnostic categories and associated malignancy risks in thyroid core needle biopsy
Chan Kwon Jung

ORIGINAL ARTICLES

- 217 Single-center study on clinicopathological and typical molecular pathologic features of metastatic brain tumor
Su Hwa Kim, Young Suk Lee, Sung Hak Lee, Yeoun Eun Sung, Ahwon Lee, Jun Kang, Jae-Sung Park, Sin Soo Jeun, Youn Soo Lee
- 232 Loss of aquaporin-1 expression is associated with worse clinical outcomes in clear cell renal cell carcinoma: an immunohistochemical study
Seokhyeon Lee, Bohyun Kim, Minsun Jung, Kyung Chul Moon

CASE REPORTS

- 238 Metastatic choroidal melanoma in the breast: a case report and review of the literature
Loay Abudalu, Vinisha Malhotra, Nabila Nasir, Sami Titi
- 242 Intrathyroidal metastasis of tonsillar squamous cell carcinoma masquerading as a primary thyroid tumor
Jai-Hyang Go

NEWSLETTER

- 246 What's new in hematopathology 2023: updates on mature T-cell neoplasms in the 5th edition of the WHO classification
Mario L. Marques-Piubelli, Roberto N. Miranda

A review of liver fibrosis and cirrhosis regression

Michael J. Lee

Department of Pathology and Cell Biology, Columbia University Medical Center, New York, NY, USA

Cirrhosis has traditionally been considered an irreversible process of end-stage liver disease. With new treatments for chronic liver disease, there is regression of fibrosis and cirrhosis, improvement in clinical parameters (i.e. liver function and hemodynamic markers, hepatic venous pressure gradient), and survival rates, demonstrating that fibrosis and fibrolysis are a dynamic process moving in two directions. Microscopically, hepatocytes push into thinning fibrous septa with eventual perforation leaving behind delicate periportal spikes in the portal tracts and loss of portal veins. Obliterated portal veins during progressive fibrosis and cirrhosis due to parenchymal extinction, vascular remodeling and thrombosis often leave behind a bile duct and hepatic artery within the portal tract. Traditional staging classification systems focused on a linear, progressive process; however, the Beijing classification system incorporates both the bidirectional nature for the progression and regression of fibrosis. However, even with regression, vascular lesions/remodeling, parenchymal extinction and a cumulative mutational burden place patients at an increased risk for developing hepatocellular carcinoma and should continue to undergo active clinical surveillance. It is more appropriate to consider cirrhosis as another stage in the evolution of chronic liver disease as a bidirectional process rather than an end-stage, irreversible state.

Key Words: Liver; Cirrhosis; Fibrosis

Received: March 20, 2023 **Revised:** May 20, 2023 **Accepted:** May 24, 2023

Corresponding Author: Michael J. Lee, MD, Department of Pathology and Cell Biology, Columbia University Medical Center, 630 West 168th Street, VC14-240A, New York, NY 10032, USA

Tel: +1-212-342-3016, E-mail: mjl2197@cumc.columbia.edu

Chronic liver disease and injury leads to regeneration of hepatocytes and fibrosis, characterized by the deposition of collagen in the extracellular matrix with replacement of hepatic parenchyma. It was initially thought that liver fibrosis with progression to cirrhosis was an irreversible process with subsequent mechanical effects (vascular remodeling, collateral circulation, portal hypertension), physiologic changes (retention of bile salts, coagulation abnormalities, metabolic disarray), and neoplastic implications (increased lifetime risk for developing hepatocellular carcinoma) [1,2]. This paradigm was initially challenged by Hans Popper in 1964 when he observed collagen resorption in idiopathic hemochromatosis patients after therapeutic phlebotomy [3,4]. In 1979, Perez-Tamayo [5] induced fibrosis and cirrhosis by chronic tetrachloride intoxication in animal models. Removal of the offending etiology caused near complete reversal of fibrosis with normal histologic findings [5].

The discussion continued to evolve until the next major breakthrough by Wanless et al. in 2000 [2], presenting serial liver biopsies from a patient with hepatitis B following antiviral treat-

ment. They demonstrated chronological progression and reversal from cirrhosis to incomplete septal cirrhosis, correlating a decreasing viral load with clinical parameters [2]. Finally, the last two decades certified that successful treatment of chronic liver disease regardless of etiology (viral, biliary, vascular, steatotic, metabolic) caused fibrosis regression. Cirrhosis was once considered an end-stage, irreversible process with orthotopic liver transplantation as an inevitable conclusion is now regarded as a dynamic, bidirectional process balancing fibrogenesis and fibrolysis [6,7].

PATHOBIOLOGY

With chronic and persistent liver injury, the liver responds by depositing extracellular matrix (ECM). This is characterized by type 1 and 3 collagen deposition in the portal tracts and lobules, and collagenous and non-collagenous ECM protein deposition in the space of Disse, which includes collagen type 3 and 4, laminin and fibronectin [8]. This wound healing response or scarring down of the liver begins when chronic liver injury causes

apoptosis of hepatocytes leading to Kupffer cell activation and cytokine release: tumor necrosis factor (TNF), platelet derived growth factor (PDGF), and endothelin-1 (ET-1). Quiescent hepatic stellate cells (HSCs) in the space of Disse are normally inactive, dormant, fat storing cells, however, TNF activates stellate cells for transformation into myofibroblast like cells, depositing ECM as collagen types 1, 3, 4, and laminin. PDGF causes proliferation of stellate cells and ET-1 leads to contraction of stellate cells and vasoconstriction, affecting vascular resistance and liver blood flow. While normal sinusoidal spaces are lined by fenestrated endothelial cells, increased ECM material and collagen deposition closes sinusoidal endothelial cell fenestrations and the space of Disse, a process called capillarization of the sinusoids, preventing protein exchange between hepatocytes and flowing plasma [8-10].

Chronic portal and lobular inflammation causing hepatocellular necrosis with subsequent parenchymal extinction not only represents hepatocellular loss but an alteration in the surrounding microvasculature as chronic inflammation causes thrombosis of small branches of the portal vein, hepatic vein, and hepatic artery. This ischemic injury leads to subsequent cycles of parenchymal loss with compounding vascular compromise and remodeling, bile ductular reaction, and collapse of the hepatocellular trabeculae. When chronic injury persists, there can be years of parenchymal, architectural, and vascular remodeling, the latter which may be irreversible [2,11,12].

In contrast, matrix metalloproteinases (MMPs) and tissue inhibitor of metalloproteinases (TIMPs) are enzymes responsible for breaking down the extracellular matrix during fibrosis regression. There are approximately nine MMPs involved in the reversal of fibrosis with varying substrate specificity. These proteases are subcategorized into the following groups: stromelysins that break down protein substrates (i.e., laminin, gelatin, and type IV collagen), collagenases that degrade collagen (i.e., type III and I collagen), and gelatinases/type IV collagenases. MMPs are balanced and regulated by TIMPs, which irreversibly bind to and inhibit MMPs and are released by HSCs and Kupffer cells [13-15].

Retinoids (vitamin A) keep stellate cells in the quiescent state and prevent conversion to an activated state, inhibiting further differentiation into a myofibroblast-like phenotype. In tissue culture, activated HSCs show loss of retinoids, however, adding retinoids to the culture medium decreased type 1 collagen synthesis and deposition. Experimental studies showed that exogenous retinoid administration reduced expression of inflammatory cytokines such as TNF- α , maintained HSCs in a quiescent state and prevented Kupffer cells from releasing fibrogenic cy-

tokines. Thus, there is an ongoing balance between fibrogenesis and fibrolysis involving an interplay of numerous factors during this dynamic, bidirectional process [16,17].

PATHOLOGIC FEATURES

The typical cirrhotic nodule is surrounded by broad, thick fibrous septae with scattered chronic inflammation and bile ductular reaction encapsulating a nodule of regenerating hepatocytes. The central veins may not be visualized because they have been compressed and undergo thrombosis. As these outflow vessels are obliterated, small, collateral vascular channels develop and act as shunts to offset the increase in portal pressure. In contrast, fibrosis regression is comprised of three components, fragmentation and regression of the scar, vascular remodeling/distortion, and parenchymal regeneration. Inflammation subsides as the balance is shifted towards fibrolysis and fibrous septa become progressively thinner and wisper (Figs. 1–3). Eventually, hepatocytes push into or split the fibrous septa causing small perforations and fragmenting the septa (Figs. 4, 5). As the liver reverses bridging fibrosis and cirrhosis, delicate periportal fibrous spikes are left behind in the portal tracts [18,19].

The portal tracts also demonstrate fibrosis regression as collagen is broken down, often leaving behind a paired bile duct and hepatic artery while the previously obliterated portal vein is not restored or visualized. This is known as a portal tract remnant. Hepatocytes prolapse or push into the fibroconnective tissue boundaries of the portal tract and are seen directly adjacent to the paired bile duct and artery (Figs. 6, 7). As the inflammation

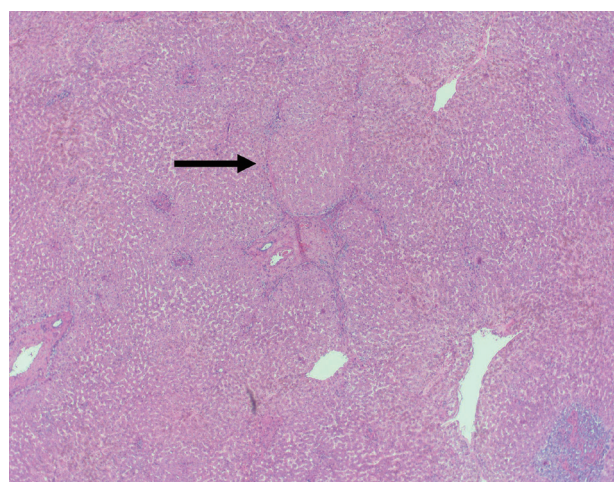


Fig. 1. On low power, a nodular architecture is apparent in fibrosis regression (arrow). Fibrous septae are thin, incomplete and interrupted.

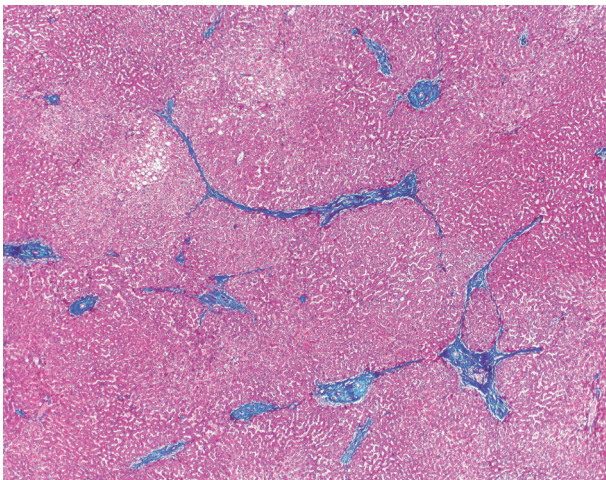


Fig. 2. Trichrome stain highlights fibrosis regression with thin, wispy, incomplete fibrous septa in a once cirrhotic liver.

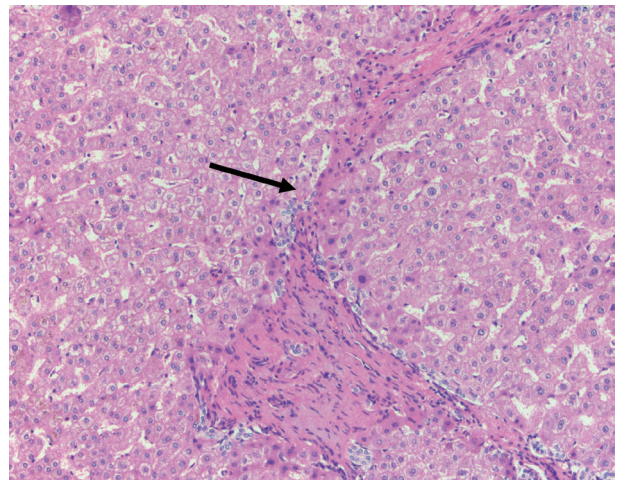


Fig. 4. With ongoing fibrolysis, hepatocytes push into the fibrous septae (arrow) eventually perforating and splitting the fibrous scar.

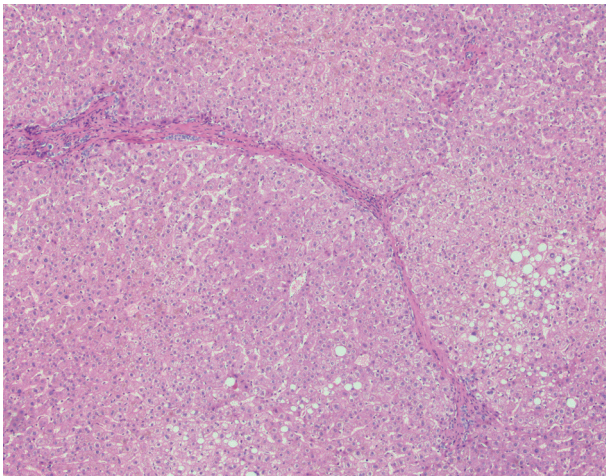


Fig. 3. Fibrous septae are thin and wispy with a paucity of chronic inflammation. There is minimal, patchy bile ductular proliferation.

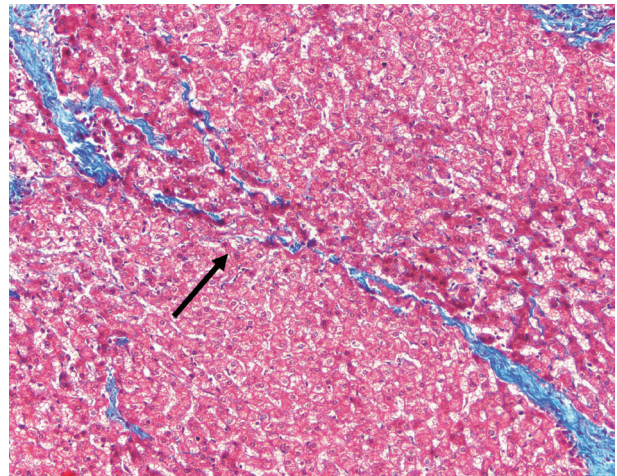


Fig. 5. Hepatocytes split the septa with ongoing perforations (arrow) (Trichrome stain).

and hepatocellular extinction subsides, parenchymal regeneration begins, sinusoidal collagen is resorbed and hepatic trabeculae restores its normal architecture [18,20,21].

CLASSIFICATION SYSTEMS

Traditional classification staging systems (i.e., Batts-Ludwig, Ishak, Metavir) characterized the architectural changes of fibrosis and cirrhosis in a linear pattern from no fibrosis to portal expansion, followed by step-wise periportal fibrosis, bridging fibrosis and ultimately cirrhosis (Table 1) [22,23]. Kutami et al. [24] introduced the Laennec classification system in 2000, which subdivided stage 4 cirrhosis into three categories: 4A, 4B, and 4C. Stage 4A was deemed mild cirrhosis with thin fibrous septa

and large nodules, 4B with at least two broad septa but small nodules and stage 4C with large, broad fibrous septa with several small nodules. While this system is easily reproducible, there has not been widespread consensus in adopting this classification scheme [24].

Due to effective treatments for chronic liver disease and the consideration of fibrosis and cirrhosis regression as a dynamic, bidirectional two-way street, Thiese et al. [18] proposed a new classification system for grading and staging hepatitis patients, the Beijing classification (Table 2). This system was proposed for the assessment of chronic viral hepatitis but has proven useful in describing activity and fibrosis for other etiologies of chronic hepatitis. It simplified grading activity and staging fibrosis and added a new, third category for determining the quality of fibro-

sis. Each biopsy is assessed a P-I-R score, predominantly progressive, indeterminate, or predominantly regressive as the major pattern of fibrosis. Predominantly progressive features show broad, thick fibrous septa with chronic inflammation, ductular reaction, parenchymal extinction, and congestion. A regressive pattern demonstrates wispy, thin fibrous septa with fragmentation, perforation, little or no inflammation and prolapsing hepatocytes into the portal tract as described earlier. Indeterminate denotes that the surgical pathologist is unable to distinctly classify a biopsy as P or R. The main benefit is that post-treatment biopsies can remain in the same stage (i.e., traditional stage 4 cirrhosis), but show significant changes in fibrosis quality (i.e., progressive to regressive or indeterminate), providing valuable prognostic information and determining response to therapy [18].

Besides a P-I-R score, liver biopsies are also graded and staged in the Beijing classification system (Table 2). Necroinflamma-

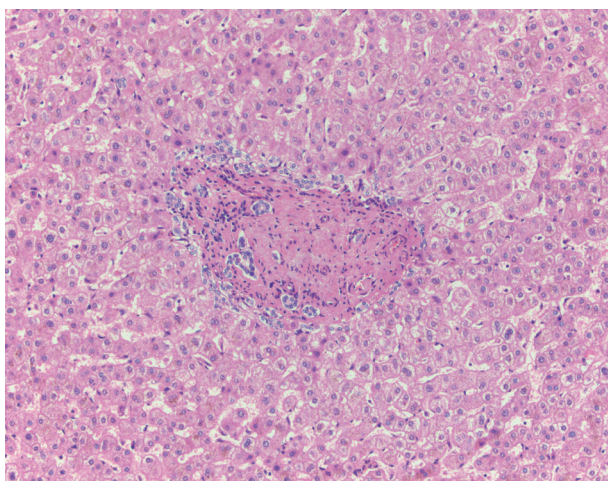


Fig. 6. Portal veins are often obliterated with vascular remodeling in advanced fibrosis and cirrhosis.

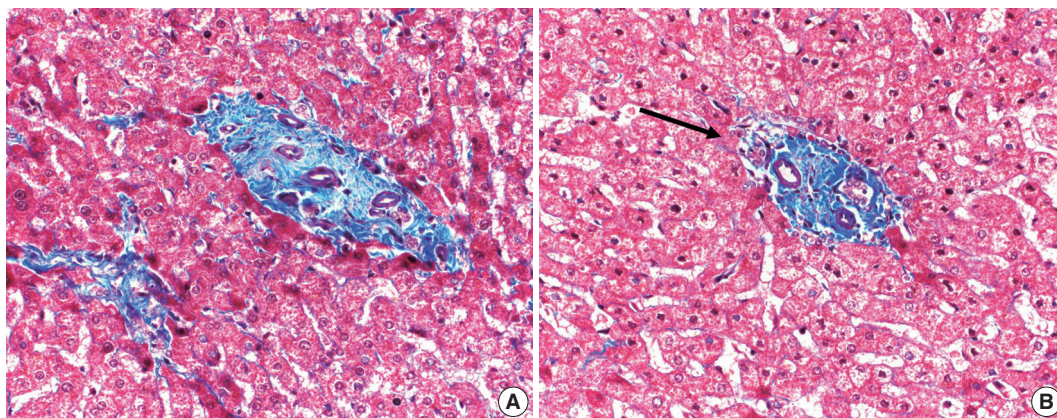


Fig. 7. Hepatocytes are in close proximity to portal tract elements (A) as they migrate into the portal tract stroma (arrow, B). Portal veins are not visualized, however, periportal thin, delicate fibrous spikes are seen (Trichrome stain).

tion or hepatitis is graded as inactive (only portal inflammation or rare interface or lobular activity), non-severe active (variable interface and lobular hepatitis), and severe active (confluent necrosis, perivenular or bridging necrosis). Fibrosis is staged as early (no fibrosis, portal fibrosis), intermediate (focal or frequent fibrous septa, bridging fibrosis) and advanced (fibrous septa with focal or diffuse nodularity) [18]. The similarities to prior adopted grading and staging classification systems are evident. This new system for microscopic evaluation of grading and staging is susceptible to intra and interobserver variability, therefore, simplifying and decreasing the number of subcategories in grading activity and staging fibrosis improves reproducibility. Interobserver agreement between pathologists adopting the P-I-R staging system was high with a Kappa value of 0.71 (substantial agreement) [18,25]. The P-I-R system is also a valuable prognostic marker independent of the grade and stage, providing a snapshot for the current state of disease that strongly correlates with hepatic venous wedge pressures (hepatic venous pressure gradient [HVPG]) and portal hypertension [26]. In patients with chronic viral hepatitis, P, I, or R was an accurate surrogate marker for clinical outcome as successful eradication and clearance of hepatotropic viruses were predominantly R and unsuccessful treatments were predominantly P or I [18].

Table 1. Batts-Ludwig classification system for staging fibrosis

Fibrosis	Score
None	0
Portal fibrosis confined to the portal tract	1
Periportal fibrosis or portal to portal fibrosis with intact architecture	2
Bridging fibrosis with architectural distortion but no cirrhosis	3
Probably or definitive cirrhosis	4

Table 2. Beijing classification system

	Description
Hepatitis assessment	
Inactive	Portal inflammation only or rare foci of interface or lobular hepatitis, no confluent necrosis
Active, non-severe	Varying degrees of interface and lobular hepatitis easily identified at low power, no confluent necrosis
Active, severe	Confluent necrosis (perivenular drop out or bridging necrosis or parenchymal collapse)
Fibrosis stage	
Early	No fibrosis or portal fibrosis
Intermediate	Fibrous septa, focal or frequent
Advanced	Fibrous septa with focal or diffuse nodularity (developing or established cirrhosis)
P-I-R fibrosis quality	
Predominantly progressive	Most of the specimen shows progressive forms of stroma
Indeterminate	Uncertain mix or balance between progressive and regressive forms of stroma
Predominantly regressive	Most of the specimen shows regressive forms of stroma

CLINICAL IMPLICATIONS

In advanced liver disease, there is increased resistance to sinusoidal blood flow which causes portal hypertension or increased portal pressures. The gold standard for measuring portal hypertension is the HVPG and a gradient of less than or equal to 5 is within normal limits. Cirrhotic patients vary widely in their clinical presentation because the severity of cirrhosis ranges from compensated and asymptomatic to decompensated cirrhosis with ascites, esophageal varices, and hepatic encephalopathy. HVPG is an accurate prognostic marker in cirrhotic patients that risk stratifies the likelihood of those complications. Clinical studies show that with cirrhosis and fibrosis regression, there is a decrease in HVPG and portal hypertension-related complications with improvements in liver function and survival rates. A comprehensive assessment is based on clinical, hemodynamic (i.e., HVPG), and histopathologic features [27-29].

There are multiple approaches to achieving reversal of fibrosis and cirrhosis. The most common method is to control or cure the primary, underlying disease. This has a proven and successful track record for hepatotropic viruses (i.e., hepatitis B and C), autoimmune hepatitis, hereditary hemochromatosis, Wilson's disease, and fatty liver disease. Anti-fibrotic agents target different steps in the pathobiology of fibrosis. These therapeutic drugs are focused on receptor-ligand interactions to prevent quiescent HSCs from transforming into activated HSCs, preventing the cascade of events that lead to deposition of ECM by inhibiting fibrogenesis, or accentuating the resolution of fibrosis through apoptosis or increased matrix degradation. There are over 500 active, clinical trials in this area of research [30].

Cirrhosis is also a major risk factor for developing hepatocellular carcinoma (HCC). With regression, there are physiologic

and mechanical/pressure improvements in the patient's condition, however, is there a reduction in the risk for developing HCC? There are two main factors that contribute to the pathobiology of HCC, the cumulative mutations of liver disease etiology (i.e., viral, metabolic, fatty liver, etc.) that form a clonal population/neoplasm and the surrounding extracellular matrix/tumor microenvironment (TME) which consists of vascular abnormalities/remodeling and the fibrous stroma [31- 33]. Even when the initial insult is removed (i.e., hepatotropic virus cleared by medication, weight loss or medication for steatohepatitis, phlebotomy for hemochromatosis, etc.) and fibrosis regression is visualized, the driver mutations within hepatocytes persist. For example, in hepatitis B, there is DNA integration into the host genome leading to genomic instability, alterations to tumor suppressor genes, and *TP53* mutations [34,35]. In non-alcoholic fatty liver disease, there are a different set of cumulative mutations, alterations in fatty acid beta-oxidation and insulin resistance [36]. As for the TME, vascular remodeling, ischemic injury, thrombosis of small blood vessels, lead to cycles of parenchymal extinction and regeneration with increased vascular endothelial growth factor expression and further genomic instability. Therefore, despite fibrosis regression, the risk for developing HCC remains high compared to the normal population and patients should continue to be actively screened and followed [32].

CONCLUSION

Cirrhosis was once thought to be an irreversible process of end-stage liver disease. This is no longer the case with treatment options for most chronic liver diseases. Fibrosis regression is characterized by thinning of the fibrous septa with hepatocytes pushing into the septa and eventual perforation. This leads to periportal

spiking within portal tracts and prolapsed hepatocytes into the boundaries of the portal tract stroma. Obliterated portal veins during progressive fibrosis and cirrhosis due to parenchymal extinction, vascular remodeling, and thrombosis often leaves behind a bile duct and hepatic artery within the portal tract. To characterize these histopathologic features, the Beijing classification system offers an accurate snapshot of a dynamic process between fibrogenesis and fibrolysis. Even with fibrosis regression, vascular lesions/remodeling, parenchymal extinction, and cumulative mutational burden persists and patients should continue to undergo clinical surveillance.

Ethics Statement

Not applicable.

Availability of Data and Material

All data generated or analyzed during the study are included in this published article (and its supplementary information files).

Code Availability

Not applicable.

ORCID

Michael J. Lee <https://orcid.org/0000-0001-6670-9109>

Conflicts of Interest

The authors declare that they have no potential conflicts of interest.

Funding Statement

No funding to declare.

References

- MacSwain RN, Burt AD, Portman B, et al. Pathology of the liver. 4th ed. Philadelphia: Saunders, 2002.
- Wanless IR, Nakashima E, Sherman M. Regression of human cirrhosis: morphologic features and the genesis of incomplete septal cirrhosis. *Arch Pathol Lab Med* 2000; 124: 1599-607.
- Hutterer F, Rubin E, Popper H. Mechanism of collagen resorption in reversible hepatic fibrosis. *Exp Mol Pathol* 1964; 3: 215-23.
- Brody JI, Mc KD, Kimball SG. Therapeutic phlebotomies in idiopathic hemochromatosis. *Am J Med Sci* 1962; 244: 575-86.
- Perez-Tamayo R. Cirrhosis of the liver: a reversible disease? *Pathol Annu* 1979; 14 Pt 2: 183-213.
- Geller SA. Coming or going? What is cirrhosis? *Arch Pathol Lab Med* 2000; 124: 1587-8.
- Chejfec G. Controversies in pathology: is cirrhosis of the liver a reversible disease? *Arch Pathol Lab Med* 2000; 124: 1585-6.
- Martinez-Hernandez A, Martinez J. The role of capillarization in hepatic failure: studies in carbon tetrachloride-induced cirrhosis. *Hepatology* 1991; 14: 864-74.
- Friedman SL. Mechanisms of hepatic fibrogenesis. *Gastroenterology* 2008; 134: 1655-69.
- Mori T, Okanoue T, Sawa Y, Hori N, Ohta M, Kagawa K. Defenestration of the sinusoidal endothelial cell in a rat model of cirrhosis. *Hepatology* 1993; 17: 891-7.
- Guido M, Sarcognato S, Russo FP, et al. Focus on histological abnormalities of intrahepatic vasculature in chronic viral hepatitis. *Liver Int* 2018; 38: 1770-6.
- Schaffner F, Poper H. Capillarization of hepatic sinusoids in man. *Gastroenterology* 1963; 44: 239-42.
- Benyon RC, Arthur MJ. Extracellular matrix degradation and the role of hepatic stellate cells. *Semin Liver Dis* 2001; 21: 373-84.
- de Meijer VE, Sverdlov DY, Popov Y, et al. Broad-spectrum matrix metalloproteinase inhibition curbs inflammation and liver injury but aggravates experimental liver fibrosis in mice. *PLoS One* 2010; 5: e11256.
- Muller D, Quantin B, Gesnel MC, Millon-Collard R, Abecassis J, Breathnach R. The collagenase gene family in humans consists of at least four members. *Biochem J* 1988; 253: 187-92.
- Yoneda A, Sakai-Sawada K, Niitsu Y, Tamura Y. Vitamin A and insulin are required for the maintenance of hepatic stellate cell quiescence. *Exp Cell Res* 2016; 341: 8-17.
- Davis BH, Pratt BM, Madri JA. Retinol and extracellular collagen matrices modulate hepatic Ito cell collagen phenotype and cellular retinol binding protein levels. *J Biol Chem* 1987; 262: 10280-6.
- Theise ND, Jia J, Sun Y, Wee A, You H. Progression and regression of fibrosis in viral hepatitis in the treatment era: the Beijing classification. *Mod Pathol* 2018; 31: 1191-200.
- Wanless IR, Wong F, Blendis LM, Greig P, Heathcote EJ, Levy G. Hepatic and portal vein thrombosis in cirrhosis: possible role in development of parenchymal extinction and portal hypertension. *Hepatology* 1995; 21: 1238-47.
- Taguchi K, Asano G. Neovascularization of pericellular fibrosis in alcoholic liver disease. *Acta Pathol Jpn* 1988; 38: 615-26.
- Wanless IR. The role of vascular injury and congestion in the pathogenesis of cirrhosis: the congestive escalator and the parenchymal extinction sequence. *Curr Hepatol Rep* 2020; 19: 40-53.
- Batts KP, Ludwig J. Chronic hepatitis: an update on terminology and reporting. *Am J Surg Pathol* 1995; 19: 1409-17.
- Bedossa P, Poynard T. An algorithm for the grading of activity in chronic hepatitis C. The METAVIR Cooperative Study Group. *Hepatology* 1996; 24: 289-93.
- Kutami R, Girgrah N, Wanless I, et al. The Laennec grading system for assessment of hepatic fibrosis: validation by correlation with wedged hepatic vein pressure and clinical features. *Hepatology* 2000; 32: 407.
- Sun Y, Zhou J, Wang L, et al. New classification of liver biopsy assessment for fibrosis in chronic hepatitis B patients before and after treatment. *Hepatology* 2017; 65: 1438-50.
- Garcia-Tsao G, Friedman S, Iredale J, Pinzani M. Now there are many (stages) where before there was one: in search of a pathophysiological classification of cirrhosis. *Hepatology* 2010; 51: 1445-9.
- Bochnakova T. Hepatic venous pressure gradient. *Clin Liver Dis (Hoboken)* 2021; 17: 144-8.
- Mauro E, Crespo G, Montironi C, et al. Portal pressure and liver stiffness measurements in the prediction of fibrosis regression after sustained virological response in recurrent hepatitis C. *Hepatology* 2018; 67: 1683-94.
- Sanyal AJ, Anstee QM, Trauner M, et al. Cirrhosis regression is associated with improved clinical outcomes in patients with nonalcoholic steatohepatitis. *Hepatology* 2022; 75: 1235-46.
- Yoon YJ, Friedman SL, Lee YA. Antifibrotic therapies: where are we

- now? *Semin Liver Dis* 2016; 36: 87-98.
31. Santhakumar C, Gane EJ, Liu K, McCaughan GW. Current perspectives on the tumor microenvironment in hepatocellular carcinoma. *Hepato Int* 2020; 14: 947-57.
 32. Lin CA, Chang LL, Zhu H, He QJ, Yang B. Hypoxic microenvironment and hepatocellular carcinoma treatment. *Hepatoma Res* 2018; 4: 26.
 33. Capece D, Fischietti M, Verzella D, et al. The inflammatory microenvironment in hepatocellular carcinoma: a pivotal role for tumor-associated macrophages. *Biomed Res Int* 2013; 2013: 187204.
 34. Levrero M, Zucman-Rossi J. Mechanisms of HBV-induced hepatocellular carcinoma. *J Hepatol* 2016; 64(1 Suppl): S84-101.
 35. Niu B, Hann HW. Hepatitis B virus-related hepatocellular carcinoma: carcinogenesis, prevention, and treatment. In: Abdeldayem HM, ed. *Updates in liver cancer*. London: IntechOpen Ltd., 2017.
 36. Peiseler M, Tacke F. Inflammatory mechanisms underlying nonalcoholic steatohepatitis and the transition to hepatocellular carcinoma. *Cancers (Basel)* 2021; 13: 730.

A stepwise approach to fine needle aspiration cytology of lymph nodes

Yosep Chong¹, Gyeongsin Park¹, Hee Jeong Cha², Hyun-Jung Kim³, Chang Suk Kang⁴, Jamshid Abdul-Ghafar¹, Seung-Sook Lee⁵

¹Department of Hospital Pathology, The Catholic University of Korea, College of Medicine, Seoul;
²Department of Pathology, Ulsan University Hospital, University of Ulsan College of Medicine, Ulsan;
³Department of Pathology, Inje University Sanggye Paik Hospital, Seoul;
⁴Department of Pathology, Samkwang Medical Laboratories, Seoul;
⁵Department of Pathology, Korea Institute of Radiological and Medical Sciences, Seoul, Korea

The cytological diagnosis of lymph node lesions is extremely challenging because of the diverse diseases that cause lymph node enlargement, including both benign and malignant or metastatic lymphoid lesions. Furthermore, the cytological findings of different lesions often resemble one another. A stepwise diagnostic approach is essential for a comprehensive diagnosis that combines: clinical findings, including age, sex, site, multiplicity, and ultrasonography findings; low-power reactive, metastatic, and lymphoma patterns; high-power population patterns, including two populations of continuous range, small monotonous pattern and large monotonous pattern; and disease-specific diagnostic clues including granulomas and lymphoglandular granules. It is also important to remember the histological features of each diagnostic category that are common in lymph node cytology and to compare them with cytological findings. It is also essential to identify a few categories of diagnostic pitfalls that often resemble lymphomas and easily lead to misdiagnosis, particularly in malignant small round cell tumors, poorly differentiated squamous cell carcinomas, and nasopharyngeal undifferentiated carcinoma. Herein, we review a stepwise approach for fine needle aspiration cytology of lymphoid diseases and suggest a diagnostic algorithm that uses this approach and the Sydney classification system.

Key Words: Cytology; Fine needle aspiration; Lymph node; Lymphoid neoplasms; Diagnosis

Received: February 22, 2023 **Revised:** May 22, 2023 **Accepted:** June 12, 2023

Corresponding Author: Yosep Chong, MD, PhD, Department of Hospital Pathology, Uijeongbu St. Mary's Hospital, College of Medicine, The Catholic University of Korea, 271 Cheonbo-ro, Uijeongbu 11765, Korea
 Tel: +82-32-820-3160, Fax: +82-32-820-3877, E-mail: ychong@catholic.ac.kr

Lymph nodes are an essential component of the human immune system. Lymphadenopathy occurs when a lymph node is large in size and number or atypical in consistency [1]. The causes of lymphadenopathy range from benign reactive lymphoid hyperplasia to malignant diseases. Although several conditions present with lymph node enlargement, the most common cause is benign lymphadenopathy (90%), including reactive hyperplasia (60%), followed by infectious or inflammatory lymphadenitis (30%). Infectious or inflammatory lymphadenitis includes Kikuchi-Fujimoto disease (KFD), tuberculosis, sarcoidosis, infectious mononucleosis, toxoplasmosis, human immunodeficiency virus infection, cat-scratch disease, drug (phenytoin) reaction, and others (Fig. 1) [1,2]. Malignant lymphadenopathies only comprise 10% of the cases, which include primary lymphomas (3%), including diffuse large B-cell lymphoma/anaplastic large cell lymphoma, follicular lymphoma (FL), mantle cell lymphoma (MCL),

peripheral T-cell lymphoma (PTCL), and Hodgkin's lymphoma (HL). Metastatic carcinomas account for 7% of cases and include metastatic papillary thyroid carcinoma, adenocarcinomas primarily from lung or breast, and poorly differentiated squamous cell, small cell, or any primary unknown carcinoma (Fig. 1) [2]. It is very unlikely to diagnose the cause of lymphadenopathy based solely on history, physical examination, or ultrasound alone.

Fine needle aspiration cytology (FNAC) has been vastly utilized as a primary diagnostic tool to examine enlarged lymph nodes and to exclude involvement of alternative organs, such as the salivary gland, head, neck, or other subcutaneous masses. It is a minimally invasive approach that allows fast diagnosis and treatment. There are few complications that have been reported for FNAC, including hemorrhage, nerve damage, and vasovagal reactions in head and neck lymph node procedures [3]. Finally, FNAC is a cost-effective procedure, especially in developing coun-

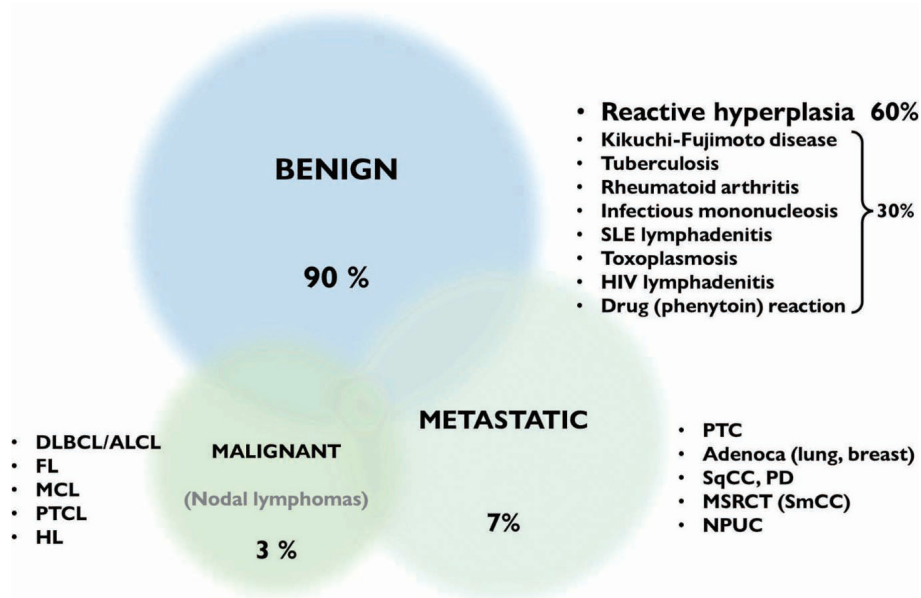


Fig. 1. Disease entity that can be found in lymph node fine needle aspiration cytology. DLBCL/ALCL, diffuse large B-cell lymphoma/anaplastic large cell lymphoma; FL, follicular lymphoma; MCL, mantle cell lymphoma; PTCL, peripheral T-cell lymphoma; HIV, human immunodeficiency virus; HL, Hodgkin's lymphoma; PTC, papillary thyroid carcinoma; SqCC, squamous cell carcinoma; MSRCT, malignant solitary fibrous tumor of the pleura; NPUC, non-papillary urothelial carcinoma; PD, poorly differentiated; SmCC, small cell carcinoma.

tries where the cost of surgical biopsy can be prohibitive [3]. However, this procedure has limitations.

In a review by Rammeh et al. [3], FNAC for head and neck masses was inconclusive in 17.7% of cases, while literature review found a rate range of 3%–30% [4,5]. This rate largely depends on the experience of cytotechnologists and cytopathologists [4,5]. There are fewer inconclusive cases when experienced cytopathologists perform the procedure, evaluate the samples, and recognize inadequate aspirates. Another limitation of FNAC is that the diagnoses of some malignant tumors (e.g., thyroid follicular carcinoma) are based only on histological criteria [2,6,7]. Moreover, the value of FNAC for verifying recurrent or residual lymphoma is well established and accepted. However, the diagnosis of primary lymphoma remains controversial [4].

A stepwise approach is required when using FNAC to diagnose the cause of lymphadenopathy. In general, up to three separate needle puncture passes with aspirates are needed to obtain a sufficient sample. Moreover, microscopic evaluation is associated with the following clinical history: signs and symptoms, radiological findings, presence of systemic inflammatory symptoms, node size and location, enlargement duration, malignancy history, medical and drug history, autoimmune disease, and risk factors for malignancy (including age, sex, race, family history, or presence of other masses in the body) [1,8,9].

In the current study, we introduce a stepwise approach for

lymph node FNAC diagnosis along with disease-specific diagnostic clues, clinical information, and ultrasonographic findings. We suggest a diagnostic algorithm that encompasses this stepwise approach and the Sydney classification system published in 2019 [10].

CLINICAL FINDINGS

Fig. 2 summarizes the stepwise approach to lymph node FNAC. Before cytological interpretation, it is important to review the clinical information. In order to formulate a proper differential diagnosis, the following clinical features are needed: age, site (cervical/inguinal), lymph node size, presence of B symptoms (fever, weight loss, night sweating), previous medical history (primary or metastatic), infectious signs, autoimmune disease, and history of drug or chemical exposure.

Radiological findings, including mostly ultrasonographic and positron emission tomography computed tomography (PET/CT) findings, are helpful to narrow the differential diagnosis (Supplementary Table S1, Supplementary Fig. S1). In benign lymphadenopathy, the lymph nodes are relatively small, oval-shaped, and hypoechoic with a regular well-demarcated border. The general architecture is preserved, with a visible hilum without obvious necrosis or calcification. In metastatic lesions, lymph nodes are usually large, round, and hypoechoic with irregular, ill-de-

finer blurred borders that suggest capsular invasion. The architecture can be destroyed by metastatic tumors, leading to a heterogeneous internal structure without a visible hilum. Cortical nodules, cystic tumor necrosis, and calcifications can occur. In malignant lymphomas, lymph nodes are continuously enlarged/conglomerated and hypoechoic with cortical thickening and no visible hilum. On PET/CT, metastatic lesions or malignant lymphomas demonstrate high fluorodeoxyglucose uptake more frequently than do normal lymph nodes.

On microscopic examination, a comprehensive interpretation of low-power patterns, high-power patterns, and disease-specific diagnostic clues is essential for successful differential diagnosis.

LOW-POWER PATTERN OF LYMPH NODE FINE NEEDLE ASPIRATION CYTOLOGY

The first step in lymph node FNAC is to assess the low-power magnification patterns. Lymphadenopathy can be broadly categorized into three patterns: reactive, metastatic, and lymphoma (Fig. 3). The reactive pattern comprises an evenly distributed smear with normal cellularity and some normal lymphoid clusters. Diverse inflammatory cells may be observed according to the type of lymphadenopathy. Necrosis or granulomas may be observed in tuberculosis or KFD. Neutrophilic smears suggest a benign condition.

The metastatic pattern involves an irregularly distributed hypercellular smear with prominent epithelial clusters and is often

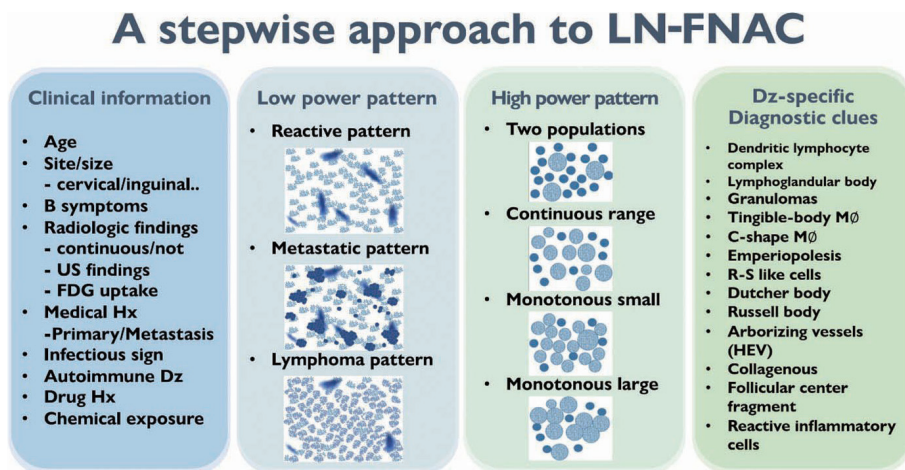


Fig. 2. A stepwise approach to lymph node fine needle aspiration cytology (LN-FNAC) interpretation. US, ultrasonography; FDG, fluorodeoxyglucose; Hx, history; Dz, disease; MΦ, macrophage; R-S, Reed-Sternberg; HEV, high endothelial venule.

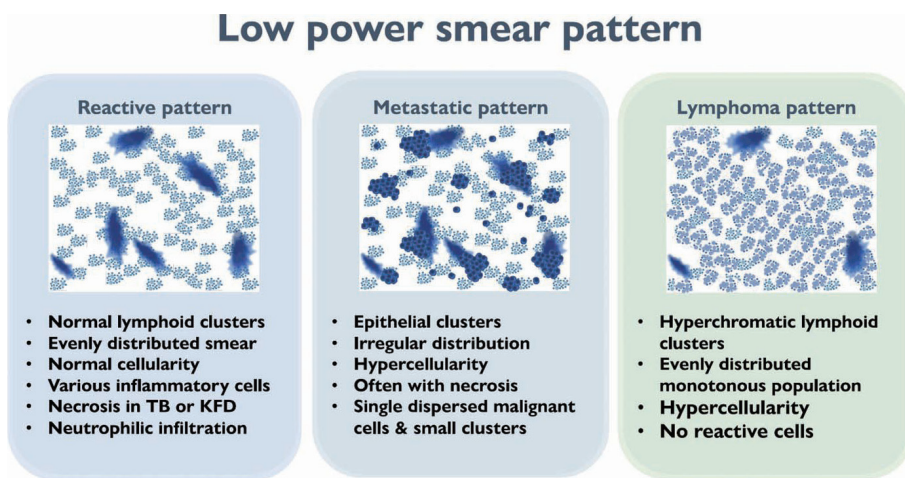


Fig. 3. Low-power smear patterns of lymph node fine needle aspiration cytology interpretation. TB, tuberculosis; KFD, Kikuchi-Fujimoto disease.

accompanied by necrosis. Single dispersed malignant cells and small-to-large clusters are observed.

The lymphoma pattern shows an evenly distributed hypercellular smear with monotonous hyperchromatic lymphoid clusters. Reactive inflammatory cells (such as neutrophils) are uncommon. Occasional multinucleated, large, atypical cells such as Reed-Sternberg cells and ill-defined granulomas with occasional eosinophils can be found in HL.

HIGH-POWER PATTERN OF LYMPH NODE FINE NEEDLE ASPIRATION CYTOLOGY

The second step for lymph node FNAC is to assess high-power magnification cell population patterns. There are four broad patterns: two-cell, continuous range, monotonously small, and monotonously large population (Fig. 4). The two-cell population pattern is a smear pattern with two distinct cell populations. This pattern can be seen in reactive hyperplasia; metastatic carcinomas; and diverse lymphomas including HL, FL, and anaplastic large cell lymphoma. Rarely, T-cell/histiocyte-rich B-cell lymphoma (TCR-BCL) and lymphomatoid granulomatosis can also present with this cytological pattern [2].

The second pattern is a smear with a continuous range of variably sized cells. In this pattern, there is an obvious dominant cell population of atypical lymphocytes and diverse inflammatory cells such as eosinophils. PTCL and angioimmunoblastic lymphoma, which are representative examples of this pattern, can

present with variable inflammatory/reactive cells.

The third pattern is a small cell population that predominantly presents as monotonously small, atypical lymphoma cells with few reactive cells. This category includes malignant small round cell tumors, such as metastatic small cell carcinoma or small round cell sarcoma, and low-grade B-cell lymphoma such as MCL or small lymphocytic lymphoma. However, malignant small round cell tumors generally have slightly larger nuclei than low-grade B-cell lymphomas.

The fourth pattern is a large cell population of mostly monotonously large atypical malignant cells. For metastasis, poorly differentiated squamous cell carcinoma (such as basaloid type) and undifferentiated nasopharyngeal carcinoma are the major differential diagnoses. Diffuse large B-cell and Burkitt lymphoma are common examples of lymphoma.

Two-cell population pattern

Reactive lymphoid hyperplasia without a specific etiology accounts for 60% of all cases and usually demonstrates polymorphic cell populations, including small and large plasmacytoid lymphocytes [11]. This hyperplasia is often accompanied by tingible-body macrophages; dendritic lymphocytic aggregates (intact follicles); and other reactive inflammatory cells, including capillaries, eosinophils, and mast cells (Fig. 5A) [11].

FL is another example of a two-cell population pattern. It demonstrates predominantly small irregular/cleaved and large cleaved/non-cleaved lymphocytes with few tingible-body macrophages,

High power cellular population pattern

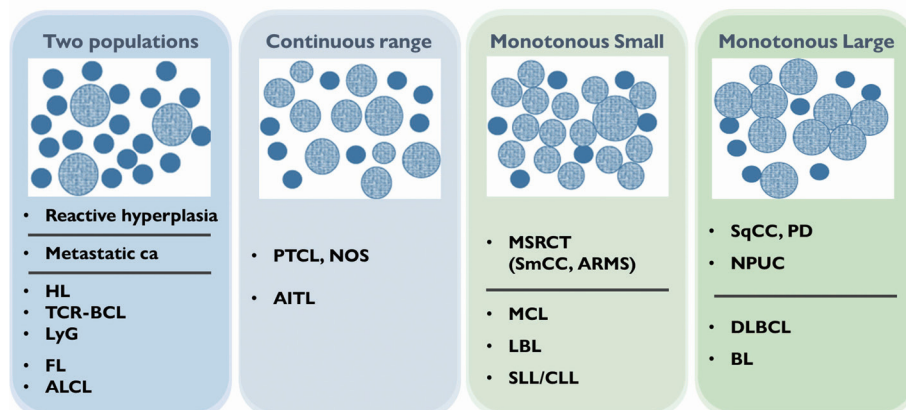


Fig. 4. High-power magnification cellular population patterns of lymph node fine needle aspiration cytology interpretation. HL, Hodgkin's Lymphoma; TCR-BCL, T-cell/histiocyte-rich B-cell lymphoma; LyG, lymphomatoid granulomatosis; FL, follicular lymphoma; ALCL, anaplastic large cell lymphoma; PTCL, NOS, peripheral T-cell lymphoma, not otherwise specified; AITL, angioimmunoblastic T-cell lymphoma; MSRCT, malignant solitary fibrous tumor of the pleura; SmCC, small cell carcinoma; ARMS, alveolar rhabdomyosarcoma; MCL, mantle cell lymphoma; LBL, lymphoblastic lymphoma; SLL/CLL, small lymphocytic lymphoma/chronic lymphocytic leukemia; SqCC, squamous cell carcinoma; PD, poorly differentiated; NPUC, non-papillary urothelial carcinoma; DLBCL, diffuse large B-cell lymphoma; BL, Burkitt lymphoma.

similar to reactive lymphoid hyperplasia (Fig. 5B). However, FL is more hypercellular, and the small lymphocytes are slightly larger than those in reactive lymphoid hyperplasia. Differential diagnosis can be challenging, although immunocytochemical staining for BCL2 may be helpful [12].

HL also demonstrates two-cell populations comprising large Reed-Sternberg cells in the background of small lymphocytes, plasma cells, and histiocytes (Fig. 5C) [13]. Because the low-power cytologic findings of Hodgkin lymphoma may resemble those of reactive lymphoid hyperplasia, it is important not to miss Reed-Sternberg cells in high-power examinations.

Rarely, differential diagnosis of metastatic carcinoma that demonstrates discohesive tumor cells with poor differentiation can be challenging as it can also present with two-cell populations, as in other examples (Fig. 5D). Tumor cells most often demonstrate adenoid or squamous differentiation, which can be useful for a correct diagnosis using high-magnification fields. Information on the clinical history or presentation of the primary cancer should be carefully verified when interpreting fine needle aspiration (FNA) slides.

Continuous range of cell size population pattern

A continuous range population pattern might be the most challenging pattern in lymph node FNA interpretation because it can

be easily misinterpreted as reactive lymphoid hyperplasia. This pattern includes peripheral T-cell and angioimmunoblastic lymphoma, which are present in the background of diverse inflammatory cells including histiocytes, plasma cells, and eosinophils.

PTCL demonstrated a marked variation in cell composition, including small, intermediate, and large cells (Fig. 6A) [14]. The biggest obstacle for proper diagnosis of PTCL is its lack of specific diagnostic features and immunocytochemical markers [15-17]. Likewise, there were no cytomorphological features specific to angioimmunoblastic T-cell lymphoma that displayed polymorphous cytomorphology (Fig. 6B). Sometimes, large cells resemble Reed-Sternberg cells and can be Epstein-Barr virus-positive, which leads to a misdiagnosis of HL.

Monotonous small cell population pattern

The third pattern involves a population of monotonously small cells and includes malignant small round cell tumors such as metastatic small cell carcinoma, alveolar rhabdomyosarcoma, and mature B-cell lymphomas (including mantle cell, lymphoblastic, and small lymphocytic lymphoma or chronic lymphocytic leukemia).

Small lymphocytic lymphoma or chronic lymphocytic leukemia demonstrated monomorphous small lymphocytes with scanty cytoplasm, smooth or minimally irregular nuclei with

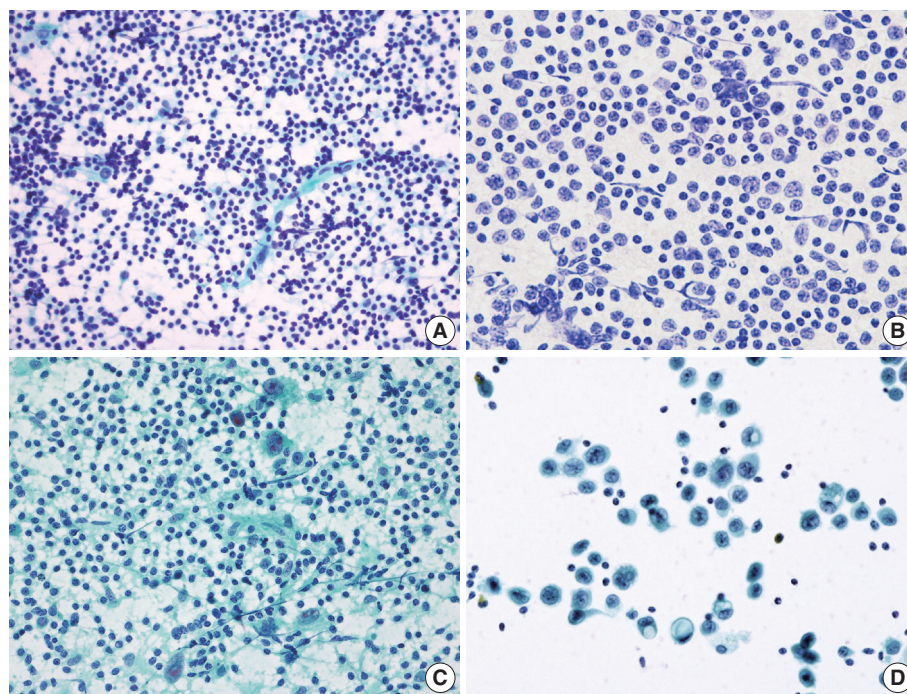


Fig. 5. Exemplary images of the two-cell population pattern. (A) Reactive hyperplasia. (B) Follicular lymphoma. (C) Hodgkin's lymphoma. (D) Metastatic adenocarcinoma.

clumped (soccer ball-like) chromatin, and inconspicuous or absent nucleoli (Fig. 7A) [18]. Occasionally, large lymphocytes such as prolymphocytes and paraimmunoblasts are observed. MCL demonstrated monomorphous small-to-intermediate-sized cells with scanty cytoplasm and irregular nuclei with fine chromatin and inconspicuous or absent nucleoli (Fig. 7B). Centroblasts or immunoblasts are absent. There may be a few histiocytes with moderately abundant eosinophilic cytoplasm, or so-called “pink histiocytes.” Lymphoblastic lymphoma demonstrates monomorphous intermediate-sized cells with scant or moderate cytoplasm and round or convoluted nuclei with finely granular chromatin and inconspicuous nucleoli [19]. The cells look small

at low power due to their blastic nature. However, they are 1.5 to 2 times larger than the small lymphocyte at high power. Occasionally, cytoplasmic vacuoles and mitoses are observed (Fig. 7C).

The most common diagnostic pitfalls in this category are malignant small round cell tumors, such as metastatic small cell carcinoma and rarely alveolar rhabdomyosarcoma. Small cell lung carcinoma commonly metastasizes to the cervical lymph nodes and demonstrates diverse cellular clusters and dispersed cells with abundant necrosis (Fig. 7D). Several important differential findings include variable-sized tumor cells with characteristic salt-and-pepper-like chromatin including frequent smudging and molding. The differential interpretation of cell aggregation and

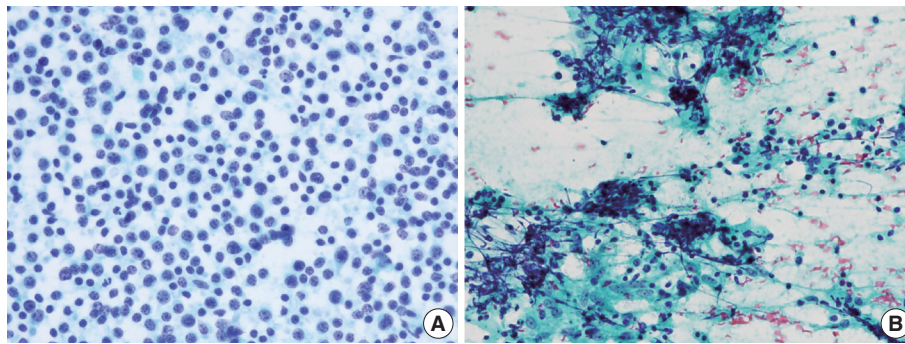


Fig. 6. Exemplary images of continuous range of variably sized cells pattern. (A) Peripheral T-cell lymphoma, not otherwise specified. (B) Angioimmunoblastic T-cell lymphoma.

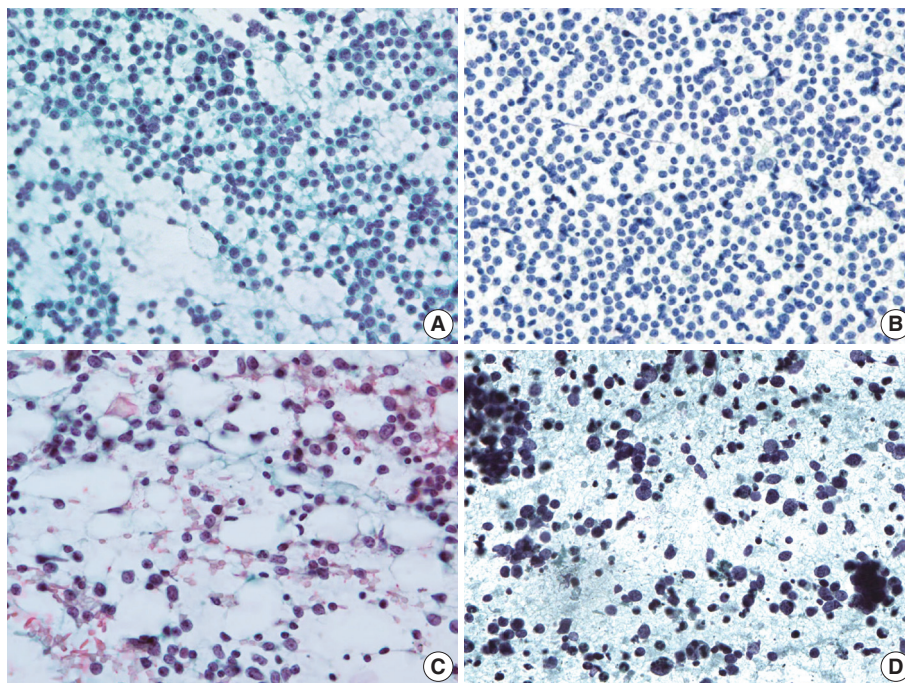


Fig. 7. Exemplary images of monotonously small population pattern. (A) Small lymphocytic lymphoma/chronic lymphocytic leukemia. (B) Mantle cell lymphoma. (C) Lymphoblastic lymphoma. (D) Metastatic small round cell tumor (small cell carcinoma).

clusters is important. Rarely, alveolar rhabdomyosarcoma can simulate the cytological features of malignant lymphomas. Therefore, the clinical presentation and history are important to avoid misdiagnosis.

Monotonous large cell population pattern

The last pattern is a monotonously large cell population pattern. This pattern can be seen in high-grade lymphomas, such as diffuse large B-cell and Burkitt lymphoma, and other metastatic carcinomas, such as poorly differentiated squamous cell and nasopharyngeal undifferentiated carcinoma. The smear of diffuse large B-cell lymphoma demonstrated a moderately to highly cellular smear of predominantly large, atypical cells that were 2.5–5 times larger than small lymphocytes or histiocytes (Fig. 8A) [20]. The tumor cell has a round or irregular nucleus with a single prominent nucleolus and scant or abundant cytoplasm. However, these cells sometimes have multiple abnormal pleomorphic nuclei that resemble those of Reed-Sternberg cells. As reactive T-cells and histiocytes are few, they usually demonstrate a monotonously large cell population. Tingible-body macrophages are variable in number, lymphoglandular bodies are common, while dendritic lymphocytic aggregates are rarely seen.

Burkitt lymphoma is another example of this pattern when the lesion involves extranodal sites. The tumor cells were typically

uniform with intermediate-sized round nuclei, coarse chromatin, two–five small nucleoli per nucleus, and scant blue cytoplasm with small intracytoplasmic vacuoles (Fig. 8B). Several characteristic features of Burkitt lymphoma include apoptosis and brisk mitoses, along with frequent tingible-body macrophages.

In this pattern, the major challenging differential diagnoses were poorly differentiated metastatic squamous cell and undifferentiated nasopharyngeal carcinomas that predominantly demonstrated singly dispersed tumor cells (Fig. 8C, D). It is important to identify tumor cells in clusters, which are uncommon in lymphoma.

DISEASE-SPECIFIC DIAGNOSTIC CLUES

In addition to the low- and high-magnification power patterns, several characteristic findings are specific or pathognomonic for certain diseases (Fig. 2). One famous example is the occasional presence of Reed-Sternberg cells in Hodgkin lymphoma, which are large, atypical cells with multiple prominent nuclei and nucleoli intermixed with diverse inflammatory cells (Fig. 9A). Another example is the Russell body or Mott cells that can be found in mature B-cell lymphomas, including lymphoplasmacytic or extranodal marginal zone lymphoma (Fig. 9B) [21]. These findings are critical for proper diagnostic use of FNA samples. There-

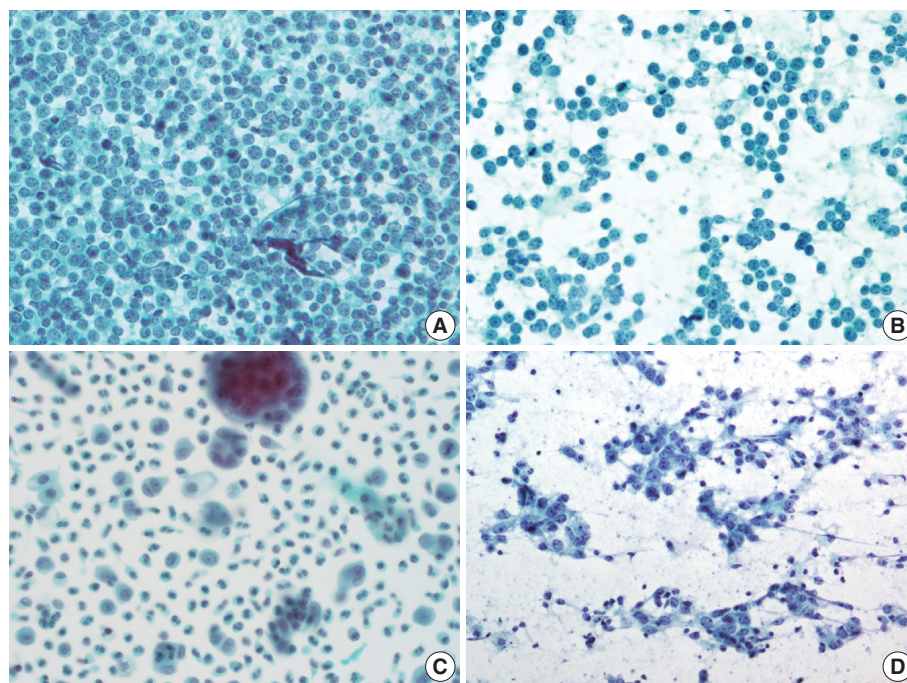


Fig. 8. Exemplary images of monotonously large population pattern. (A) Diffuse large B-cell lymphoma. (B) Burkitt lymphoma. (C) Squamous cell carcinoma, poorly differentiated. (D) Undifferentiated carcinoma, nasopharynx.

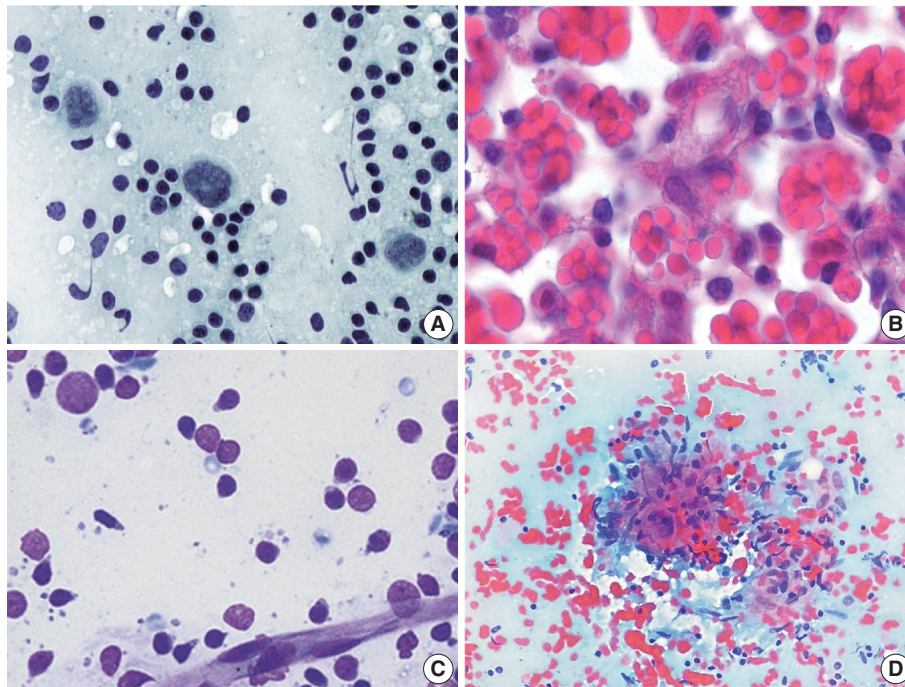


Fig. 9. Disease-specific diagnostic clues. (A) Reed-Sternberg cells in Hodgkin's lymphoma. (B) Russell body (Mott cells) in mature B-cell lymphoma such as lymphoplasmacytic lymphoma. (C) Lymphoglandular bodies in reactive hyperplasia. (D) Ill-defined granuloma in tuberculosis.

fore, it is important to be familiar with these disease-specific diagnostic clues. Lymphoglandular bodies, also called hyaline bodies or lymphoid globules, are round, pale, basophilic fragments of cytoplasm with smooth borders in lymphoid tissues. Francis et al. [22] reported that lymphoglandular bodies were found in >90% of non-Hodgkin lymphomas, 86% of reactive lymphadenitis, and 66% of Hodgkin lymphomas (Fig. 9C). Granulomas with caseous necrosis are suspicious for tuberculosis, while those that are small tight granuloma clusters without necrosis are suspicious for sarcoidosis (Fig. 9D). Granulomas can also be found in toxoplasmosis, cat-scratch disease, and HL. Other diagnostic clues include dendritic lymphocyte complexes in reactive hyperplasia, tingible-body macrophages in highly proliferative lymphomas such as Burkitt lymphoma, C-shaped macrophages in KFD, emperipolesis in Rosai-Dorfman disease, and melanin-containing macrophages in dermatopathic lymphadenopathy. Additionally, Dutcher bodies are intranuclear inclusions of cytoplasm (pseudoinclusions) found in plasma cells and were originally described in Waldenstrom macroglobulinemia and IgA multiple myeloma. Arborizing vessels (high endothelial venules) can be found in the lymph node FNA of follicular dendritic cell-derived tumors, such as Castleman disease. A necrotic background is a common finding in several high-grade malignant lymphomas and metastatic carcinomas including diffuse large

B-cell lymphomas or metastatic squamous cell carcinomas and in benign lymphadenopathies such as tuberculosis and necrotizing histiocytic lymphadenitis (KFD) [23].

SYDNEY CLASSIFICATION

In 2019, a steering committee of international cytopathologists involved in lymph node FNAC developed a system for reporting lymph node FNAC in the International Cytology Congress in Sydney. They ultimately published The Sydney system after five rounds of circulation among committee members based on a review of the international literature and the expertise of the members (Table 1).

This system defined the following five diagnostic reporting categories according to the cytological findings: inadequate/non-diagnostic (L1), benign (L2), atypical, undermined significance/atypical lymphoid uncertain significance (AUS/ALUS) (L3), suspicious (L4), and malignant (L5) [2]. The inadequate/non-diagnostic category includes cases that cannot be diagnosed properly owing to scant cellularity, extensive necrosis, or technical limitations that cannot be overcome. Repeat FNAC, core needle, or excision biopsy was recommended in these cases. The benign category includes cases of suppurative and granulomatous inflammation and specific infections that demonstrate a heteroge-

Table 1. The Sydney classification system

Diagnostic reporting categories	Explanation	Post-LN-FNAC management recommendations	Exemplary findings
Inadequate/non-diagnostic (L1)	Low cellularity	LN-FNAC repetition and/or CNB or excision	-
Benign (L2)	Reactive hyperplasia Benign lymphadenitis	Clinical F/U or specific Tx depending on the Dx	-
AUS/ALUS (L3)	Possibly benign, not fully supported by cytology and ancillary technique	LN-FNAC repetition with acquisition of material for ancillary studies and/or CNB or excision	Two-cell population that cannot exclude follicular lymphoma Monotonously small cell population that cannot exclude low-grade B-cell lymphomas such as marginal zone B-cell lymphoma, small cell lymphoma/chronic lymphocytic leukemia, mantle cell lymphoma, and lymphoblastic lymphoma
Suspicious (L4)	Possibly malignant, not fully supported by cytology and ancillary technique	LN-FNAC repetition with acquisition of material for appropriate ancillary studies and/or CNB or excision	Monotonously small and/or medium-sized, monomorphic atypical lymphoid cells suspicious of lymphoma, but cytomorphology alone is not sufficient for diagnosis, polymorphous lymphoid smears in which few Reed-Sternberg-like cells are detected, large cell or Burkitt lymphomas with scanty cellular, and smears in which atypical cells suspicious for metastasis are detected but are too scant to be diagnostic
Malignant (L5)	(NHL, HL, metastases)	Histological biopsy requested (not requested for HL/NHL relapses or metastasis from known or clearly indicated primary tumor, etc.)	Small-to-medium-sized cells of non-Hodgkin lymphomas supported by evidence of clonality and all the entities in which cytopathological features alone are sufficient to identify malignancy as large cell non-Hodgkin's lymphoma. This category also includes Hodgkin's lymphoma in which there is an appropriate cellular background and diagnostic Reed-Sternberg cells as well as metastatic neoplasms

LN-FNAC, lymph node fine needle aspiration cytology; CNB, core needle biopsy; F/U, follow-up; Tx, therapy; Dx, diagnosis; NHL, non-Hodgkin lymphoma.

neous lymphoid population (two-cell population). The AUS/ALUS category includes cases with two-cell populations in which the features suggest a reactive process; however, FL cannot be excluded; or the atypical cells are not lymphoid cells (AUS); or there is a monotonously small cell population for which low-grade B-cell lymphomas cannot be excluded. The suspicious category includes cases with small and/or medium-sized monomorphic atypical lymphoid cells that are suspicious of lymphoma, but cytomorphology alone is insufficient to make the diagnosis. The suspicious category includes polymorphous lymphoid smears containing a few Reed-Sternberg-like cells, large cell or Burkitt lymphomas with scanty cellular cells, or atypical cells that are suspicious for metastasis are detected but are too scant to be diagnosed. The malignant category includes small- to medium-sized cells of non-HLs supported by evidence of clonality and all cases in which cytopathological features alone are sufficient to identify large cell non-HLs. This category also includes HL in cases in which there is an appropriate cellular background, diagnostic Reed-Sternberg cells, and metastatic neoplasms.

The authors of the Sydney system proposed that this standardized system may improve the quality of the procedure, the handling of material for diagnostic ancillary testing, the understanding of the report, and the communication between the cytopatholo-

gist and the clinician. Recently, an Indian research group evaluated the malignancy risk in 6,983 lymph node FNACs by retrospectively reviewing cases with the Sydney system [24]. The diagnoses using the Sydney system were discordant in 10.7% of histologic diagnoses. The overall diagnostic accuracy of this system was 89.3%. The malignancy risk was 11.5% and 99.6% for the benign and malignant categories, respectively. Inter- and intraobserver variabilities were noted for categories 3 and 4, respectively. The authors reported a relatively high malignancy risk of 27.5% in the inadequate/non-diagnostic categories. For these cases, they recommended a repeat FNAC according to the Sydney system recommendations. Collectively, the authors concluded that application of the Sydney system can help achieve uniformity, reproducibility, and risk stratification in lymph node FNAC. However, multicenter studies with larger samples are needed to validate the utility of the Sydney system.

SUGGESTED DIAGNOSTIC ALGORITHM FOR LYMPH NODE FINE NEEDLE ASPIRATION CYTOLOGY

Herein, we suggest a diagnostic algorithm for lymph node FNAC that encompasses a stepwise approach and the Sydney

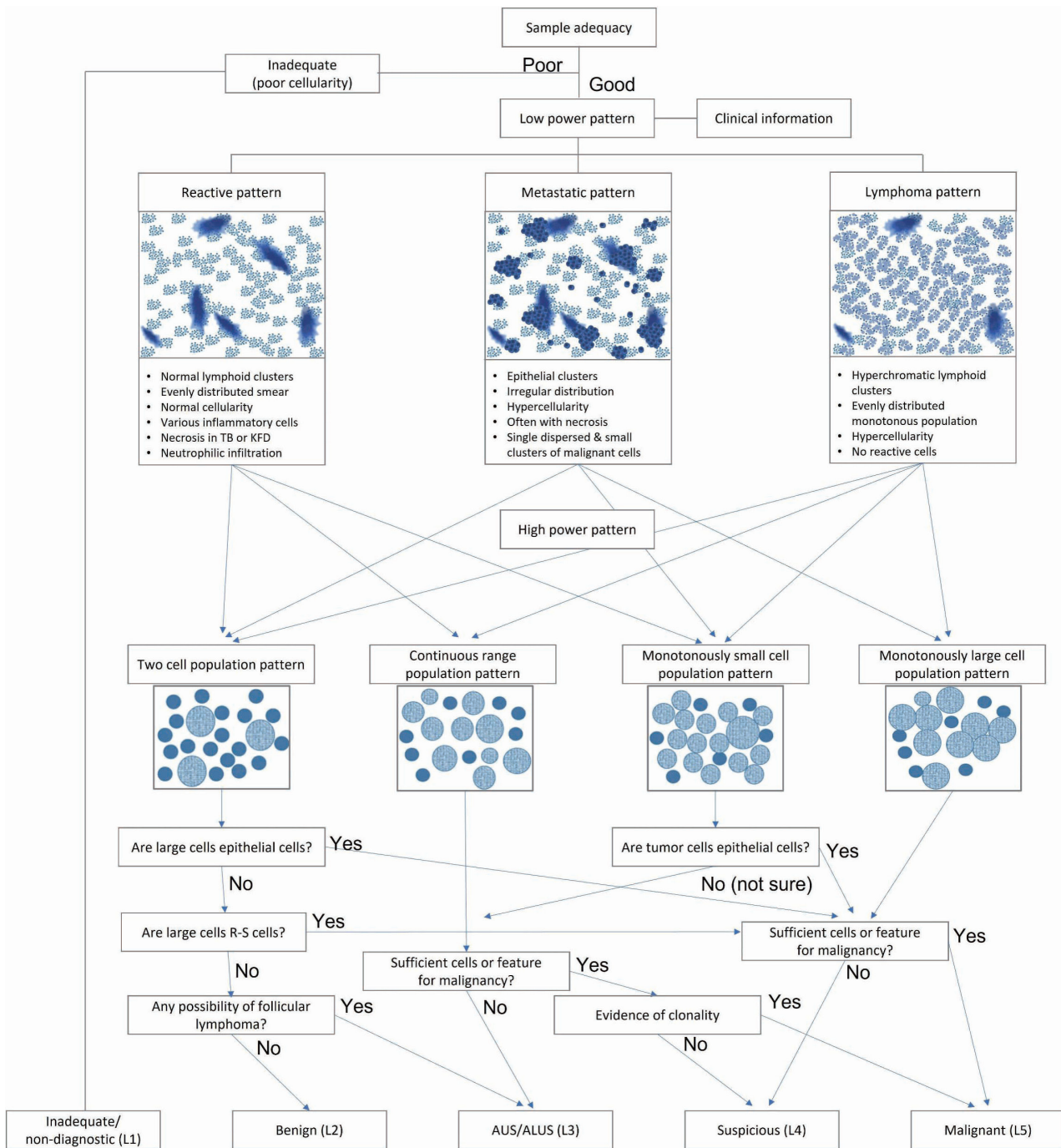


Fig. 10. Diagnostic algorithm for lymph node fine needle aspiration cytology.

classification system (Fig. 10). Sample adequacy should be evaluated; if there is insufficient cellularity for proper evaluation or the smearing condition is poor due to dry artifacts, then the sample can be categorized as inadequate/non-diagnostic (L1). Once the clinical information is reviewed, the low-power pattern can be evaluated under a microscope. Reactive patterns can present

as two-cell populations, a continuous range, or a monotonously small cell population. Metastatic patterns can present as two-cell populations of monotonously small or large cell populations. Lymphoma can present with all kinds of patterns at high-power magnification. A large cell population in the two-cell population pattern should be thoroughly reviewed if it has epithelial features to

exclude the possibility of a metastatic lesion. If there is no chance of metastasis, FL remains a possibility. FL should be considered in cases of multiple enlarged lymph nodes in elderly patients with hypercellular smears and several small lymphocytes that are slightly larger than usual. Immunocytochemical staining for BCL2 can be helpful for diagnosis in such cases. When FL cannot be excluded and immunocytochemical staining is unavailable, an ALUS diagnosis can be made.

If there are large cells are clearly epithelial, and cytologic atypia is evident, the case can be diagnosed as malignant or suspicious according to the level of evidence. This is true regardless of the high-power pattern of a two-cell, monotonously small, or large cell population. A monotonously large cell population is mostly found in high-grade B-cell lymphomas, such as diffuse large B-cell or Burkitt lymphoma; however, such cases can also be diagnosed as malignant or suspicious according to the level of evidence. Monotonously small cell population patterns can be quite challenging because certain features can be difficult to distinguish between lymphomas and small cell carcinoma (such as mild cytologic atypia in lymphoma). If there are enough cytological features for small cell carcinoma, a case can be diagnosed as malignant or suspicious according to the level of evidence. If there is no definite evidence that the tumor cells are epithelial, lymphomas or other rare mesenchymal malignant tumors should be excluded. In such cases, cytological findings and additional IHC or molecular studies might be required. These cases can be diagnosed as AUS/ALUS, suspicious, or malignant according to the level of evidence. The continuous range population pattern is predominantly from possible T-cell lymphomas. Clonality tests, such as TCR gene rearrangement, are required for a more conclusive diagnosis.

The Sydney system has an inevitable limitation in that the epithelial or lymphomatous nature of the lesion is not clearly separated into different categories and is not emphasized due to the ambiguity of the lymph node features on FNAC. In other words, even though a diagnosis was made on a certain case using the Sydney system, it is still unclear whether the case is lymphoid or metastatic. The L3 category, which includes AUS and ALUS, is a good example. It is often quite challenging to discriminate a certain lesion as lymphoid or epithelial in origin. The aforementioned study by the Indian group mentioned intra- and interobserver variabilities in the diagnosis of category III. However, further in-depth knowledge of lesion nature might be warranted. In cases in which the FNAC features favor certain diseases, the cases should be described specifically as “AUS, favor poorly differentiated carcinoma,” “ALUS, favor atypical lymphoprolifera-

tive disease (Infectious mononucleosis, Kikuchi-Fujimoto disease, Rosai-Dorfman disease),” or “ALUS, cannot exclude low-grade lymphoma.” Since the previous study reported a high malignancy rate of 66.7% in the AUS/ALUS category, it is important to deliver any evidence that supports either lymphoid or metastatic lesion. However, it is also important not to conduct unnecessary excisional biopsy.

CONCLUSION

Lymph node FNAC encompasses diverse diseases, including benign and malignant lymphoma and metastasis, whose cytologic findings often resemble each other. A stepwise diagnostic approach combining clinical findings (age, sex, site, multiplicity, ultrasonography findings), low-power pattern (reactive, metastatic, lymphoma pattern), high-power population pattern (two-cell, continuous range, monotonously small, and monotonously large population patterns), and disease-specific diagnostic clues (granulomas, etc.) can help in comprehensive FNAC diagnosis. It is important to remember representative traits of each diagnostic category, including diagnostic pitfalls that share the cytologic findings of other categories.

Supplementary Information

The Data Supplement is available with this article at <https://doi.org/10.4132/jptm.2023.06.12>.

Ethics Statement

This study was reviewed and approved by the Institutional Review Board of the Catholic University of Korea College of Medicine (UC21ZISI0138).

Availability of Data and Material

The datasets generated or analyzed during the study are available from the corresponding author on reasonable request.

Code Availability

Not applicable.

ORCID

Yosep Chong	https://orcid.org/0000-0001-8615-3064
Gyeongsin Park	https://orcid.org/0000-0002-9727-5566
Hee Jeong Cha	https://orcid.org/0000-0001-8744-5747
Hyung-Jung Kim	https://orcid.org/0000-0002-6617-4578
Jamshid Abdul-Ghafar	https://orcid.org/0000-0002-6575-8870

Author Contributions

Conceptualization: YC, SSL, CSK. Data curation: YC, JAG, CSK, SSL, HJC, HJK, GP. Funding acquisition: YC. Investigation: YC, SSL. Methodology: YC. Project administration: YC. Resources: YC, CSK, SSL, HJC, HJK, GP. Supervision: SSL, GP, CSK. Validation: YC, JAG. Visualization: YC, JAG. Writing—original draft: YC, JAG. Writing—review & editing: YC, SSL, HJC, HJK, CSK, GP. Approval of final manuscript: all authors.

Conflicts of Interest

Y.C., a contributing editor of the *Journal of Pathology and Translational Medicine*, was not involved in the editorial evaluation or decision to publish this article. All remaining authors have declared no conflicts of interest.

Funding Statement

This study was supported by a Korean Society for Cytopathology grant (No. 2021-01).

References

- Zhou J, Li F, Meng L, et al. Fine needle aspiration cytology for lymph nodes: a three-year study. *Br J Biomed Sci* 2016; 73: 28-31.
- Cibas ES, Ducatman BS. *Cytology: diagnostic principles and clinical correlates*. 5th ed. Maryland Heights: Elsevier Inc., 2020.
- Rammeh S, Romdhane E, Sassi A, et al. Accuracy of fine-needle aspiration cytology of head and neck masses. *Diagn Cytopathol* 2019; 47: 394-9.
- Houcine Y, Romdhane E, Blel A, et al. Evaluation of fine needle aspiration cytology in the diagnosis of cervical lymph node lymphomas. *J Craniomaxillofac Surg* 2018; 46: 1117-20.
- Rammeh S, Ben Rejeb H, M'Farrej M K, et al. Cervical node fine needle aspiration: factors influencing the failure rate. *Rev Stomatol Chir Maxillofac Chir Orale* 2014; 115: 85-7.
- Heo I, Park S, Jung CW, et al. Fine needle aspiration cytology of parathyroid lesions. *Korean J Pathol* 2013; 47: 466-71.
- Agarwal AM, Bentz JS, Hungerford R, Abraham D. Parathyroid fine-needle aspiration cytology in the evaluation of parathyroid adenoma: cytologic findings from 53 patients. *Diagn Cytopathol* 2009; 37: 407-10.
- Gronkiewicz JJ, Vade A. Cervical lymph node fine needle aspiration in patients with no history of malignancy. *Ultrasound Q* 2013; 29: 323-6.
- Hong SA, Jung H, Kim SS, et al. Current status of cytopathology practice in Korea: impact of the coronavirus pandemic on cytopathology practice. *J Pathol Transl Med* 2022; 56: 361-9.
- Al-Abbadi MA, Barroca H, Bode-Lesniewska B, et al. A proposal for the performance, classification, and reporting of lymph node fine-needle aspiration cytopathology: the Sydney system. *Acta Cytol* 2020; 64: 306-22.
- Duraiswami R, Margam S, Chandran P, Prakash A. Spectrum of pathologies on FNAC evaluation of peripheral lymph nodes at a tertiary care center in hyderabad: a retrospective study. *Int J Adv Med* 2017; 4: 27-33.
- Cho J. Basic immunohistochemistry for lymphoma diagnosis. *Blood Res* 2022; 57: 55-61.
- Kuppers R, Hansmann ML. The Hodgkin and Reed/Sternberg cell. *Int J Biochem Cell Biol* 2005; 37: 511-7.
- Jaffe ES, Nicolae A, Pittaluga S. Peripheral T-cell and NK-cell lymphomas in the WHO classification: pearls and pitfalls. *Mod Pathol* 2013; 26 Suppl 1: S71-87.
- de Leval L, Savilo E, Longtine J, Ferry JA, Harris NL. Peripheral T-cell lymphoma with follicular involvement and a CD4+/bcl-6+ phenotype. *Am J Surg Pathol* 2001; 25: 395-400.
- Huang Y, Moreau A, Dupuis J, et al. Peripheral T-cell lymphomas with a follicular growth pattern are derived from follicular helper T cells (TFH) and may show overlapping features with angioimmunoblastic T-cell lymphomas. *Am J Surg Pathol* 2009; 33: 682-90.
- Dobay MP, Lemonnier F, Missiaglia E, et al. Integrative clinicopathological and molecular analyses of angioimmunoblastic T-cell lymphoma and other nodal lymphomas of follicular helper T-cell origin. *Haematologica* 2017; 102: e148-51.
- Rizzo K, Nassiri M. Diagnostic workup of small B cell lymphomas: a laboratory perspective. *Lymphoma* 2012; 2012: 346084.
- Jacobs JC, Katz RL, Shabb N, el-Naggar A, Ordonez NG, Pugh W. Fine needle aspiration of lymphoblastic lymphoma: a multiparameter diagnostic approach. *Acta Cytol* 1992; 36: 887-94.
- Sukswai N, Lyapichev K, Khoury JD, Medeiros LJ. Diffuse large B-cell lymphoma variants: an update. *Pathology* 2020; 52: 53-67.
- el-Okda M, Hyeh Y, Xie SS, Hsu SM. Russell bodies consist of heterogeneous glycoproteins in B-cell lymphoma cells. *Am J Clin Pathol* 1992; 97: 866-71.
- Francis IM, Das DK, al-Rubah NA, Gupta SK. Lymphoglandular bodies in lymphoid lesions and non-lymphoid round cell tumours: a quantitative assessment. *Diagn Cytopathol* 1994; 11: 23-7.
- Jimenez-Heffernan JA, Diaz Del Arco C, Adrados M. A cytological review of follicular dendritic cell-derived tumors with emphasis on follicular dendritic cell sarcoma and unicentric Castleman disease. *Diagnostics (Basel)* 2022; 12: 406.
- Gupta P, Gupta N, Kumar P, et al. Assessment of risk of malignancy by application of the proposed Sydney system for classification and reporting lymph node cytopathology. *Cancer Cytopathol* 2021; 129: 701-18.

Reevaluating diagnostic categories and associated malignancy risks in thyroid core needle biopsy

Chan Kwon Jung^{1,2}

¹Department of Hospital Pathology, College of Medicine, The Catholic University of Korea, Seoul;
²Cancer Research Institute, College of Medicine, The Catholic University of Korea, Seoul, Korea

As the application of core needle biopsy (CNB) in evaluating thyroid nodules rises in clinical practice, the 2023 Korean Thyroid Association Management Guidelines for Patients with Thyroid Nodules have officially recognized its value for the first time. CNB procures tissue samples preserving both histologic structure and cytologic detail, thereby supplying substantial material for an accurate diagnosis and reducing the necessity for repeated biopsies or subsequent surgical interventions. The current review introduces the risk of malignancy within distinct diagnostic categories, emphasizing the implications of noninvasive follicular thyroid neoplasm with papillary-like nuclear features on these malignancy risks. Prior research has indicated diagnostic challenges associated with follicular-patterned lesions, resulting in notable variation within indeterminate diagnostic categories. The utilization of mutation-specific immunostaining in CNB enhances the accuracy of lesion classification. This review underlines the essential role of a multidisciplinary approach in diagnosing follicular-patterned lesions and the potential of mutation-specific immunostaining to strengthen diagnostic consensus and inform patient management decisions.

Key Words: Thyroid nodule; Thyroid neoplasms; Biopsy, Core needle; Mutation; Practice guideline

Received: June 11, 2023 **Revised:** June 17, 2023 **Accepted:** June 19, 2023

Corresponding Author: Chan Kwon Jung, MD, PhD, Department of Pathology, Seoul St. Mary's Hospital, College of Medicine, The Catholic University of Korea, 222 Banpo-daero, Seocho-gu, Seoul 06591, Korea

Tel: +82-2-2258-1622, Fax: +82-2-2258-1627, E-mail: ckjung@catholic.ac.kr

Core needle biopsy (CNB) has been established as an alternative to fine needle aspiration (FNA) cytology in assessing thyroid nodules, particularly in cases where initial FNA results are non-diagnostic or indeterminate [1,2]. Recent studies advocate CNB as a primary diagnostic tool [1-7]. CNB of the thyroid yields tissue samples that maintain histologic structure and cytologic detail. Moreover, CNB provides substantial tissue for histologic examination and supplementary ancillary testing [8,9]. CNB allows for an exact diagnosis and reduces the need for repeated biopsies or subsequent surgical interventions in cases such as lymphoma, medullary thyroid carcinoma, anaplastic thyroid carcinoma, other rare thyroid diseases, and diseases of non-thyroid origin [1,9].

With CNB becoming increasingly prevalent in clinical practice, issues have been raised about the appropriate use of diagnostic categories and the corresponding risk of malignancy (ROM). In Korea, the inaugural pathology reporting system for thyroid

CNB was introduced in 2015 and later revised in 2019 by the Clinical Practice Guidelines Development Committee of the Korean Thyroid Association [9,10]. Despite the Korean Endocrine Pathologists reaching a consensus on the pathology report of thyroid CNB [9,10], the implied ROM for each diagnostic category has yet to be quantified. In the course of calculating the malignancy risk estimates within the diagnostic categories, various factors warrant consideration. These encompass patient demographics, criteria for nodule selection, differences in pathologist expertise and the application of diagnostic criteria, possible overestimation of malignancy risk for some diagnostic categories based exclusively on post-surgical thyroid cases, publication bias, and the surgically proven histological diagnosis of noninvasive follicular thyroid neoplasm with papillary-like nuclear features (NIFTP). Recently, the 2023 Korean Thyroid Association Management Guidelines for Patients with Thyroid Nodules made a significant stride by addressing the implied ROM for each diag-

nostic category for the first time [11]. Accordingly, this article presents a concise review that illuminates these recent updates concerning the ROM within thyroid CNB categories.

FORMAT OF THYROID CORE NEEDLE BIOPSY REPORTS

Thyroid CNB reports adhere to a structured format consisting of a diagnostic category, a subcategory, and a microscopic description (Table 1) [9]. The six diagnostic categories include (1) nondiagnostic (category I); (2) benign lesion (category II); (3) indeterminate lesion (category III); (4) follicular neoplasm (category IV); (5) suspicious for malignancy (category V); and (6) malignant (category VI). Categories III and IV are further divided into subcategories based on the status of nuclear atypia, architectural atypia, or oncocyctic atypia. Subcategories that exhibit nuclear atypia (categories IIIa, IIIc, and IVb) raise concerns for conditions such as papillary thyroid carcinoma and NIFTP, which are typically associated with a higher ROM compared to subcategories

that display architectural or oncocyctic atypia [8,12-16].

RISK OF MALIGNANCY OF THYROID CORE NEEDLE BIOPSY DIAGNOSTIC CATEGORIES

Based on retrospective studies in the literature, the frequency and ROM for each category are summarized in Table 2. The ROM estimates for each category are based on clinical follow-up and surgically resected nodules. Benign nodules within category II were clinically confirmed based on additional benign results from FNA or CNB and stable or reduced nodule size observed over a 1-year ultrasound follow-up period. Pathological confirmations on surgical specimens were used for nodules within categories I, III, IV, V, and VI.

The method of estimating the cancer risk, which is based on histologic follow-up, overestimates the ROM, particularly for the categories I–III, where there is selection bias given the relatively small proportion of nodules that undergo excision. Although NIFTP is a surgical disease and cannot be preoperatively diag-

Table 1. Diagnostic categories of thyroid core needle biopsy

Diagnostic category
Category I. Nondiagnostic or unsatisfactory
Non-tumor adjacent thyroid tissue only
Extrathyroid tissue only (e.g., skeletal muscle, mature adipose tissue)
Acellular specimen (e.g., acellular fibrotic tissue, acellular hyalinized tissue, cystic fluid only)
Blood clot only
Other
Category II. Benign lesion
Benign follicular nodule
Hashimoto's thyroiditis
Subacute granulomatous thyroiditis
Nonthyroidal lesion (e.g., parathyroid lesions, benign neurogenic tumors, benign lymph node)
Other
Category III. Indeterminate lesion
IIIa. Indeterminate follicular lesion with nuclear atypia
IIIb. Indeterminate follicular lesion with architectural atypia
IIIc. Indeterminate follicular lesion with nuclear and architectural atypia
IIId. Indeterminate follicular lesion with oncocyctic atypia
IIIe. Indeterminate lesion, not otherwise specified
Category IV. Follicular neoplasm
IVa. Follicular neoplasm, conventional type
IVb. Follicular neoplasm with nuclear atypia
IVc. Oncocyctic (Hürthle cell) neoplasm
IVd. Follicular neoplasm, not otherwise specified
Category V. Suspicious for malignancy
Suspicious for papillary thyroid carcinoma, medullary thyroid carcinoma, poorly differentiated thyroid carcinoma, metastatic carcinoma, lymphoma, etc.
Category VI. Malignant
Papillary thyroid carcinoma, poorly differentiated thyroid carcinoma, differentiated high-grade thyroid carcinoma, anaplastic thyroid carcinoma, medullary thyroid carcinoma, lymphoma, metastatic carcinoma, etc

Adapted with permission from *Journal of Pathology and Translational Medicine* [9].

Table 2. Diagnostic frequency and implied risk of malignancy according to the diagnostic category of thyroid CNB

CNB diagnostic category	Diagnostic frequency (%) ^a	Risk of malignancy based on final diagnosis from clinical and/or surgical follow-up (%) ^b	Change in risk of malignancy due to NIFTP ^c
I. Nondiagnostic	2 (2–3)	33 (18–50)	No significant change
II. Benign lesion	46 (40–53)	4 (2–6)	No significant change
III. Indeterminate lesion	10 (7–14)	39 (32–45)	24% Decrease (24%–34%)
IV. Follicular neoplasm	7 (5–9)	52 (46–57)	20% Decrease (37%–45%)
V. Suspicious for malignancy	2 (2–3)	98 (96–100)	No significant change
VI. Malignant	28 (23–34)	100	No significant change

^a95% Confidence intervals of pooled proportions from meta-analysis of literature [3-5,7,12-14,17,20-32]; ^bMeta-analysis based pooled proportions and 95% confidence intervals for confirmed clinical and surgical pathology follow-up [4,5,7,12-14,17,22,23,25-33]; ^cInfluence of noninvasive follicular thyroid neoplasm with papillary-like nuclear features (NIFTP) on malignancy risk in thyroid core needle biopsy (CNB) diagnostic categories. NIFTP appears to reduce the risk of malignancy in the diagnostic category of the thyroid CNB reporting system. The alterations in malignancy risk within categories III and IV were inferred from shifts in malignancy risk identified in three retrospective studies [13,14,17].

nosed on CNB or FNA specimens, the morphologic features of NIFTP tend to lead to classification on CNB/FNA as either category III, IV, or V, thereby impacting the resultant ROM calculations [13,14,17,18]. The ROM for each category is shown when including and excluding NIFTP in malignancy, information that might help guide more conservative clinical management of some nodules. The presence of NIFTP lowers the ROM within the diagnostic category of the thyroid CNB reporting system. The corresponding modifications in the ROM within categories III and IV have been deduced from the observed shifts in malignancy risk from three retrospective studies [13,14,17].

DIAGNOSTIC CHALLENGES IN FOLLICULAR-PATTERNED LESIONS ON CORE NEEDLE BIOPSY

CNB has emerged as a viable alternative to FNA, serving to decrease inconclusive results in the diagnosis of thyroid nodules. Nonetheless, follicular-patterned lesions presented in CNB continue to pose a significant challenge to pathologists, often falling within diagnostic categories II, III, or IV. The diagnostic rates of CNB categories may fluctuate based on pathologists' diagnostic thresholds for follicular-patterned lesions [13,14,17].

The histologic architecture and the status of the tumor capsule are critical determinants in diagnosing follicular-patterned lesions. Within the context of CNB specimens, follicular proliferative lesions characterized by a discernible tumor capsule are typically classified as category IV (follicular neoplasm) [9,10]. Conversely, in specimens where a tumor capsule is not apparent, these lesions are generally classified as category II (benign) in the absence of nuclear or architectural atypia, or category III (indeterminate follicular lesion) when nuclear or architectural atypia is present.

In addition to the condition of the tumor capsule, the histologic

architecture also plays a significant role in determining the diagnosis of follicular-patterned lesions. A microfollicular proliferative lesion, distinctly separated from the surrounding normal parenchyma by a fibrous capsule, leans towards a diagnosis of a category IV (follicular neoplasm). In contrast, a CNB specimen exhibiting a primarily microfollicular or trabecular growth pattern, but lacking a discernible fibrous capsule or adjacent non-lesional tissue, typically falls into category IIIb (indeterminate follicular lesion with architectural atypia). This categorization stems from the uncertainty regarding the presence of a tumor capsule in the lesion. This subcategory exhibits no nuclear atypia. However, certain pathologists might classify such cases under category IV, particularly when ultrasound imaging reveals a solitary nodule with a peripheral hypoechoic halo indicative of a tumor capsule. It is noteworthy that, even if a follicular-patterned lesion presents a definitive fibrous capsule, if the lesion exhibits a macrofollicular pattern rather than microfollicular or trabecular patterns, some pathologists might lean towards categorizing it as category III [15,16]. This preference is motivated by the understanding that a macrofollicular pattern is characteristic of benign thyroid diseases, even when a definitive fibrous capsule associated with a macrofollicular proliferative lesion is present.

A comparison of the diagnostic categories from three major Korean hospitals, all of which perform a high volume of thyroid CNBs, reveals a noticeable variation. One hospital reported the frequencies of categories II, III, and IV as 38.1%, 17.6%, and 10.2%, respectively [14]. Another hospital reported the frequencies as 38.3%, 24.5%, and 7.6%, respectively [17]. Contrastingly, at our institution, the frequencies were markedly different at 60.9%, 1.2%, and 17.5%, respectively [13]. It is noteworthy that the occurrence of category III was significantly lower in our hospital than in the others, while the incidences of categories II and IV were comparatively higher in our hospital than the others.

CNB tends to diagnose category IV “follicular neoplasms” more frequently than FNA [13,17,19], leading to an increased number of patients undergoing surgery based on CNB diagnoses compared to FNA. While the rate of follicular neoplasms diagnosed using CNB may differ significantly across various institutions, potentially due to the variability in how different observers interpret architectural or nuclear atypia in CNB, the ROMs found post-surgery for these follicular neoplasms remain consistent [13,14,17]. This consistency is observed irrespective of whether the initial diagnosis was made via CNB or FNA [13].

CLASSIFICATION OF FOLLICULAR-PATTERNED LESIONS USING MUTATION-SPECIFIC IMMUNOSTAINING IN CORE NEEDLE BIOPSY

Immunostaining has served as an essential tool, supplementing standard methodologies in clarifying differential diagnoses in surgical pathology. This straightforward and economical technique facilitates the identification of lineage or cell type in histopathology and cytopathology. The recent emergence of innovative markers, particularly mutation-specific markers and those bearing translational significance, has substantially transformed the paradigm of immunohistochemistry (IHC). These progressive strides have notably influenced clinical practice and investigative pursuits within the field of thyroid disease.

The *RAS* genetic variants, typically found to be mutually exclusive with *BRAF* variants, are the most common oncogenic changes observed in follicular-patterned thyroid tumors [5,34,35]. Of all *RAS* variants identified in thyroid tumors, *RAS* Q61R is the most prevalent [8,36]. IHC for *RAS* Q61R, using the SP174 antibody, has proven to be an accurate method for detecting thyroid tumors harboring the *RAS* Q61R variant [8,37]. While *RAS* variants are not inherently sensitive or specific markers for thyroid cancers, their detection in preoperative FNA or CNB samples exhibiting indeterminate results usually prompts a diagnostic lobectomy. Thus, for CNB samples wherein histologic morphologies complicate the differential diagnosis between categories III and IV, a positive result for *RAS* Q61R IHC often simplifies the diagnostic process, favoring a categorization into category IV. In cases where a CNB specimen primarily displays a microfollicular or trabecular growth pattern without a discernible fibrous capsule, it is typically diagnosed as an indeterminate follicular lesion (category III). However, a positive *RAS* Q61R result in such a case could lead to a revised diagnosis of a follicular neoplasm (category IV) (Figs. 1, 2).

When CNB samples display nuclear atypia yet lack sufficient histologic features for a definitive malignancy diagnosis, they may be assigned to category IIIa (Indeterminate follicular lesion with nuclear atypia) or category V (suspicious for malignancy) based on the extent of nuclear atypia and the quantity of atypical cells

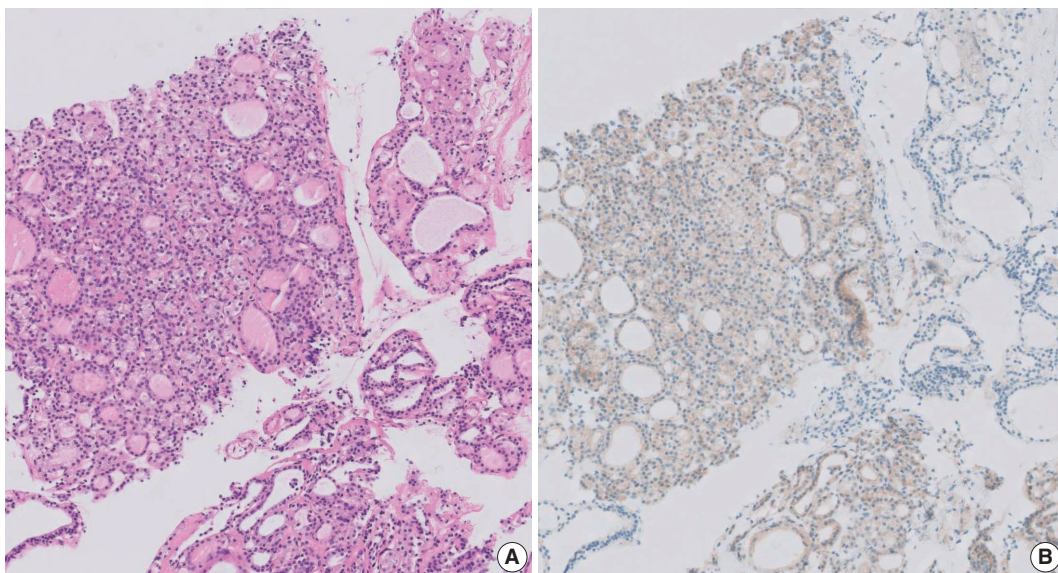


Fig. 1. Core needle biopsy of a microfollicular proliferative lesion exhibiting morphological differences from adjacent thyroid tissue. (A) Although the lesion is distinctly segregated from surrounding tissue, the absence of a discernible tumor capsule typically leads to its categorization under category III based on histomorphology. (B) Immunohistochemistry for *RAS* Q61R clearly delineates immunostaining-positive tumor cells from the immunostaining-negative normal thyroid tissue. Ultimately, with the incorporation of immunostaining results, the specimen should be appropriately diagnosed as follicular neoplasm, conventional type (category IVa).

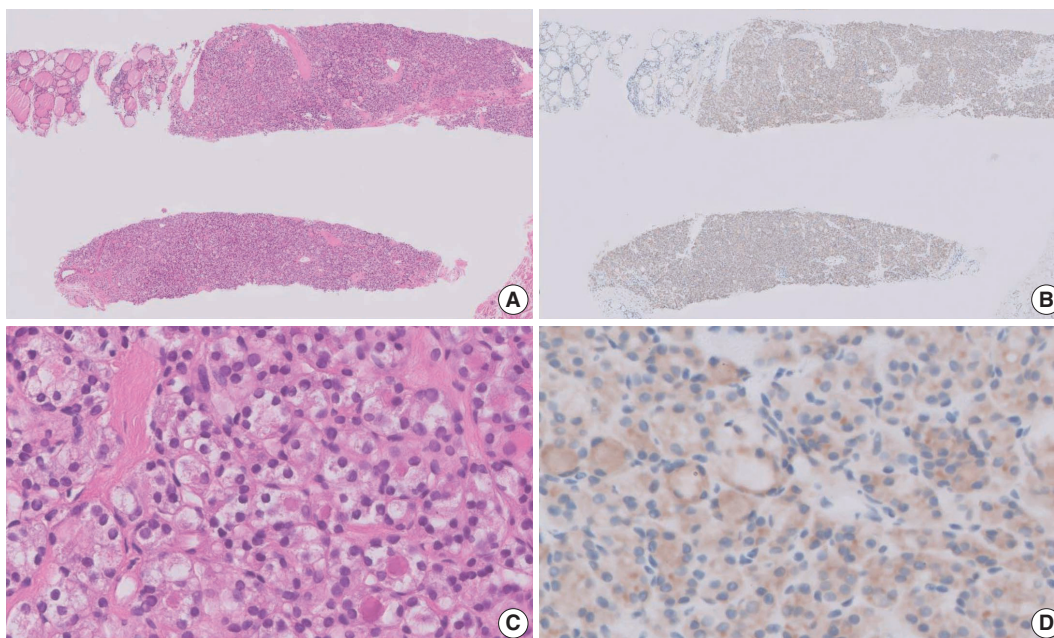


Fig. 2. The core needle biopsy displays a microfollicular proliferative lesion that exhibits morphological differences from the adjacent thyroid tissue, but lacks a fibrous capsule (A). (B) The tumor component tests positive for RAS Q61R immunostaining. (C) A high-power view reveals microfollicles lined by tumor cells exhibiting nuclear atypia and thin fibrous bands within the stroma. (D) Tumor cells show cytoplasmic and membranous positivity for RAS Q61R. This specimen should be appropriately classified as a follicular neoplasm with nuclear atypia (category IVb). After conducting a diagnostic lobectomy, the definitive pathological diagnosis was confirmed as an invasive encapsulated follicular variant of papillary thyroid carcinoma.

involved. In such situations, employing BRAF VE1 IHC to detect the *BRAF* p.V600E variant can be valuable for differential diagnosis (Fig. 3). Given the demonstrated reliability of BRAF VE1 IHC in identifying the *BRAF* p.V600E across different tumor types, including thyroid cancers [34,38], a positive result from this method has the potential to clarify indeterminate CNB results, typically pointing towards a definitive diagnosis of papillary thyroid carcinoma.

RISK STRATIFICATION OF PREOPERATIVELY DIAGNOSED INDETERMINATE FOLLICULAR-PATTERNED LESIONS

Recently, our team established that CNB categories III and IV could be classified into two distinct risk groups based on histologic features of nuclear atypia and IHC for RAS Q61R [8]. CNBs exhibiting nuclear atypia or RAS Q61R expression were identified as high-risk, bearing an average NIFTP/malignancy risk of 75.5%. In contrast, CNBs without these findings were marked as low-risk, having a risk of approximately 34.9%. RAS Q61R IHC has shown high sensitivity and specificity for identifying the *RAS* p.Q61R variant and demonstrates a positive pre-

dictive value of 74.3% and a negative predictive value of 55.5% for diagnosing NIFTP/malignancy in CNB categories III and IV. Follicular lesions exhibiting both nuclear atypia and RAS Q61R expression carry an 86% NIFTP/malignancy risk. Therefore, in patients classified as CNB category III/IV, the presence of nuclear atypia or RAS Q61R expression signifies a heightened risk of NIFTP/malignancy, which may necessitate consideration for surgical resection (Figs. 4, 5). On the other hand, thyroid nodules lacking nuclear atypia and RAS Q61R expression, which present a lower likelihood of NIFTP/malignancy, might be suitable for observation without further intervention. This approach can potentially assist in the management of patients presenting with indeterminate CNB results.

In patients preoperatively diagnosed with follicular neoplasm (category IV), nodule size plays a critical role in surgical decision-making due to the rising ROM associated with increasing nodule size. The 2023 Korean Thyroid Association Management Guidelines for Patients with Thyroid Nodules states that surgical intervention is typically favored for follicular neoplasms of 2 cm or more, given the escalating malignancy risk [11]. Even for tumors smaller than 2 cm, a malignancy risk exists, necessitating consideration of diagnostic surgery based on individual clinical findings

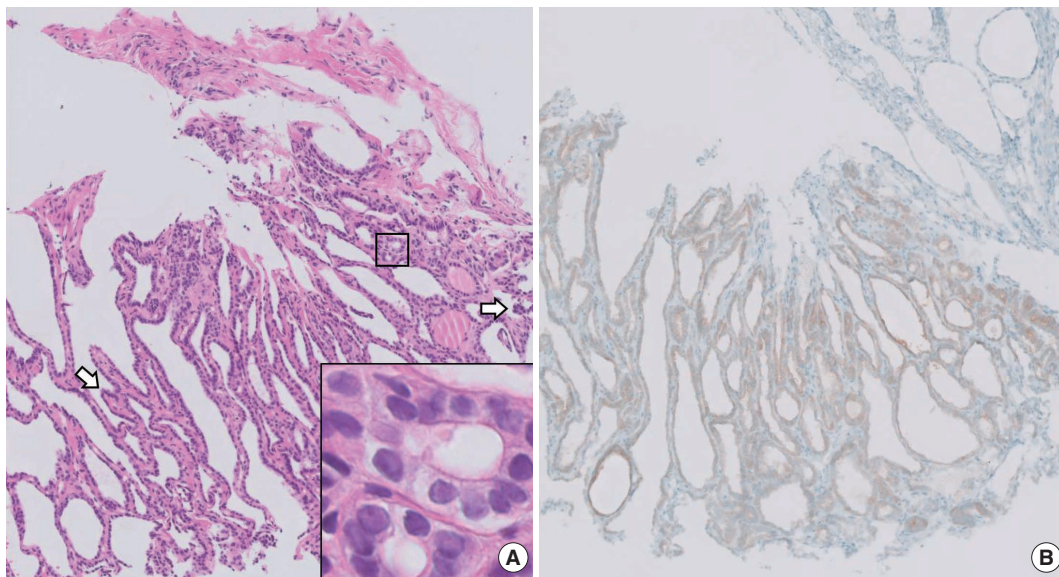


Fig. 3. The core needle biopsy specimen exhibits both follicular and abortive papillary architecture. (A) In light of the nuclear atypia and predominantly follicular growth, the diagnostic considerations span from category III to IV. (B) The positive result for BRAF VE1 immunostaining confirmed the diagnosis, categorizing the specimen as category VI - papillary thyroid carcinoma. The inset image provides a magnified view of the indicated region as a square, facilitating the observation of nuclear atypia. Arrows indicate abortive papillae.

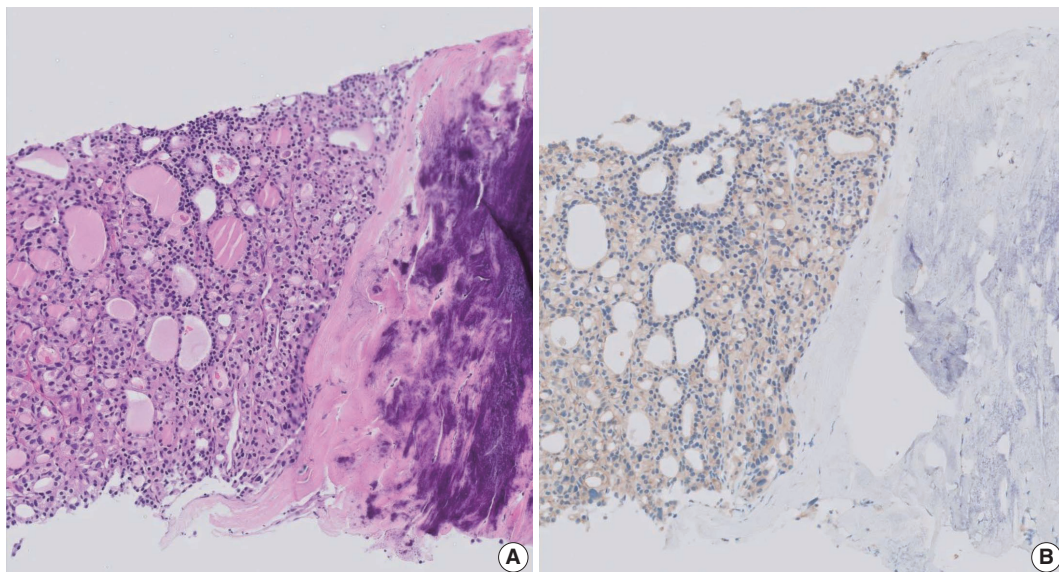


Fig. 4. The core needle biopsy specimen reveals a microfollicular proliferative lesion surrounded by a thick fibrous capsule (A) and exhibiting positivity for RAS Q61R immunostaining (B). Considering these characteristics, the specimen can be confidently classified as follicular neoplasm, conventional type (category IVa). After a diagnostic lobectomy, the tumor was conclusively identified as follicular thyroid carcinoma.

[11]. A meta-analysis of 14 observational studies involving 2,016 thyroid nodules diagnosed as follicular neoplasms (category IV) demonstrated that in comparison to their smaller counterparts, nodules measuring 4 cm or larger, 3 cm or larger, and 2 cm or larger were associated with a respective 2.29-fold (95% confidence interval [CI], 1.68 to 3.11), 2.39-fold (95% CI, 1.45 to

3.95), and 1.63-fold (95% CI, 1.13 to 2.35) increase in ROM for thyroid nodules of various sizes [39-52].

Molecular marker tests can facilitate malignancy assessment and inform decisions regarding ultrasound monitoring or surgical interventions. These decisions should account for patient preferences, clinical feasibility, and evaluations supplemented by ul-

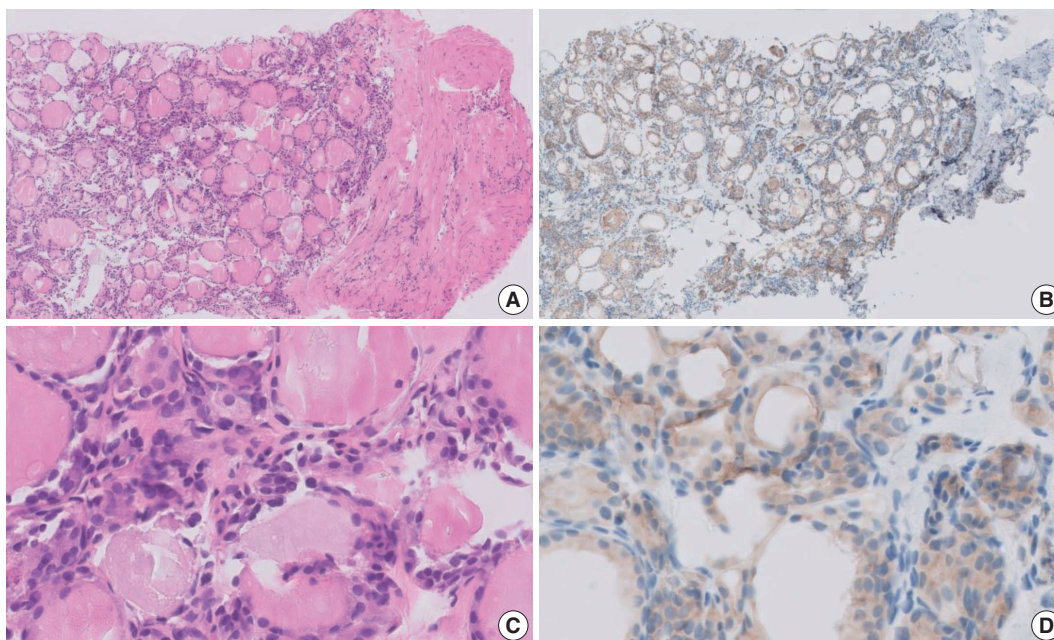


Fig. 5. The core needle biopsy specimen reveals a follicular proliferative lesion characterized by follicles of varying sizes and a discernible fibrous capsule (A), and demonstrates positivity for RAS Q61R immunostaining (B). (C) A high-power view reveals follicles lined by tumor cells exhibiting nuclear atypia, intermixed with follicles comprised of cells with no nuclear atypia. (D) Tumor cells show cytoplasmic and membranous positivity for RAS Q61R. The specimen was diagnosed as a follicular neoplasm with nuclear atypia (category IVb). Following a diagnostic lobectomy, the definitive pathological diagnosis was established as noninvasive follicular thyroid neoplasm with papillary-like nuclear features.

trasound findings [20]. While next-generation sequencing (NGS)-based molecular panel testing is predominantly employed in Western countries, such molecular NGS testing for diagnostic or prognostic prediction on preoperative biopsy specimens is not currently permitted in Korea [11].

CONCLUSION

The use of CNB for the evaluation of thyroid nodules has seen an increasing trend due to its potential as an alternative to FNA cytology. The 2023 Korean Thyroid Association Management Guidelines for Patients with Thyroid Nodules have recognized the value of CNB for the first time. Despite its advantages, the diagnosis of follicular-patterned lesions remains subject to interobserver variability. Therefore, a multidisciplinary approach emphasizing clinicopathologic correlation is essential. Furthermore, the utilization of mutation-specific immunostaining can enhance diagnostic consensus and contribute meaningfully to patient management by informing clinical decision-making processes.

Ethics Statement

Not applicable.

Availability of Data and Material

Data sharing not applicable to this article as no datasets were generated or analyzed during the study.

Code Availability

Not applicable.

ORCID

Chan Kwon Jung <https://orcid.org/0000-0001-6843-3708>

Conflicts of Interest

C.K.J., the editor-in-chief of the *Journal of Pathology and Translational Medicine*, was not involved in the editorial evaluation or decision to publish this article.

Funding Statement

This research was supported by a grant (HI21C0940) from the Korean Health Technology R&D Project, Ministry of Health and Welfare, Republic of Korea.

References

1. Na DG, Baek JH, Jung SL, et al. Core needle biopsy of the thyroid: 2016 consensus statement and recommendations from Korean Society of Thyroid Radiology. *Korean J Radiol* 2017; 18: 217-37.
2. Liu N, Meng Z, Jia Q, et al. Ultrasound-guided core needle biopsy for differential diagnosis of thyroid nodules: a systematic review and meta-analysis. *Mol Clin Oncol* 2017; 6: 825-32.
3. Trimboli P, Nasrollah N, Guidobaldi L, et al. The use of core needle

- biopsy as first-line in diagnosis of thyroid nodules reduces false negative and inconclusive data reported by fine-needle aspiration. *World J Surg Oncol* 2014; 12: 61.
4. Suh CH, Baek JH, Lee JH, et al. The role of core-needle biopsy as a first-line diagnostic tool for initially detected thyroid nodules. *Thyroid* 2016; 26: 395-403.
 5. Kim HC, Kim YJ, Han HY, et al. First-line use of core needle biopsy for high-yield preliminary diagnosis of thyroid nodules. *AJNR Am J Neuroradiol* 2017; 38: 357-63.
 6. Zhang M, Zhang Y, Fu S, Lv F, Tang J. Thyroid nodules with suspicious ultrasound findings: the role of ultrasound-guided core needle biopsy. *Clin Imaging* 2014; 38: 434-8.
 7. Ahn HS, Youn I, Na DG, Kim SJ, Lee MY. Diagnostic performance of core needle biopsy as a first-line diagnostic tool for thyroid nodules according to ultrasound patterns: Comparison with fine needle aspiration using propensity score matching analysis. *Clin Endocrinol (Oxf)* 2021; 94: 494-503.
 8. Kim M, Jeon S, Jung CK. Preoperative risk stratification of follicular-patterned thyroid lesions on core needle biopsy by histologic subtyping and RAS variant-specific immunohistochemistry. *Endocr Pathol* 2023; 34: 247-56.
 9. Jung CK, Baek JH, Na DG, Oh YL, Yi KH, Kang HC. 2019 Practice guidelines for thyroid core needle biopsy: a report of the Clinical Practice Guidelines Development Committee of the Korean Thyroid Association. *J Pathol Transl Med* 2020; 54: 64-86.
 10. Jung CK, Min HS, Park HJ, et al. Pathology reporting of thyroid core needle biopsy: a proposal of the Korean Endocrine Pathology Thyroid Core Needle Biopsy Study Group. *J Pathol Transl Med* 2015; 49: 288-99.
 11. Park YJ, Lee EK, Song YS, et al. 2023 Korean Thyroid Association management guidelines for patients with thyroid nodules. *Int J Thyroidol* 2023; 16: 1-31.
 12. Choe J, Baek JH, Park HS, Choi YJ, Lee JH. Core needle biopsy of thyroid nodules: outcomes and safety from a large single-center single-operator study. *Acta Radiol* 2018; 59: 924-31.
 13. Kim K, Bae JS, Kim JS, Jung SL, Jung CK. Diagnostic performance of thyroid core needle biopsy using the revised reporting system: comparison with fine needle aspiration cytology. *Endocrinol Metab (Seoul)* 2022; 37: 159-69.
 14. Na HY, Woo JW, Moon JH, et al. Preoperative diagnostic categories of noninvasive follicular thyroid neoplasm with papillary-like nuclear features in thyroid core needle biopsy and its impact on risk of malignancy. *Endocr Pathol* 2019; 30: 329-39.
 15. Ahn SH, Park SY, Choi SI. Comparison of consecutive results from fine needle aspiration and core needle biopsy in thyroid nodules. *Endocr Pathol* 2017; 28: 332-8.
 16. Yoon RG, Baek JH, Lee JH, et al. Diagnosis of thyroid follicular neoplasm: fine-needle aspiration versus core-needle biopsy. *Thyroid* 2014; 24: 1612-7.
 17. Chung SR, Baek JH, Lee JH, et al. Risk of malignancy according to the sub-classification of atypia of undetermined significance and suspicious follicular neoplasm categories in thyroid core needle biopsies. *Endocr Pathol* 2019; 30: 146-54.
 18. Na HY, Park SY. Noninvasive follicular thyroid neoplasm with papillary-like nuclear features: its updated diagnostic criteria, preoperative cytologic diagnoses and impact on the risk of malignancy. *J Pathol Transl Med* 2022; 56: 319-25.
 19. Ahn SH. Usage and diagnostic yield of fine-needle aspiration cytology and core needle biopsy in thyroid nodules: a systematic review and meta-analysis of literature published by Korean authors. *Clin Exp Otorhinolaryngol* 2021; 14: 116-30.
 20. Son HM, Kim JH, Kim SC, et al. Distribution and malignancy risk of six categories of the pathology reporting system for thyroid core-needle biopsy in 1,216 consecutive thyroid nodules. *Ultrasonography* 2020; 39: 159-65.
 21. Suh CH, Baek JH, Choi YJ, et al. Efficacy and safety of core-needle biopsy in initially detected thyroid nodules via propensity score analysis. *Sci Rep* 2017; 7: 8242.
 22. Ahn HS, Seo M, Ha SM, Kim HS. Comparison of the diagnostic efficacy of ultrasound-guided core needle biopsy with 18- versus 20-gauge needles for thyroid nodules. *J Ultrasound Med* 2018; 37: 2565-74.
 23. Choe JY, Kwak Y, Kim M, et al. Utility of a formatted pathologic reporting system in thyroid core needle biopsy: a validation study of 1998 consecutive cases. *Clin Endocrinol (Oxf)* 2018; 88: 96-104.
 24. Chung SR, Baek JH, Park HS, et al. Ultrasound-pathology discordant nodules on core-needle biopsy: malignancy risk and management strategy. *Thyroid* 2017; 27: 707-13.
 25. Ha EJ, Baek JH, Lee JH, et al. Core needle biopsy can minimise the non-diagnostic results and need for diagnostic surgery in patients with calcified thyroid nodules. *Eur Radiol* 2014; 24: 1403-9.
 26. Ha EJ, Baek JH, Lee JH, et al. Sonographically suspicious thyroid nodules with initially benign cytologic results: the role of a core needle biopsy. *Thyroid* 2013; 23: 703-8.
 27. Joo L, Na DG, Kim JH, Seo H. Comparison of core needle biopsy and repeat fine-needle aspiration in avoiding diagnostic surgery for thyroid nodules initially diagnosed as atypia/follicular lesion of undetermined significance. *Korean J Radiol* 2022; 23: 280-8.
 28. Kim YH, Kwon HJ, Kim EK, Kwak JY, Moon HJ, Yoon JH. Applying ultrasound-guided core needle biopsy for diagnosis of thyroid masses: preliminary results from a single institution. *J Ultrasound Med* 2015; 34: 1801-8.
 29. Park JY, Yi SY, Baek SH, Lee YH, Kwon HJ, Park HJ. Diagnostic efficacy, performance and safety of side-cut core needle biopsy for thyroid nodules: comparison of automated and semi-automated biopsy needles. *Endocrine* 2022; 76: 341-8.
 30. Sung JY, Na DG, Kim KS, et al. Diagnostic accuracy of fine-needle aspiration versus core-needle biopsy for the diagnosis of thyroid malignancy in a clinical cohort. *Eur Radiol* 2012; 22: 1564-72.
 31. Xiong Y, Yan L, Nong L, Zheng Y, Li T. Pathological diagnosis of thyroid nodules based on core needle biopsies: comparative study between core needle biopsies and resected specimens in 578 cases. *Diagn Pathol* 2019; 14: 10.
 32. Hong MJ, Na DG, Kim SJ, Kim DS. Role of core needle biopsy as a first-line diagnostic tool for thyroid nodules: a retrospective cohort study. *Ultrasonography* 2018; 37: 244-53.
 33. Suh CH, Baek JH, Lee JH, et al. The role of core-needle biopsy in the diagnosis of thyroid malignancy in 4580 patients with 4746 thyroid nodules: a systematic review and meta-analysis. *Endocrine* 2016; 54: 315-28.
 34. Agarwal S, Bychkov A, Jung CK. Emerging biomarkers in thyroid practice and research. *Cancers (Basel)* 2021; 14: 204.
 35. Jung CK, Bychkov A, Kakudo K. Update from the 2022 World Health Organization classification of thyroid tumors: a standardized diagnostic approach. *Endocrinol Metab (Seoul)* 2022; 37: 703-18.
 36. Burge RA, Hobbs GA. Chapter two - Not all RAS mutations are

- equal: a detailed review of the functional diversity of *RAS* hot spot mutations. In: O'Bryan JP, Piazza GA, eds. *Advances in Cancer Research*. Vol. 153. New York: Academic Press, 2022; 29-61.
37. Saliba M, Katabi N, Dogan S, Xu B, Ghossein RA. *NRAS* Q61R immunohistochemical staining in thyroid pathology: sensitivity, specificity and utility. *Histopathology* 2021; 79: 650-60.
 38. Chang S, Choi YL, Shim HS, Lee GK, Ha SY; Korean Cardiopulmonary Pathology Study Group. Usefulness of *BRAF* VE1 immunohistochemistry in non-small cell lung cancers: a multi-institutional study by 15 pathologists in Korea. *J Pathol Transl Med* 2022; 56: 334-41.
 39. Baloch ZW, Fleisher S, LiVolsi VA, Gupta PK. Diagnosis of "follicular neoplasm": a gray zone in thyroid fine-needle aspiration cytology. *Diagn Cytopathol* 2002; 26: 41-4.
 40. Choi YJ, Yun JS, Kim DH. Clinical and ultrasound features of cytology diagnosed follicular neoplasm. *Endocr J* 2009; 56: 383-9.
 41. Giorgadze T, Rossi ED, Fadda G, Gupta PK, Livolsi VA, Baloch Z. Does the fine-needle aspiration diagnosis of "Hurthle-cell neoplasm/follicular neoplasm with oncocytic features" denote increased risk of malignancy? *Diagn Cytopathol* 2004; 31: 307-12.
 42. Gulcelik NE, Gulcelik MA, Kuru B. Risk of malignancy in patients with follicular neoplasm: predictive value of clinical and ultrasonographic features. *Arch Otolaryngol Head Neck Surg* 2008; 134: 1312-5.
 43. Kim HJ, Mok JO, Kim CH, et al. Preoperative serum thyroglobulin and changes in serum thyroglobulin during TSH suppression independently predict follicular thyroid carcinoma in thyroid nodules with a cytological diagnosis of follicular lesion. *Endocr Res* 2017; 42: 154-62.
 44. Kuru B, Kefeli M. Risk factors associated with malignancy and with triage to surgery in thyroid nodules classified as Bethesda category IV (FN/SFN). *Diagn Cytopathol* 2018; 46: 489-94.
 45. Lubitz CC, Faquin WC, Yang J, et al. Clinical and cytological features predictive of malignancy in thyroid follicular neoplasms. *Thyroid* 2010; 20: 25-31.
 46. Parikh PP, Allan BJ, Lew JI. Surgeon-performed ultrasound predictors of malignancy in patients with Hurthle cell neoplasms of the thyroid. *J Surg Res* 2013; 184: 247-52.
 47. Petric R, Perhavec A, Gazic B, Besic N. Preoperative serum thyroglobulin concentration is an independent predictive factor of malignancy in follicular neoplasms of the thyroid gland. *J Surg Oncol* 2012; 105: 351-6.
 48. Raber W, Kaserer K, Niederle B, Vierhapper H. Risk factors for malignancy of thyroid nodules initially identified as follicular neoplasia by fine-needle aspiration: results of a prospective study of one hundred twenty patients. *Thyroid* 2000; 10: 709-12.
 49. Raparia K, Min SK, Mody DR, Anton R, Amrikachi M. Clinical outcomes for "suspicious" category in thyroid fine-needle aspiration biopsy: patient's sex and nodule size are possible predictors of malignancy. *Arch Pathol Lab Med* 2009; 133: 787-90.
 50. Roth MY, Witt RL, Steward DL. Molecular testing for thyroid nodules: review and current state. *Cancer* 2018; 124: 888-98.
 51. Tuttle RM, Lemar H, Burch HB. Clinical features associated with an increased risk of thyroid malignancy in patients with follicular neoplasia by fine-needle aspiration. *Thyroid* 1998; 8: 377-83.
 52. Williams MD, Suliburk JW, Staerckel GA, et al. Clinical significance of distinguishing between follicular lesion and follicular neoplasm in thyroid fine-needle aspiration biopsy. *Ann Surg Oncol* 2009; 16: 3146-53.

Single-center study on clinicopathological and typical molecular pathologic features of metastatic brain tumor

Su Hwa Kim¹, Young Suk Lee¹, Sung Hak Lee¹, Yeoun Eun Sung¹, Ahwon Lee¹,
Jun Kang¹, Jae-Sung Park², Sin Soo Jeun², Youn Soo Lee¹

Departments of ¹Hospital Pathology and ²Neurosurgery, Seoul St. Mary's Hospital, College of Medicine, The Catholic University of Korea, Seoul, Korea

Background: The metastatic brain tumor is the most common brain tumor. The aim of this study was to demonstrate the clinicopathological and molecular pathologic features of brain metastases (BM). **Methods:** A total of 269 patients were diagnosed with BM through surgical resection at Seoul St. Mary's Hospital from January 2010 to March 2020. We reviewed the clinicopathological features and molecular status of primary and metastatic brain tissues using immunohistochemistry and molecular pathology results. **Results:** Among 269 patients, 139 males and 130 females were included. The median age of primary tumor was 58 years (range, 13 to 87 years) and 86 patients (32.0%) had BM at initial presentation. Median BM free interval was 28.0 months (range, 1 to 286 months). The most frequent primary site was lung 46.5% (125/269), and followed by breast 15.6% (42/269), colorectum 10.0% (27/269). Epidermal growth factor receptor (*EGFR*) mutation was found in 50.8% (32/63) and 58.0% (40/69) of lung primary and BM, respectively. In both breast primary and breast cancer with BM, luminal B was the most frequent subtype at 37.9% (11/29) and 42.9% (18/42), respectively, followed by human epidermal growth factor receptor 2 with 31.0% (9/29) and 33.3% (14/42). Triple-negative was 20.7% (6/29) and 16.7% (7/42), and luminal A was 10.3% (3/29) and 7.1% (3/42) of breast primary and BM, respectively. In colorectal primary and colorectal cancer with BM, *KRAS* mutation was found in 76.9% (10/13) and 66.7% (2/3), respectively. **Conclusions:** We report the clinicopathological and molecular pathologic features of BM that can provide useful information for understanding the pathogenesis of metastasis and for clinical trials based on the tumor's molecular pathology.

Key Words: Brain metastases; Clinical pathology; Molecular pathology

Received: April 4, 2023 Revised: May 23, 2023 Accepted: June 10, 2023

Corresponding Author: Youn Soo Lee, MD, PhD, Department of Hospital Pathology, Seoul St. Mary's Hospital, College of Medicine, The Catholic University of Korea, 222 Banpo-daero, Seocho-gu, Seoul 06591, Korea
Tel: +82-2-2258-1626, Fax: +82-2-2258-1628, E-mail: lys9908@catholic.ac.kr

Brain metastases (BM) are common in patients with solid malignancies and are the most common intracranial tumor in adults. Compared to primary malignant brain tumors, BM occurs approximately 10 times more frequently [1]. Although the actual incidence of BM is difficult to determine, estimates of BM incidence range from 8.3 to 14.3 per 100,000 [2,3]. As the use of magnetic resonance imaging (MRI) expands, cancer is not only detected early, but systemic therapy is gradually improved, which increases the survival rate of cancer patients and consequently increases the incidence of BM [4].

Imaging modalities such as computed tomography and MRI have increased the surgical resection of BM, and neurosurgical management has been shown to increase patient survival and enhance neurological performance [5,6]. At 2019 Congress of

Neurological Surgeons Guidelines on the Role of Surgery in the Management of Adults with Metastatic Brain Tumors, the adult patients newly diagnosed with metastatic brain tumors, except for radiosensitive tumors, surgery plus whole brain radiation therapy are recommended as first-line treatments if the following three conditions are satisfied: (1) single BM, (2) favorable performance status, and (3) limited extracranial disease [7].

According to increased neurosurgical operation for metastatic brain tumor, the number of surgical pathologic specimens has also recently increased. Molecular pathology analyses of these BM tissues can offer additional clinical gains. To date, some studies on epidemiology and pathology of patients with BM have been conducted. In the epidemiologic research of BM, some studies have been conducted based on patients with BM, but most mo-

lecular pathological studies were performed targeting primary cancer patients such as lung cancer and breast cancer, and studies based on BM cases nearly have not been conducted. We performed an analysis encompassing the epidemiological and molecular pathological characteristics of metastatic brain tumors based on BM patients. Therefore, this is the first study of patients with BM in South Korea in the past decade.

In this retrospectively collected data of patients with BM, we studied epidemiology, pathologic and molecular features of BM. We specifically address metastatic brain tumors from the three major primary cancers in which BM predominates: lung cancer, breast cancer, and colon cancer, with a focus on the therapy-associated molecular alterations and their clinicopathological implications. We collected extensive data using next-generation sequencing (NGS), immunohistochemistry (IHC), in situ hybridization, and sequencing. In this study, some specific data, which are emphasized in clinical importance among them, were selected and analyzed for comparison. We addressed epidermal growth factor receptor (*EGFR*), anaplastic lymphoma kinase (*ALK*), and *KRAS* status in lung cancer, human epidermal growth factor receptor 2 (*HER2*) and hormone receptor conversion in breast cancer, and *KRAS* and *NRAS* status in colorectal cancer.

MATERIALS AND METHODS

Patients

From January 2010 to March 2020, patients diagnosed with BM were identified from our institutional database. A total of 269 patients underwent surgical resection for intra-axial lesion of the BM. We retrospectively reviewed the electronic medical records for these patients, including demographic information, clinical characteristics, and surgical pathology reports. Among these, the most frequent primary tumors, that is, lung cancer ($n = 125$), breast cancer ($n = 42$), and colorectal cancer ($n = 27$), were reviewed their protein expression and molecular pathological status. Due to the molecular pathology studies for primary tumor and BM were performed at the physician's request for treatment decision, the tests were not uniform between patients.

Immunohistochemistry

IHC for estrogen receptor (ER), progesterone receptor (PR), *HER2*, Ki-67 index, and *ALK* was performed on formalin-fixed paraffin-embedded (FFPE) tumor specimens. Primary antibodies used for immunohistochemical staining were ER (prediluted, SP1, Roche Tissue Diagnostics, Tucson, AZ, USA), PR (prediluted, 1E2, Roche Tissue Diagnostics), *HER2* (prediluted, 4B5,

Roche Tissue Diagnostics), Ki67 (prediluted, MIB-1, Roche Tissue Diagnostics), and *ALK* (prediluted, D5F3, Roche Tissue Diagnostics). Immunohistochemical staining was performed using an automated Ventana Benchmark XT slide stainer (Roche Tissue Diagnostics). The staining results of ER and PR were interpreted using the Allred scoring system [8]. The proportion score was evaluated according to the proportion of positive-stained tumor cells as follows: 0 (0% positive), 1 (<1% positive), 2 (1% to 10% positive), 3 (11% to 33% positive), 4 (34% to 66% positive), and 5 ($\geq 67\%$ positive). Intensity was scored according to the average staining intensity of tumor cells, which is as follows: 0 (none), 1 (weak), 2 (intermediate), and 3 (strong). Positive and negative were evaluated by the sum of proportion and intensity scores, and a sum score > 2 was interpreted as positive.

HER2 staining results were interpreted according to the American Society of Clinical Oncology (ASCO)/College of American Pathologists (CAP) guidelines [9,10]. The criteria for reporting *HER2* test results are as follows: score 0 (negative, no staining observed or membrane staining that is incomplete and is faint/barely perceptible and within $\leq 10\%$ of tumor cells), score 1+ (negative, incomplete membrane staining that is faint/barely perceptible and within $> 10\%$ of tumor cells), score 2+ (equivocal, weak to moderate complete membrane staining in $> 10\%$ of tumor cells or complete membrane staining that is intense but within $\leq 10\%$ of tumor cells), and score 3+ (positive, complete membrane staining that is intense and $> 10\%$ of tumor cells). *HER2* results were scored from 0 to 3+ according to the criteria presented in the guideline, and in the case of 2+, subsequent analysis of *HER2* amplification by silver in situ hybridization was performed.

Ki-67 proliferation index was evaluated either by manual counting with 'eyeballing' or using automated digital image analysis. All stained invasive tumor cells were included for evaluation, regardless of staining intensity. Slides were scanned with an iScan Coreo slide scanner (Roche Tissue Diagnostics) and analyzed with Virtuoso software (Roche Tissue Diagnostics). Ki-67 was counted from more than 1,000 invasive tumor cells in at least three high-power fields (400 \times), including one hotspot area and two average areas, according to the recommendations of the International Ki67 in Breast Cancer Working Group [11].

In situ hybridization

ALK rearrangement was detected from FFPE by fluorescence in situ hybridization (FISH) using *ALK* (2p23) Break Apart Probe Kit (Leica Biosystems, Melbourne, Australia) or LSI *ALK* Dual Color Probe Kit (Abbott, Chicago, IL, USA). Since 2015, Vysis

ALK Dual Color Break Apart FISH Probe Kit (Abbott) has been used for *ALK* analysis. *HER2* amplification status was determined by using *HER2* Dual ISH Probe Cocktail Assay (Roche Diagnostics, Risch-Rotkreuz, Switzerland).

Sequence analysis

Sanger direct sequencing, peptide nucleic acid (PNA)-mediated real-time polymerase chain reaction (PCR), and pyrosequencing were used for sequence analysis, and the DNA extraction method was the same for each. DNA was extracted from FFPE tumor specimen using Maxwell 16 FFPE purification kit (Promega, Madison, WI, USA), according to manufacturer's protocol. DNA concentration was measured by Nano drop (Thermo Fisher Scientific, Waltham, MA, USA). Sanger direct sequencing was used to analyze *EGFR* exons 18, 19, 20, 21 and *KRAS*. After DNA extraction, PCR was performed using HotStar Taq Plus DNA Polymerase (Qiagen, Hilden, Germany). As forward primers, 5'-ACTGCTTTCCAGCATGGTGAGG-3' for *EGFR* exon 18, 5'-GTGGCACCATCTCACAATTGCC-3' for *EGFR* exon 19, 5'-ATGCGTCTTCACCTGGAAGG-3' for *EGFR* exon 20, 5'-CCTGAA TTCGGATGCAGAGCTTC-3' for *EGFR* exon 21, 5'-GGTGAGTTTGTATTTAAAAGG-3' for *KRAS* exon 2, and 5'-GGTGCACCTGTAATAATCCAGAC-3' for *KRAS* exon 3 were used. After initial denaturation at 95°C for 5 minutes, the following process was performed for 40 cycles. 94°C for 30 seconds, 60°C (*EGFR* exon 18) or 57°C (*EGFR* exon 19, 20, and 21) or 50°C (*KRAS* exon 2 and 3) for 30 seconds, and 72°C for 30 seconds. A final extension was performed at 72°C for 7 minutes. Sequencing was performed using Applied Biosystems 3730XL (Thermo Fisher Scientific) with the BigDye Terminator v.3.1 Cycle Sequencing kit (Applied Biosystems, Foster City, CA, USA). Since 2013, Applied Biosystems 3500 XL (Thermo Fisher Scientific) has been used. Pyrosequencing of *NRAS* codon 12, 13 and 61 region was performed using ThreascreeN *NRAS* Pyro kit (Qiagen). *NRAS* PCR conditions were as follows: initial denaturation at 95°C for 15 min, 42 cycles at 95°C for 30 seconds, 53°C for 30 seconds, and 72°C for 30 seconds, and final extension was performed at 72°C for 10 minutes. Streptavidin sepharose beads (GE Healthcare, Pittsburgh, PA, USA) and PCR product were dispensed into PyroMark Q24 plate wells, and the pyrosequencing results were analyzed using PyroMark Q24 software (ver. 2.0.6). PNA-mediated real-time PCR clamping method was used to analyze *EGFR* exons 18, 19, 20, 21 and *NRAS* codons 12, 13, 59, 61, 117, and 146. The extracted DNA was amplified using the PANAMutyper R *EGFR* kit (PANAGENE, Daejeon, Korea). PCR was performed using the CFX96 Real-Time PCR

Detection System (Bio-Rad, Hercules, CA, USA) for *EGFR* and the QuantStudio 5 Real-Time PCR Instrument for *NRAS*. The results were analyzed using the PANAMutyper Analyzer (PANAGENE).

Next-generation sequencing

Genomic DNA was extracted from dissected FFPE samples using the RecoverAll Total Nucleic Acid Isolation Kit (Thermo Fisher Scientific) according to the manufacturer's instructions. DNA concentration was measured by Nano drop and Qubit dsDNA HS Assay Kit (Thermo Fisher Scientific). DNA library construction was performed using the Ion AmpliSeq Library kit 2.0 (Thermo Fisher Scientific) according to the manufacturer's protocol and quantified by quantitative polymerase chain reaction. IonTorrent S5 XL Sequencer (Thermo Fisher Scientific) was used for sequencing, and sequencing data were analyzed by Ion Reporter v5.4 (Thermo Fisher Scientific). Since December 2019, OncoPrint Comprehensive Assay v3 panel and Ion Reporter v5.10 (Thermo Fisher Scientific) have been used.

Breast cancer subtype classification

Breast cancer subtype were classified as follows: Luminal A (ER and/or PR positive, HER2 negative, Ki-67 \leq 20%), luminal B (HER2 negative type: ER and/or PR positive, HER2 negative, Ki-67 > 20%, HER2 positive type: ER and/or PR positive, HER2 positive, any Ki-67), HER2-enriched (ER and PR negative, HER2 positive), and triple-negative (ER, PR, and HER2 negative) [12]. In our institution, the Ki-67 cutoff value is 20% [13].

Statistical analysis

Difference comparisons between groups were performed using the chi-square test. A p-value of < 0.05 was set as the level of statistical significance. Statistical analyses were performed utilizing R software (ver. 4.2.1, R core team 2022, R Foundation for Statistical Computing, Vienna, Austria).

RESULTS

Clinical characteristics

Two hundred sixty-nine patients were diagnosed with BM for the surgically resected brain specimen, including 139 men and 130 women (Table 1). The median age at diagnosis of primary tumor was 58 years (range, 13 to 87 years). Of these patients, 86 (32.0%) had synchronous BM at initial presentation. The median interval between diagnosis of primary tumor and metastatic brain tumor was 28 months (range, 1 to 286 months). Most metastatic

Table 1. Clinical characteristics of patients with metastatic brain tumor

	No. of patients (%)	Age ^a (yr)		Sex, n (%)		Timing of BM, n (%)			BM free interval (mo)			BM location, n (%)		
		Mean±SD	Median (range)	Male	Female	Meta	Syn		Mean±SD	Median (range)		Supra	Infra	Both
Total	269 (100)	57.45±11.9	58 (13-87)	139 (51.7)	130 (48.3)	183 (68.0)	86 (32.0)		44.0±45.6	28 (1-286)		200 (74.4)	28 (10.4)	41 (15.2)
Lung	125 (46.5)	61.8±10.4	62 (38-87)	81 (64.8)	44 (35.2)	59 (47.2)	66 (52.8)		31.6±38.1	20 (4-217)		99 (79.2)	10 (8.0)	16 (12.8)
Breast	42 (15.6)	47.3±10.0	46 (28-68)	0	42 (100)	41 (97.6)	1 (2.4)		57.9±53.2	39 (1-215)		26 (61.9)	4 (9.5)	12 (28.6)
Colorectum	27 (10.0)	59.0±8.0	58 (40-76)	13 (48.1)	14 (51.9)	24 (88.9)	3 (11.1)		52.2±35.0	41 (12-146)		14 (51.9)	8 (29.6)	5 (18.5)
Kidney	18 (6.7)	57.8±10.0	54 (38-72)	16 (88.9)	2 (11.1)	16 (88.9)	2 (11.1)		67.6±71.3	57 (3-286)		15 (83.3)	1 (5.6)	2 (11.1)
Liver	14 (5.2)	53.4±12.0	53 (36-74)	12 (85.7)	2 (14.3)	12 (85.7)	2 (14.3)		32.2±33.4	22 (7-129)		14 (100)	0	0
Ovary	7 (2.6)	56.6±7.4	56 (44-66)	0	7 (100)	7 (100)	0		34.4±21.8	28 (13-79)		2 (28.6)	4 (57.1)	1 (14.3)
Uterus	5 (1.9)	53.2±8.4	52 (41-64)	0	5 (100)	5 (100)	0		18.6±20.3	13 (4-54)		5 (100)	0	0
Skin	5 (1.9)	47.4±13.2	43 (36-70)	1 (20.0)	4 (80.0)	4 (80.0)	1 (20.0)		73.8±57.4	77 (5-136)		4 (80.0)	0	1 (20.0)
Unknown	5 (1.9)	63.8±17.0	67 (35-80)	3 (60.0)	2 (40.0)	0	5 (100)					3 (60.0)	0	2 (40.0)
GB and EBD	3 (1.1)	65.3±6.3	68 (58-70)	2 (66.7)	1 (33.3)	0	3 (100)					2 (66.7)	0	1 (33.3)
Stomach	2 (0.7)	57.5±10.6	58 (50-65)	1 (50.0)	1 (50.0)	1 (50.0)	1 (50.0)		54±54	54 (54)		2 (100)	0	0
Peritoneum	2 (0.7)	51.0±4.2	51 (48-54)	0	2 (100)	2 (100)	0		42±38.2	42 (15-69)		1 (50.0)	0	1 (50.0)
Pituitary gland	1 (0.4)		51		Female		Meta			11				Supra
PNS	1 (0.4)		48		Male		Meta			18				Supra
Nasopharynx	1 (0.4)		50		Male		Meta			37				Supra
Larynx	1 (0.4)		60		Male		Meta			94				Supra
Esophagus	1 (0.4)		72		Male		Meta			14				Supra
Thymus	1 (0.4)		61		Male		Meta			23				Supra
Heart	1 (0.4)		51		Female		Meta			13				Supra
Mediastinum	1 (0.4)		13		Female		Meta			10				Supra
Jejunum	1 (0.4)		71		Male		Syn			0				Supra
Vessel	1 (0.4)		73		Male		Syn			0				Supra
Bone	1 (0.4)		33		Female		Meta			3				Supra
Bladder	1 (0.4)		69		Male		Meta			7				Infra
Prostate	1 (0.4)		56		Male		Meta			58				Supra
Testis	1 (0.4)		28		Male		Meta			26				Supra

In the median BM free interval, synchronous BM cases set the time lag to zero.

BM, brain metastasis; SD, standard deviation; Meta, metachronous; Syn, synchronous; Supra, supratentorial; Infra, infratentorial; GB, gall bladder; EBD, extrahepatic bile ducts; PNS, paranasal sinus.

^aAge at diagnosis of primary tumor.

brain tumors (74.4%) were located in the supratentorial region. The most frequent primary tumors were lung cancers (46.5%), followed by breast cancer (15.6%), and colon cancer (10.0%).

Lung was the most frequent site of origin of BM, occupying 125 out of 269 cases (46.5%). The median age at diagnosis of primary tumor was 62 years (range, 38 to 87 years). Many of these patients were male (81/125, 64.8%). More than half of the cases (66/125, 52.8%) were diagnosed with BM at initial presentation and the median BM-free interval was 20 months (range, 4 to 217 months). The location of BM was supratentorial in 79.2% (99/125).

For breast cancer (15.6%), which had the second highest incidence of BM, all 42 patients were female. The median age at diagnosis of primary cancer was 46 years (range, 28 to 68 years), and most of them (41/42, 97.6%) developed BM over time. There was a median interval of 39 months between diagnosis of BM and primary cancer (range, 1 to 215 months). Twenty-six of the 42 patients (61.9%) had BM in the supratentorial region.

Colorectal cancer was the third most common primary cancer, accounting for 10.0% (n = 27). The median age at diagnosis of colorectal cancer was 58 years (range, 40 to 76 years). There was no significant difference in the sex, with males and females accounting for 48.1% (13/27) and 51.9% (14/27), respectively. Most of them (24/27, 88.9%) had metachronous BM, with a median interval of 41 months from primary cancer diagnosis to BM diagnosis (range, 12 to 146 months). Fifty-one point nine percent (14/27) were supratentorial metastases.

Other additional clinical characteristics according to the primary tumor are shown in Table 1. Overall, among patients with BM, patients with primary lung cancer, gallbladder and extrahepatic bile duct cancer were older than patients with the other types of primary cancer, and breast and skin cancer patients were younger. Lung, kidney, and liver cancers showed male predominance, 64.8%, 88.9%, and 85.7% in males, respectively. On the other hand, skin cancers showed female predominance, 80% in females.

The histological types of the primary tumors with brain metastasis

The histological types of the primary tumors are summarized in Table 2. In the case of lung cancer, most were non-small cell lung cancers (NSCLC, 92.0%) and small cell lung cancers were 8.0%. Among NSCLC, the most frequent histologic type was adenocarcinoma, followed by squamous cell carcinoma and adenocarcinoma. In breast cancer, invasive breast carcinoma of no special type (90.4%) was the most common, followed

by invasive lobular carcinoma (4.8%) and mucinous carcinoma (4.8%) in equal proportions. Most of colon cancer were adenocarcinoma. Concerning kidney, clear cell renal cell carcinomas (RCC) were most frequent (94.4%) and chromophobe RCC is in one case. In liver, all cases were hepatocellular carcinoma. All of ovary cancer were high grade serous carcinoma, and all of skin cancer were malignant melanoma. In uterine cancer, endometrioid carcinoma was four cases (80.0%) and undifferentiated carcinoma was one case (20.0%). In five cases of unknown of primary tumor, the histologic types were adenocarcinoma in three cases, small cell neuroendocrine carcinoma and poorly differentiated carcinoma in one case each. The other diverse primary sites and histologic types are described in Table 2.

Molecular pathology of lung cancer with brain metastasis

Molecular pathology studies were applied to 71 metastatic brain lesions and 63 primary lung lesions. This study was not totally paired with primary and metastatic lesions in all cases, but was performed on paired lesions in some cases. *EGFR* mutation or amplification, *KRAS* mutations, and *ALK* rearrangement status were evaluated. In primary tumors, *EGFR* mutations were observed in 50.8% of cases (Table 3). Exon19 deletion was the most frequent genotype (17 cases), followed by exon21 p.L858R (8 cases). In metastatic brain tumors, 58.0% of cases were *EGFR*-mutant types. As with primary tumors, exon19 deletion and exon21 p.L858R mutations were the most frequent, 19 cases and eight cases, respectively. Multiple mutation sites were detected in four cases of primary tumors and eight cases of metastatic brain tumors. Exon20 p.T790M mutations were much more detected in BM (6 cases) than lung primary (1 cases). Detailed mutation sites of *EGFR* are shown in Table 3. Correlations between *EGFR* status and clinicopathological characteristics are listed in Table 4. There was no significant correlation between *EGFR* status and age, timing of BM, BM location, and histologic type except sex. *EGFR*-mutant type was observed more frequently in females (p = .002). Of the 125 cases, 33 cases were studied for *EGFR* mutations in both primary lung cancer and paired metastatic brain tissues (Table 5). Eight cases of *EGFR*-wild type and 25 cases of *EGFR*-mutant type were observed. *EGFR* mutation sites were changed in nine cases. In six cases, exon20 p.T790M was additionally found in the existing mutation. In one of the three cases, *EGFR* amplification was additionally confirmed in addition to the existing mutation, in one case, exon18 E709G disappeared from the existing mutation, and in the other case, exon19 del and exon21 L833S disappeared from the existing mutations and *EGFR* amplification appeared.

Table 2. Histologic diagnosis according to the sites of primary tumor

Histologic diagnosis	No. (%)
Lung (n = 125)	
NSCLC	115 (92.0)
Adenocarcinoma	78
Squamous cell carcinoma	12
Adenosquamous carcinoma	10
Poorly differentiated carcinoma	8
Mucinous adenocarcinoma	2
Large cell carcinoma	2
Combined carcinoma	2
Sarcomatoid carcinoma	1
SCLC	10 (8.0)
Breast (n = 42)	
Invasive breast carcinoma of no special type	38 (90.4)
Invasive lobular carcinoma	2 (4.8)
Mucinous carcinoma	2 (4.8)
Colorectum (n = 27)	
Adenocarcinoma, NOS	24 (88.9)
Mucinous adenocarcinoma	2 (7.4)
Signet-ring cell carcinoma	1 (3.7)
Kidney (n = 18)	
Clear cell renal cell carcinoma	17 (94.4)
Chromophobe renal cell carcinoma	1 (5.6)
Liver (n = 14)	
Hepatocellular carcinoma	14 (100)
Ovary (n = 7)	
High grade serous carcinoma	7 (100)
Uterus (n = 5)	
Endometrioid carcinoma	4 (80.0)
Undifferentiated carcinoma	1 (20.0)
Skin (n = 5)	
Malignant melanoma	5 (100)
Unknown (n = 5)	
Adenocarcinoma	3 (60.0)
Small cell neuroendocrine carcinoma	1 (20.0)
Poorly differentiated carcinoma	1 (20.0)
Gall bladder (n = 2)	
Tubular adenocarcinoma	2 (100)
EBD (n = 1)	
Cholangiocarcinoma	1 (100)
Stomach (n = 2)	
Adenocarcinoma	1 (50.0)
Poorly cohesive carcinoma with signet ring cell component	1 (50.0)
Peritoneum (n = 2)	
Peritoneal serous adenocarcinoma	2 (100)
Pituitary gland (n = 1)	
Pituitary carcinoma	1 (100)
PNS (n = 1)	
Sinonasal adenocarcinoma, intestinal type	1 (100)
Nasopharynx (n = 1)	
Non-keratinizing squamous cell carcinoma	1 (100)
Larynx (n = 1)	
Neuroendocrine carcinoma	1 (100)

(Continued)

Histologic diagnosis	No. (%)
Esophagus (n = 1)	
Squamous cell carcinoma	1 (100)
Thymus (n = 1)	
Thymic squamous cell carcinoma	1 (100)
Heart (n = 1)	
Leiomyosarcoma	1 (100)
Mediastinum (n = 1)	
Choriocarcinoma	1 (100)
Jejunum (n = 1)	
Adenosquamous carcinoma	1 (100)
Vessel (n = 1)	
Aortic intimal sarcoma	1 (100)
Bone (n = 1)	
Osteosarcoma	1 (100)
Bladder (n = 1)	
Poorly differentiated carcinoma	1 (100)
Prostate (n = 1)	
Prostatic acinar adenocarcinoma	1 (100)
Testis (n = 1)	
Mixed germ cell tumor	1 (100)

NSCLC, non-small cell lung cancer; SCLC, small cell lung cancer; NOS, not otherwise specified; EBD, extrahepatic bile ducts; PNS, paranasal sinus.

Four cases of primary lung tumors and three cases of metastatic brain tumors were *KRAS*-mutant, and the detected mutation sites were codon 12 (3 cases) and codon 13 (1 case) in primary brain tumors and codon 12 in metastatic brain tumors (Table 3).

ALK rearrangement was detected in five cases of lung and six cases of brain, respectively, and one case was examined by IHC in the brain, and all other cases were confirmed by FISH (Table 3).

Protein expression profile and molecular subtypes of breast cancer with brain metastasis

In 42 breast cancer BM cases, 29 primary tumors and 42 metastatic brain tumors were studied for protein expression status. Detailed data and resultant molecular subtypes are shown in Table 6. In both breast and brain, the most frequent subtype was luminal B type (37.9% and 42.9%), followed by HER2-enriched type (31.0% and 33.3%) and triple-negative type (20.7% and 16.7%). Among 42 cases of breast cancer BM, protein expression in both primary and paired metastatic brain tumors was studied in 29 cases. In primary tumors, ER, PR, and HER2 positive cases were 14/29 (48.3%), 11/29 (37.9%), and 16/29 (55.2%), respectively, and in metastatic brain tumors, 12/29 (41.4%), 7/29 (24.1%), and 17/29 (58.6%), respectively (Fig. 1). Receptor status discordances between primary and paired metastatic brain tumors were observed in a total of 11 out of 29 cases. There were two cases of ER status conversion, both of which were positive to negative conversion. PR status conversion occurred in a total

of eight cases, with positive to negative conversion in six cases and negative to positive conversion in two cases. HER2 conversion was negative to positive in one case (Table 7). Accordingly,

Table 3. Molecular profile of lung cancer with brain metastasis

Molecular status	Primary tumor (n=63)	Brain metastasis (n=71)
EGFR status		
Wild type	31 (49.2)	29 (42.0)
Mutant type	32 (50.8)	40 (58.0)
Exon18		
E709_T710 del insD (SD, NGS)	1 (1.6)	1 (1.5)
G719 (PNA)	0	1 (1.5)
Exon19		
Deletion (SD, PNA, NGS)	17 (27.0)	19 (27.6)
Exon20		
S768I (PNA, NGS)	1 (1.6)	0
Exon21		
L858R (PNA, NGS)	8 (12.7)	8 (11.6)
T854I (SD)	0	1 (1.5)
L861Q (SD)	1 (1.6)	0
Exon18 + Exon21		
E709G + L858R (SD)	1 (1.6)	0
G719 + L861Q (PNA)	1 (1.6)	1 (1.5)
Exon19 + Exon20		
Deletion + T790M (PNA)	1 (1.6)	5 (7.3)
Exon19 + Exon21		
Deletion + L858R, L833S (SD)	1 (1.6)	0
Exon21 + Exon20		
L858R + T790M (PNA)	0	1 (1.5)
L858R + S768I (PNA, NGS)	0	1 (1.5)
Exon21 + amp		
L858R (PNA, NGS)	0	2 (2.9)
Not determined	0	2
ALK rearrangement status		
Positive		
FISH	5 (9.3)	7 (13.5)
IHC	5 (9.3)	6 (11.6)
IHC	0	1 (1.9)
Negative		
FISH	49 (90.7)	45 (86.5)
IHC	41 (75.9)	42 (80.7)
IHC	8 (14.8)	3 (5.8)
Not determined	9	19
KRAS status		
Wild type		
	28 (87.5)	30 (90.9)
Mutant type		
G12C	4 (12.5)	3 (9.1)
G12A	1 (3.1)	1 (3.0)
G12A	1 (3.1)	1 (3.0)
G12D	1 (3.1)	1 (3.0)
G13C	1 (3.1)	0
Not determined	31	38

Values are presented as number (%).

EGFR, epidermal growth factor receptor; SD, Sanger direct sequencing; NGS, next-generation sequencing; PNA, peptide nucleic acid-mediated real-time PCR clamping; amp, amplification; ALK, anaplastic lymphoma kinase; FISH, fluorescence in situ hybridization; IHC, immunohistochemistry;

one case each of luminal A type and luminal B type was converted to HER2-enriched type (Fig. 2).

Molecular pathology of colorectal cancer with brain metastasis

Among 27 cases of colorectal cancer BM, 14 cases of primary tumors and three cases of metastatic brain tumors were studied for the molecular status. In primary tumors and metastatic brain tumors, 13 cases and three cases were analyzed for *KRAS* mutation and eight cases and two cases for *NRAS* mutation, respectively. In primary tumors, *KRAS* mutations were observed in 76.9% (10/13) and no *NRAS* mutations were detected. In metastatic brain tumors, *KRAS* mutations were observed in 66.7% (2/3) and no *NRAS* mutations were detected (Table 8). In primary tumors, *KRAS* mutations were most frequently observed in codon 12 of exon 2 (6 cases), and the other detected mutation sites are described in Table 8. Multiple mutations in *KRAS* were not observed. Two cases of *KRAS* mutations in metastatic brain

Table 4. Correlation between EGFR status and clinicopathological characteristics in lung cancer with brain metastasis (n=99)

	EGFR status		p-value
	Wild type (n=52)	Mutant type (n=47)	
Age (yr)			.566
>60	28 (53.9)	28 (59.6)	
≤60	24 (46.1)	19 (40.4)	
Sex			.002
Male	39 (75.0)	21 (44.7)	
Female	13 (25.0)	26 (55.3)	
Timing of BM			.582
Synchronous	27 (51.9)	27 (57.5)	
Metachronous	25 (48.1)	20 (42.6)	
BM location			.414
Supratentorial	40 (76.9)	41 (87.2)	
Infratentorial	4 (7.7)	2 (4.3)	
Both	8 (15.4)	4 (8.5)	
Histologic type			.054
NSCLC			
Adenocarcinoma	31 (59.6)	42 (89.4)	
Squamous cell carcinoma	6 (11.5)	0	
Adenosquamous carcinoma	4 (7.7)	3 (6.4)	
Poorly differentiated carcinoma	4 (7.7)	2 (4.2)	
Mucinous adenocarcinoma	2 (3.9)	0	
Large cell carcinoma	1 (1.9)	0	
Combined carcinoma	1 (1.9)	0	
Sarcomatoid carcinoma	1 (1.9)	0	
SCLC	2 (3.9)	0	

Values are presented as number (%). n=99; primary tumor (n=30), metastatic brain tumor (n=36), matched primary and metastatic brain tumor (n=33). EGFR, epidermal growth factor receptor; BM, brain metastasis; NSCLC, non-small cell lung cancer; SCLC, small cell lung cancer.

Table 5. Concordance of subtypes of *EGFR* mutation in primary lung cancer and paired brain metastasis (n=33)

Patient	Sex	Age (yr)	Primary lung tumor	Metastatic brain tumor
P1	F	48	Wild type	Wild type
P2	M	63	Wild type	Wild type
P3	M	46	Wild type	Wild type
P4	M	64	Wild type	Wild type
P5	M	58	Wild type	Wild type
P6	F	44	Wild type	Wild type
P7	M	52	Wild type	Wild type
P8	F	50	Wild type	Wild type
P9	F	67	Exon18 E709_T710 del insD	Exon18 E709_T710 del insD
P10	M	59	Exon19 del	Exon19 del
P11	M	62	Exon19 del	Exon19 del
P12	M	65	Exon19 del	Exon19 del
P13	M	47	Exon19 del	Exon19 del
P14	F	61	Exon19 del	Exon19 del
P15	F	64	Exon19 del	Exon19 del
P16	F	63	Exon19 del	Exon19 del
P17	F	59	Exon19 del	Exon19 del
P18	F	68	Exon19 del	Exon19 del
P19	F	53	Exon19 del	Exon19 del
P20	M	53	Exon19 del	Exon19 del
P21	F	69	Exon19 del	Exon19 del
P22	F	63	Exon21 L858R	Exon21 L858R
P23	M	46	Exon21 L858R	Exon21 L858R
P24	M	55	Exon18 G719, Exon21 L861Q	Exon18 G719, Exon21 L861Q
P25	M	59	Exon18 E709G, Exon21 L858R	Exon21 L858R
P26	F	52	Exon19 del	Exon19 del, Exon20 T790M
P27	M	66	Exon19 del	Exon19 del, Exon20 T790M
P28	F	76	Exon19 del	Exon19 del, Exon20 T790M
P29	F	66	Exon19 del	Exon19 del, Exon20 T790M
P30	F	65	Exon19 del	Exon19 del, Exon20 T790M
P31	M	58	Exon19 del, Exon21 L858R, Exon21 L833S	Exon21 L858R, EGFR Amp
P32	F	60	Exon21 L858R	Exon21 L858R, EGFR Amp
P33	M	54	Exon21 L858R	Exon21 L858R, Exon20 T790M

EGFR, epidermal growth factor receptor; Amp, amplification.

tumors were observed at codons 12 and 13 of exon 2, respectively, and both mutations were consistent with mutations in the primary tumors. Correlations between *KRAS* status and clinicopathological characteristics are listed in Table 9. There was no significant correlation between *EGFR* status and age, sex, and BM location except timing of BM. Most of the wild type were diagnosed with BM at initial presentation (2/3), while mutant types were mostly metachronous (9/10) ($p = .041$).

DISCUSSION

This study analyzed the 10-year epidemiology and molecular pathological characteristics of BM patients. In particular, molecular pathological analysis was performed on metastatic brain tumor tissues of lung cancer, breast cancer, and colorectal cancer

with high BM incidence. As stated in several studies, lung cancer (43%–51%), breast cancer (15%–16%), and melanoma (7%–16%) are known as the three most common primary cancers that metastasize to the brain, followed by renal cancer (7%–9%) and colorectal cancer (0.6%–9%) [2,14–17]. In this study, the most common primary lesions of BM were lung (46.5%), breast (15.6%), and colorectum (10.0%), followed by kidney (6.7%), liver (5.2%), and ovary (2.6%), uterus (1.9%), skin (1.9%), and unknown (1.9%) in the order, and 8.1% in other lesions. This difference appears to be due to the incidence of primary cancer. In the United States and Europe, the incidence of melanoma is frequent at 3.7% to 5.2% but in South Korea it is only 0.3%, while the incidence of liver cancer is higher at 5.2% than in the United States and Europe (2.2%) [18–20]. The BM incidence of colorectal cancer in this study is relatively higher than the results

of western countries' previous studies. The reasons for this are that the oncologic outcome has improved with the development of the surgical technique and adjuvant chemotherapy in colon cancer, and the detection rate of small brain lesions has increased due to increased number of performed brain imaging procedure, including brain MRI, which has been covered by medical insurance in South Korea.

Table 6. Protein expression profile and molecular subtype of breast cancer with brain metastasis

Molecular status	Primary tumor (n=29)	brain metastasis (n=42)	p-value
ER status			.957
Positive	14 (48.3)	20 (47.6)	
Negative	15 (51.7)	22 (52.4)	
PR status			.541
Positive	11 (37.9)	13 (31.0)	
Negative	18 (62.1)	29 (69.1)	
HER2 status			.702
Positive	16 (55.2)	23 (56.1)	
Negative	13 (44.8)	18 (43.9)	
Not determined	0	1	
Ki-67 index			.055
>20%	15 (51.7)	31 (73.8)	
≤20%	14 (48.3)	11 (26.2)	
Subtype			.921
Luminal A	3 (10.3)	3 (7.1)	
Luminal B	11 (37.9)	18 (42.9)	
HER2	9 (31.0)	14 (33.3)	
Triple negative	6 (20.7)	7 (16.7)	

Values are presented as number (%).

ER, estrogen receptor; PR, progesterone receptor; HER2, human epidermal growth factor receptor 2.

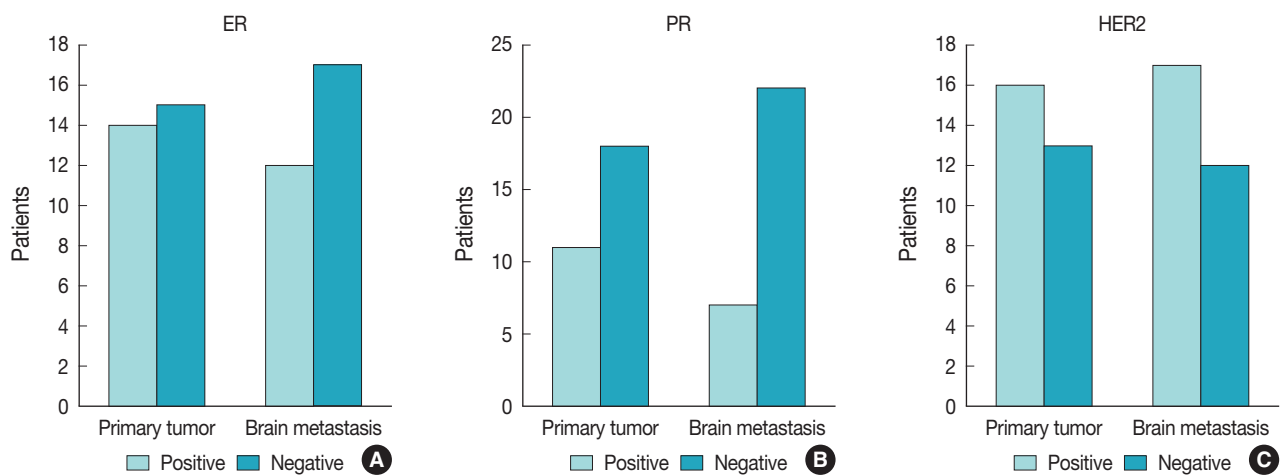


Fig. 1. Expression patterns of hormone receptors and HER2 in primary tumors and brain metastases by immunohistochemistry. (A) ER expression pattern. (B) PR expression pattern. (C) HER2 expression pattern. ER, estrogen receptor; PR, progesterone receptor; HER2, human epidermal growth factor receptor 2.

Among the three BM-prone primary sites, the median age at diagnosis of primary cancer was 62 years old for lung cancer, 46 years old for breast cancer, and 58 years old for colorectal cancer, and, with lung cancer patients being the oldest and breast cancer patients being the youngest. These results showed similar tendencies to the results of previous studies. In a study of 309 patients with BM, the median age at diagnosis of primary cancer was reported as 60 years for NSCLC, 61 years for small cell lung cancer, 57 years for colon cancer, and 50 years for breast cancer [15]. Of the 269 patients with BM, 51.7% were male. In the case of lung cancer patients with BM, 64.8% were male and 35.2% were female. All patients with BM from breast cancer were female, while there was minimal sex disparity among patients with colorectal cancer BM. These results are similar to study that analyzed patients diagnosed with BM from 1973 to 2001 [2]. According to this study, 7,167 patients (60.9%) were male and 4,596 (39.1%) female patients with BM from lung cancer, with a high proportion of males. The majority of patients with BM from breast cancer were female, with only 19 males and 2,616 females. There were 414 males and 365 females with BM from colorectal cancer patients, and no significant difference was observed by sex. According to the incidence of major carcinomas by sex in South Korea, lung cancer was more common in males, and breast cancer was far more common in females [20]. Colorectal cancer has a slight male predominance, and there is no significant difference in the sex ratio. Considering this, the difference in the proportion of BM patients by sex in our study also seems to depend on the incidence of primary cancer, as in the above study.

The natural history of progression from primary cancer to BM

Table 7. Receptor conversion between primary breast cancer and paired brain metastasis (n=29)

Primary tumor	Brain metastasis		Total
	Positive	Negative	
ER status			
Positive	12 (41.4)	2 (6.9)	14 (48.3)
Negative	0	15 (51.7)	15 (51.7)
Total	12 (41.4)	17 (58.6)	29 (100)
PR status			
Positive	5 (17.2)	6 (20.7)	11 (37.9)
Negative	2 (6.9)	16 (55.2)	18 (62.1)
Total	7 (24.1)	22 (75.9)	29 (100)
HER2 status			
Positive	16 (55.2)	0	16 (55.2)
Negative	1 (3.4)	12 (41.4)	13 (44.8)
Total	17 (58.6)	12 (41.4)	29 (100)

Values are presented as number (%).

ER, estrogen receptor; PR, progesterone receptor; HER2, human epidermal growth factor receptor 2.

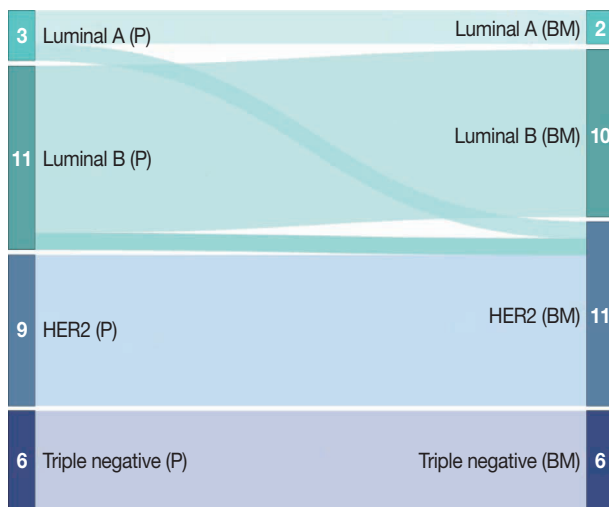


Fig. 2. Subtype conversion between primary tumor and brain metastases. P, primary tumor; BM, brain metastasis; HER2, HER2-enriched subtype.

varies depending on the site of the primary tumor. According to a study analyzing the incidence and mortality of synchronous BM in the United States, the most common primary tumor site in patients with synchronous BM was the lung (80.3%) [21]. Likewise, in our study, lung cancer was the most frequently diagnosed at the same time as the primary tumor at 52.8%. In a retrospective cohort study of 2419 patients [14], median time interval from diagnosis of primary cancer to diagnosis of BM was as follows; lung cancer (11 months), breast cancer (44 months), and colorectal cancer (33 months). In contrast, our results demonstrate the median time interval was lung cancer (20 months), breast cancer (39 months), and colorectal cancer (41 months).

Table 8. Molecular profile of colorectal cancer with brain metastasis

Molecular status	Primary tumor (n=14)	Brain metastasis (n=14)
<i>KRAS</i> status		
Wild type	3 (23.1)	1 (33.3)
Mutant type	10 (76.9)	2 (66.7)
Exon2		
G12C	2 (15.4)	
G12V	2 (15.4)	1 (33.3)
G12D	2 (15.4)	
G12_G13 insG	1 (7.7)	
G13D	1 (7.7)	1 (33.3)
Exon3		
Q61H	1 (7.7)	
Q61L	1 (7.7)	
Not determined	1	11
<i>NRAS</i> status		
Wild type	8 (100)	2 (100)
Mutant type	0	0
Not determined	6	12

Values are presented as number (%).

Table 9. Correlation between *KRAS* status and clinicopathological characteristics in colorectal cancer with brain metastasis (n=13)

	<i>KRAS</i> status		p-value
	Wild type (n=3)	Mutant type (n=10)	
Age (yr)			.913
>60	1 (33.3)	3 (30.0)	
≤60	2 (66.7)	7 (70.0)	
Sex			.913
Male	2 (66.7)	7 (70.0)	
Female	1 (33.3)	3 (30.0)	
Primary site			.188
Colon	0	4 (40.0)	
Rectum	3 (100)	6 (60.0)	
Timing of BM			.041
Synchronous	2 (66.7)	1 (10.0)	
Metachronous	1 (33.3)	9 (90.0)	
BM location			.492
Supratentorial	2 (66.7)	7 (70.0)	
Infratentorial	1 (33.3)	1 (10.0)	
Both	0	2 (20.0)	

Values are presented as number (%).

BM, brain metastasis.

Lung cancer had the shortest free interval, showing a similar result to previous studies, but the primary cancer with the longest free interval was colorectal cancer, not breast cancer.

Berghoff et al. [14] reported a supratentorial predominance for the location at diagnosis of BM. Our result shows also supratentorial predominance (79.2%).

As described in Table 2, we summarized the histological types of primary tumors in 269 patients with BM. NSCLC was the

most common type with BM at 92.0% in lung cancer. While previous studies reported that NSCLC accounts for 66.4 to 86.3% of lung cancer cases [14,16], the results in our study showed a slightly higher rate. Among NSCLC, adenocarcinoma (67.8%) was the most frequent, followed by squamous cell carcinoma (10.4%) and adenosquamous carcinoma (8.7%). A study of 975 patients with early-stage NSCLC found that 48% of patients with BM had adenocarcinoma and 32% had squamous cell carcinoma [22]. According to a population-based study, invasive ductal carcinoma (IDC, now changed to invasive breast carcinoma of no special type) was the most common histological type in 64.6% of patients with BM from breast cancer [23]. Another study reported that 81.1% of cases were IDC [4]. In our study, invasive breast carcinoma of no special type was the majority at 90.4%. Yang et al. [24] reported that 84.5% of 401 patients with colorectal cancer BM were adenocarcinoma, 6.7% were mucinous adenocarcinoma, 5.5% were other types, and 3.2% were unknown. As a result of our study, adenocarcinoma, NOS accounted for 88.9% of colorectal cancer BM, followed by mucinous adenocarcinoma in 7.4% and signet-ring cell carcinoma in 3.7%.

Metastatic lung cancer

Molecular pathology analysis provides information on NSCLC oncogenes that are responsive to targeted therapy, such as *EGFR* mutations, *ALK* rearrangements, and *KRAS* mutations. *EGFR* mutations in NSCLC patients occur in about 17.4% of Caucasians and 38.8% of Asians [25], and *EGFR* mutations in BM were found in 3.9%–6.2% and 44.4%–61.2% of Caucasians and Asians, respectively [26–30]. In this study, *EGFR* mutations were observed in 50.8% of primary tumors and 58.0% of BM. These results, similar to previous studies, indicate that *EGFR* mutations in NSCLC and BM have clear ethnic and geographical differences.

Discordances in *EGFR* mutations between NSCLC and BM have been reported at 22.5% to 32.0% [29–31]. In our study, the *EGFR* mutation was altered in nine patients with BM. Exon20 p.T790M and *EGFR* amplification were additionally found in the existing mutation, and in two patients, some of the mutations present in primary lung cancer were disappeared. One patient had exon18 E709G and exon21 L858R in primary lung cancer and only exon21 L858R in metastatic cancer. The other patient had exon19 del, exon21 L858R, and exon21 L833S in primary lung cancer and exon21 L858R and *EGFR* amplification in metastatic cancer. These findings can be explained by tumor heterogeneity associated with genetic changes such as cancer stem cell theory, clonal evolution, and chromosomal instability. In ad-

dition to genetic heterogeneity, epigenetic and microenvironmental changes can contribute to tumor heterogeneity [32,33].

Most NSCLC patients with *EGFR* mutations respond to treatment with first-generation *EGFR* tyrosine kinase inhibitors (TKIs) [34] but develop drug resistance within 1 to 2 years, approximately 50%–60% due to acquired *EGFR* T790M mutation [35,36]. For patients who have progressed after treatment with an *EGFR* TKI, the molecular pathology analyses of the BM tissue should be considered to determine whether to continue treatment with an *EGFR* inhibitor or switch to another TKI, such as the T790M mutation-specific brain penetration inhibitor osimertinib.

EML4-ALK is a tyrosine kinase generated by gene fusion and appears in about 3%–5% of NSCLC patients [37–39]. *ALK*-positive NSCLC patients have been reported to have a higher risk of developing BM than *ALK*-negative patients [40]. Rangachari et al. [41] analyzed NSCLC patients and found that 23.8% of NSCLC patients with *ALK* rearrangements had BM at initial diagnosis. In this study, *ALK* rearrangement was detected in 9.3% of primary tumors and 13.5% of BM, respectively. One case was examined by IHC in the brain, and all other cases were confirmed by FISH. A highly reactive *ALK* inhibitor, crizotinib is the treatment of choice for NSCLC patients with *ALK* rearrangement. However, crizotinib has a problem of poor blood-brain barrier penetration [42]. In contrast, alectinib and brigatinib have been proven to penetrate the central nervous system and show excellent efficacy [43,44], so it is important to analyze the *ALK* mutation status of BM in establishing a treatment plan for BM of NSCLC.

KRAS mutations are prevalent mutations in human cancers, and occur in about 20%–40% of lung adenocarcinomas [45,46]. According to Kalikaki et al. [47], in paired primary tumor and BM specimens, *KRAS* mutations were found in 20% and 8% of primary tumors and BM, respectively. In this study, *KRAS* mutations were found in 12.5% and 9.1% of primary tumors and BM, respectively. Considering that the incidence of *KRAS* mutations in lung adenocarcinoma is 25%–33% in Europe and the United States, which is higher than in Asia (5%–8%) [48], the lower incidence of primary tumors' *KRAS* mutations in our study seems to be due to geographical or racial differences. On the other hand, the incidence of *KRAS* mutations in lung cancer was higher in our study (12.5%) than in Asia (5%–8%), which seems to be due to the analysis of lung cancer tissues with BM. Evaluation of *KRAS* mutations in BM paired with primary lung carcinoma using NGS revealed a higher incidence of *KRAS* mutations in lung cancer with BM [49]. In both lung cancer and BM, *KRAS*

mutations have been reported to be most prevalent in the G12C subtype [48,49], and sotorasib targeting G12C was approved by the U.S. Food and Drug Administration in 2021 for patients with locally advanced or metastatic NSCLC. Thus, *KRAS* profile analysis can serve as a basis for suggesting customized treatment for NSCLC and NSCLC BM patients with *KRAS* mutations.

Molecular alterations in *EGFR*, *ALK*, and *KRAS* in patients with NSCLC BM are significant information for planning treatment including drug selection. In this way, as molecular pathology develops and its influence gradually expands, pathologists should focus on molecular study in addition to histological examination and diagnosis.

Metastatic breast cancer

Hormone receptor and HER2 status in breast cancer play an important role in determining the direction of treatment. Several studies have reported discordance in receptor (ER, PR, and HER2) status between primary tumors and paired metastatic tumors. The conversion rates for each receptor were broad, ranging from 7.3% to 29.2% for ER, 2.4% to 38.1% for PR, and 2.3% to 23.8% for HER2 [4,50-58]. In this study, the conversion rates of receptors were 6.9% for ER, 27.6% for PR, and 3.4% for HER2. The conversion rates of PR and HER2 were within the range of previous studies, while the conversion rates of ER were comparatively lower. The reason for these results is not clear. Receptor conversion reported in another study conducted in South Korea was different from our study (ER, 9.5%, PR, 38.1%, HER2, 23.8%) [4]. In addition, no clear racial or geographic trends were found associated with a wide range of receptor conversion rates reported in previous studies. Although the exact reason is not known, it is thought that the receptor conversion may vary according to the unknown characteristics of the patients included in the study. A multicenter analysis of subtype switching reported that subtype conversion occurred due to changes in the receptor status, and the HER2 enriched and triple-negative types increased [58]. In this study, ERs were converted from positive to negative (2/2), PRs were predominantly converted from positive to negative (6/8), and HER2 was converted from negative to positive. Accordingly, one case each of luminal A type and luminal B type was converted to HER2-enriched type. Although the exact mechanisms by which discordance in receptor expression occurs have not been elucidated, several explanations have been made. Turner et al. [59] introduced three explanations, including the selection of existing clones that may have been obscured by bulk tumors, changes in molecular expression of hormone receptors and HER2, or both of these possibilities occur-

ring. In addition, inadequate fixation of the tumor tissue may also contribute to receptor conversion. Yildiz-Aktas et al. [60] reported that a delayed fixation time contributed to reduced immunostaining of hormone receptors and HER2 receptors. The ASCO/CAP guidelines recommend that cold ischemia time must be recorded and samples should be fixed in 10% neutral buffered formalin for 6 to 72 hours [61].

Receptor discrepancy between the primary tumor and BM may affect treatment decisions, so receptor status testing in BM tissue should be performed. ASCO Clinical Practice Guidelines recommend biopsy to determine ER, PR, and HER2 status in patients with newly diagnosed metastases, as receptor discrepancies can be found in the primary tumor and metastases [62].

Metastatic colon cancer

The *RAS* gene family consists of the proto-oncogenes *KRAS*, *NRAS*, and *HRAS*, and *RAS* mutations appear in various cancers. According to a study analyzing the COSMIC (The Catalog of Somatic Mutations in Cancer) database, the *KRAS*, *NRAS*, and *HRAS* mutation rates in the large intestine were 33%, 3%, and <1%, respectively [63]. Roussille et al. [64] reported that *KRAS* mutations were observed in 56% of primary tumor and 74% of BM, respectively, and *NRAS* mutations were observed in 6% and 11%, respectively. In primary tumors and BM, *KRAS* mutations were observed at exon 2 codon 12 and codon 13, and the most frequent were G12D and G12V [64]. Our results show that *KRAS* mutations were observed in 76.9% of primary tumors and 66.7% of BM, and *NRAS* mutations were not detected in either. In primary tumors, *KRAS* mutations were most frequently observed in exon 2 codon 12. In two cases of BM, *KRAS* mutations were observed in exon 2 codons 12 and 13, respectively. In our study, the incidence of *KRAS* mutations in primary tumors was 76.9%, which was higher than the previous study result of 56%. Differences in *KRAS* mutation rates in primary cancers are probably due to regional and ethnic differences. In a study researching *KRAS* mutation frequencies in Caucasian colorectal cancer patients, *KRAS* mutations were found in 38.3% [65]. A study of colorectal cancer patients in South Korea reported that *KRAS* mutations were found in 45.9% [66]. Meanwhile, the *KRAS* mutation rate of primary cancer was higher in this study compared to 30%–40% in previous studies [65,66], which seems to be because the study was conducted on BM patients. *RAS* mutation analysis in colorectal cancer patients reported that *RAS* mutations affect the increased incidence of lung, bone and BM [67]. As a result of our study, *KRAS* status in metastatic brain tumors was analyzed in three patients and found 66.7% of

mutations, but this is too small a number to discuss.

The incidence of *NRAS* mutations is low, as reported in 4% or 3.2% of colorectal cancer patients [65,68]. In our study, *NRAS* status was analyzed in eight cases of primary cancer and two cases of BM, so the results of the study do not represent the incidence of *NRAS* mutations. Therefore, additional studies with more patients should be conducted.

Molecular alterations different from the information obtained in the primary tumor can occur in the BM, and these differences can be detected by analysis of the molecular profile, providing clinical advantages in the selection of candidate targeted therapies. As the NGS platform is covered by medical insurance in South Korea, it has recently become a standard procedure in many institutions. NGS analysis of resected metastatic brain tumor tissue specimens provided treatment-associated mutations, contributing to the development of drug resistance.

A multidisciplinary approach is often required to discuss treatment plans for BM, and the molecular tumor board plays an important role in discussing the opinions of multiple medical experts, including pathologists. Molecular tumor board helps in the understanding of the results of molecular analysis and is of benefit in establishing treatment plans and clinical trial enrollment in patients with genetic alterations available to targeted therapy [69]. As the field of molecular medicine develops, the role of the pathologist as an important member of multidisciplinary teams is increasing. In particular, molecular studies are becoming more important in diagnosis and management due to discordance in target molecular mutations between BM and primary tumors. Therefore, in addition to the pathological diagnosis, pathologists will have to provide information on the molecular biomarkers.

For the first time, our study provided clinicopathological and molecular features of patients with BM in South Korea. The main limitation of this study is it's the single-center, retrospective design and molecular analysis results in the unpaired samples since most patients which were performed surgery of BM did not have analyzed molecular status for primary cancer. Moreover, we only included patients who underwent surgical resection of the BM tumor, so population selection bias occurred. Therefore, further studies on comparative analysis targeting primary cancer paired with BM should be conducted.

Ethics Statement

This study was approved by the Institutional Review Board of Seoul St. Mary's Hospital (KC17RES1033). Formal written informed consent was not required with a waiver by the appropriate IRB and/or national research ethics committee.

Availability of Data and Material

The datasets generated or analyzed during the study are available from the corresponding author on reasonable request.

Code Availability

Not applicable.

ORCID

Su Hwa Kim	https://orcid.org/0000-0001-8046-4988
Young Suk Lee	https://orcid.org/0000-0003-4794-639X
Sung Hak Lee	https://orcid.org/0000-0003-1020-5838
Yeoun Eun Sung	https://orcid.org/0000-0002-9408-0085
Ahwon Lee	https://orcid.org/0000-0002-2523-9531
Jun Kang	https://orcid.org/0000-0002-7967-0917
Jae-Sung Park	https://orcid.org/0000-0002-9827-9913
Sin Soo Jeun	https://orcid.org/0000-0001-8421-6455
Youn Soo Lee	https://orcid.org/0000-0002-1653-6315

Author Contributions

Conceptualization: YSL (Youn Soo Lee). Data curation: SHK, YSL (Young Suk Lee). Formal analysis: SHK, YSL (Young Suk Lee). Investigation: YSL (Youn Soo Lee), SHL, YES, AL, JK, JSP, SSJ. Supervision: YSL (Youn Soo Lee). Visualization: SHK. Writing—original draft: SHK, YSL (Youn Soo Lee), YSL (Young Suk Lee). Writing—review & editing: SHK, YSL (Youn Soo Lee). Approval of final manuscript: all authors.

Conflicts of Interest

S.H.L., a contributing editor of the *Journal of Pathology and Translational Medicine*, was not involved in the editorial evaluation or decision to publish this article. All remaining authors have declared no conflicts of interest.

Funding Statement

No funding to declare.

References

- Sacks P, Rahman M. Epidemiology of brain metastases. *Neurosurg Clin N Am* 2020; 31: 481-8.
- Barnholtz-Sloan JS, Sloan AE, Davis FG, Vigneau FD, Lai P, Sawaya RE. Incidence proportions of brain metastases in patients diagnosed (1973 to 2001) in the Metropolitan Detroit Cancer Surveillance System. *J Clin Oncol* 2004; 22: 2865-72.
- Counsell CE, Collie DA, Grant R. Incidence of intracranial tumours in the Lothian region of Scotland, 1989-90. *J Neurol Neurosurg Psychiatry* 1996; 61: 143-50.
- Jung J, Lee SH, Park M, et al. Discordances in ER, PR, and HER2 between primary breast cancer and brain metastasis. *J Neurooncol* 2018; 137: 295-302.
- Sundaresan N, Galicich JH. Surgical treatment of brain metastases: clinical and computerized tomography evaluation of the results of treatment. *Cancer* 1985; 55: 1382-8.
- Schackert G, Steinmetz A, Meier U, Sobottka SB. Surgical management of single and multiple brain metastases: results of a retrospective study. *Onkologie* 2001; 24: 246-55.
- Nahed BV, Alvarez-Breckenridge C, Brastianos PK, et al. Congress of neurological surgeons systematic review and evidence-based guidelines on the role of surgery in the management of adults with metastatic brain tumors. *Neurosurgery* 2019; 84: E152-5.
- Allred DC, Harvey JM, Berardo M, Clark GM. Prognostic and pre-

- dictive factors in breast cancer by immunohistochemical analysis. *Mod Pathol* 1998; 11: 155-68.
9. Wolff AC, Hammond ME, Allison KH, et al. Human epidermal growth factor receptor 2 testing in breast cancer: American Society of Clinical Oncology/College of American Pathologists clinical practice guideline focused update. *J Clin Oncol* 2018; 36: 2105-22.
 10. Wolff AC, Hammond ME, Hicks DG, et al. Recommendations for human epidermal growth factor receptor 2 testing in breast cancer: American Society of Clinical Oncology/College of American Pathologists clinical practice guideline update. *J Clin Oncol* 2013; 31: 3997-4013.
 11. Dowsett M, Nielsen TO, A'Hern R, et al. Assessment of Ki67 in breast cancer: recommendations from the International Ki67 in Breast Cancer working group. *J Natl Cancer Inst* 2011; 103: 1656-64.
 12. Goldhirsch A, Winer EP, Coates AS, et al. Personalizing the treatment of women with early breast cancer: highlights of the St Gallen International Expert Consensus on the Primary Therapy of Early Breast Cancer 2013. *Ann Oncol* 2013; 24: 2206-23.
 13. Jeong YS, Kang J, Lee J, Yoo TK, Kim SH, Lee A. Analysis of the molecular subtypes of preoperative core needle biopsy and surgical specimens in invasive breast cancer. *J Pathol Transl Med* 2020; 54: 87-94.
 14. Berghoff AS, Schur S, Fureder LM, et al. Descriptive statistical analysis of a real life cohort of 2419 patients with brain metastases of solid cancers. *ESMO Open* 2016; 1: e000024.
 15. Stark AM, Stohring C, Hedderich J, Held-Feindt J, Mehdorn HM. Surgical treatment for brain metastases: prognostic factors and survival in 309 patients with regard to patient age. *J Clin Neurosci* 2011; 18: 34-8.
 16. Sperduto PW, Chao ST, Sneed PK, et al. Diagnosis-specific prognostic factors, indexes, and treatment outcomes for patients with newly diagnosed brain metastases: a multi-institutional analysis of 4,259 patients. *Int J Radiat Oncol Biol Phys* 2010; 77: 655-61.
 17. Christensen TD, Spindler KL, Palshof JA, Nielsen DL. Systematic review: brain metastases from colorectal cancer: incidence and patient characteristics. *BMC Cancer* 2016; 16: 260.
 18. Siegel RL, Miller KD, Fuchs HE, Jemal A. Cancer statistics, 2022. *CA Cancer J Clin* 2022; 72: 7-33.
 19. Dyba T, Randi G, Bray F, et al. The European cancer burden in 2020: incidence and mortality estimates for 40 countries and 25 major cancers. *Eur J Cancer* 2021; 157: 308-47.
 20. Kang MJ, Won YJ, Lee JJ, et al. Cancer statistics in Korea: incidence, mortality, survival, and prevalence in 2019. *Cancer Res Treat* 2022; 54: 330-44.
 21. Che W, Liu J, Fu T, Wang X, Lyu J. Recent trends in synchronous brain metastasis incidence and mortality in the United States: ten-year multicenter experience. *Curr Oncol* 2022; 29: 8374-89.
 22. Hubbs JL, Boyd JA, Hollis D, Chino JP, Saynak M, Kelsey CR. Factors associated with the development of brain metastases: analysis of 975 patients with early stage nonsmall cell lung cancer. *Cancer* 2010; 116: 5038-46.
 23. Sun MS, Yun YY, Liu HJ, Yu ZH, Yang F, Xu L. Brain metastasis in de novo breast cancer: an updated population-level study from SEER database. *Asian J Surg* 2022; 45: 2259-67.
 24. Yang L, He W, Xie Q, et al. Brain metastases in newly diagnosed colorectal cancer: a population-based study. *Cancer Manag Res* 2018; 10: 5649-58.
 25. Zhang YL, Yuan JQ, Wang KF, et al. The prevalence of *EGFR* mutation in patients with non-small cell lung cancer: a systematic review and meta-analysis. *Oncotarget* 2016; 7: 78985-93.
 26. Villalva C, Duranton-Tanneur V, Guilloteau K, et al. *EGFR*, *KRAS*, *BRAF*, and *HER-2* molecular status in brain metastases from 77 NSCLC patients. *Cancer Med* 2013; 2: 296-304.
 27. Nicos M, Krawczyk P, Jarosz B, et al. Screening for gene mutations in central nervous system metastases of non-small-cell lung cancer. *Brain Pathol* 2018; 28: 295-7.
 28. Luo D, Ye X, Hu Z, et al. *EGFR* mutation status and its impact on survival of Chinese non-small cell lung cancer patients with brain metastases. *Tumour Biol* 2014; 35: 2437-44.
 29. Rau KM, Chen HK, Shiu LY, et al. Discordance of mutation statuses of epidermal growth factor receptor and K-ras between primary adenocarcinoma of lung and brain metastasis. *Int J Mol Sci* 2016; 17: 524.
 30. Kim KM, Lee SH, Kim SM, et al. Discordance of epidermal growth factor receptor mutation between brain metastasis and primary non-small cell lung cancer. *Brain Tumor Res Treat* 2019; 7: 137-40.
 31. Gow CH, Chang YL, Hsu YC, et al. Comparison of epidermal growth factor receptor mutations between primary and corresponding metastatic tumors in tyrosine kinase inhibitor-naive non-small-cell lung cancer. *Ann Oncol* 2009; 20: 696-702.
 32. Cheng X, Chen H. Tumor heterogeneity and resistance to *EGFR*-targeted therapy in advanced nonsmall cell lung cancer: challenges and perspectives. *Onco Targets Ther* 2014; 7: 1689-704.
 33. Marusyk A, Polyak K. Tumor heterogeneity: causes and consequences. *Biochim Biophys Acta* 2010; 1805: 105-17.
 34. Rosell R, Moran T, Queralt C, et al. Screening for epidermal growth factor receptor mutations in lung cancer. *N Engl J Med* 2009; 361: 958-67.
 35. Yu HA, Arcila ME, Rekhtman N, et al. Analysis of tumor specimens at the time of acquired resistance to *EGFR*-TKI therapy in 155 patients with *EGFR*-mutant lung cancers. *Clin Cancer Res* 2013; 19: 2240-7.
 36. Sequist LV, Waltman BA, Dias-Santagata D, et al. Genotypic and histological evolution of lung cancers acquiring resistance to *EGFR* inhibitors. *Sci Transl Med* 2011; 3: 75ra26.
 37. Koivunen JP, Mermel C, Zejnullahu K, et al. *EML4-ALK* fusion gene and efficacy of an *ALK* kinase inhibitor in lung cancer. *Clin Cancer Res* 2008; 14: 4275-83.
 38. Wong DW, Leung EL, So KK, et al. The *EML4-ALK* fusion gene is involved in various histologic types of lung cancers from nonsmokers with wild-type *EGFR* and *KRAS*. *Cancer* 2009; 115: 1723-33.
 39. Perner S, Wagner PL, Demicheli F, et al. *EML4-ALK* fusion lung cancer: a rare acquired event. *Neoplasia* 2008; 10: 298-302.
 40. Fallet V, Cadranet J, Doubre H, et al. Prospective screening for *ALK*: clinical features and outcome according to *ALK* status. *Eur J Cancer* 2014; 50: 1239-46.
 41. Rangachari D, Yamaguchi N, VanderLaan PA, et al. Brain metastases in patients with *EGFR*-mutated or *ALK*-rearranged non-small-cell lung cancers. *Lung Cancer* 2015; 88: 108-11.
 42. Costa DB, Kobayashi S, Pandya SS, et al. CSF concentration of the anaplastic lymphoma kinase inhibitor crizotinib. *J Clin Oncol* 2011; 29: e443-5.
 43. Barlesi F, Dingemans AM, Yang JC, et al. Updated efficacy and safety from the global phase II NP28673 study of alectinib in patients (pts) with previously treated *ALK+* non-small-cell lung cancer (NSCLC). *Ann Oncol* 2016; 27(Suppl 6): VI437.

44. Kim DW, Tiseo M, Ahn MJ, et al. Brigatinib in patients with crizotinib-refractory anaplastic lymphoma kinase-positive non-small-cell lung cancer: a randomized, multicenter phase II trial. *J Clin Oncol* 2017; 35: 2490-8.
45. Cancer Genome Atlas Research Network. Comprehensive molecular profiling of lung adenocarcinoma. *Nature* 2014; 511: 543-50.
46. Imielinski M, Berger AH, Hammerman PS, et al. Mapping the hallmarks of lung adenocarcinoma with massively parallel sequencing. *Cell* 2012; 150: 1107-20.
47. Kalikaki A, Koutsopoulos A, Trypaki M, et al. Comparison of *EGFR* and *K-RAS* gene status between primary tumours and corresponding metastases in NSCLC. *Br J Cancer* 2008; 99: 923-9.
48. Timar J, Kashofer K. Molecular epidemiology and diagnostics of *KRAS* mutations in human cancer. *Cancer Metastasis Rev* 2020; 39: 1029-38.
49. Vassella E, Kashani E, Zens P, et al. Mutational profiles of primary pulmonary adenocarcinoma and paired brain metastases disclose the importance of *KRAS* mutations. *Eur J Cancer* 2021; 159: 227-36.
50. Yonemori K, Tsuta K, Shimizu C, et al. Immunohistochemical profiles of brain metastases from breast cancer. *J Neurooncol* 2008; 90: 223-8.
51. Hoefnagel LD, van de Vijver MJ, van Slooten HJ, et al. Receptor conversion in distant breast cancer metastases. *Breast Cancer Res* 2010; 12: R75.
52. Omoto Y, Kurosumi M, Hozumi Y, et al. Immunohistochemical assessment of primary breast tumors and metachronous brain metastases, with particular regard to differences in the expression of biological markers and prognosis. *Exp Ther Med* 2010; 1: 561-7.
53. Brogi E, Murphy CG, Johnson ML, et al. Breast carcinoma with brain metastases: clinical analysis and immunoprofile on tissue microarrays. *Ann Oncol* 2011; 22: 2597-603.
54. Duchnowska R, Dziadziuszko R, Trojanowski T, et al. Conversion of epidermal growth factor receptor 2 and hormone receptor expression in breast cancer metastases to the brain. *Breast Cancer Res* 2012; 14: R119.
55. Shen Q, Sahin AA, Hess KR, et al. Breast cancer with brain metastases: clinicopathologic features, survival, and paired biomarker analysis. *Oncologist* 2015; 20: 466-73.
56. Thomson AH, McGrane J, Mathew J, et al. Changing molecular profile of brain metastases compared with matched breast primary cancers and impact on clinical outcomes. *Br J Cancer* 2016; 114: 793-800.
57. Jiabin C, Jinmei Z, Huiqiang Z, et al. Conversion of ER, PR, HER2 and Ki-67 and prognosis in breast cancer metastases to the brain. *Front Neurol* 2022; 13: 1002173.
58. Hulsbergen AFC, Claes A, Kavouridis VK, et al. Subtype switching in breast cancer brain metastases: a multicenter analysis. *Neuro Oncol* 2020; 22: 1173-81.
59. Turner KM, Yeo SK, Holm TM, Shaughnessy E, Guan JL. Heterogeneity within molecular subtypes of breast cancer. *Am J Physiol Cell Physiol* 2021; 321: C343-54.
60. Yildiz-Aktas IZ, Dabbs DJ, Bhargava R. The effect of cold ischemic time on the immunohistochemical evaluation of estrogen receptor, progesterone receptor, and HER2 expression in invasive breast carcinoma. *Mod Pathol* 2012; 25: 1098-105.
61. Allison KH, Hammond ME, Dowsett M, et al. Estrogen and progesterone receptor testing in breast cancer: ASCO/CAP guideline update. *J Clin Oncol* 2020; 38: 1346-66.
62. Van Poznak C, Harris LN, Somerfield MR. Use of biomarkers to guide decisions on systemic therapy for women with metastatic breast cancer: American Society of Clinical Oncology clinical practice guideline. *J Oncol Pract* 2015; 11: 514-6.
63. Prior IA, Lewis PD, Mattos C. A comprehensive survey of Ras mutations in cancer. *Cancer Res* 2012; 72: 2457-67.
64. Roussille P, Tachon G, Villalva C, et al. Pathological and molecular characteristics of colorectal cancer with brain metastases. *Cancers (Basel)* 2018; 10: 504.
65. Bozyk A, Krawczyk P, Reszka K, et al. Correlation between *KRAS*, *NRAS* and *BRAF* mutations and tumor localizations in patients with primary and metastatic colorectal cancer. *Arch Med Sci* 2022; 18: 1221-30.
66. Lee SH, Chung AM, Lee A, et al. *KRAS* mutation test in Korean patients with colorectal carcinomas: a methodological comparison between Sanger sequencing and a real-time PCR-based assay. *J Pathol Transl Med* 2017; 51: 24-31.
67. Yaeger R, Cowell E, Chou JF, et al. *RAS* mutations affect pattern of metastatic spread and increase propensity for brain metastasis in colorectal cancer. *Cancer* 2015; 121: 1195-203.
68. Li Y, Xiao J, Zhang T, Zheng Y, Jin H. Analysis of *KRAS*, *NRAS*, and *BRAF* mutations, microsatellite instability, and relevant prognosis effects in patients with early colorectal cancer: a cohort study in East Asia. *Front Oncol* 2022; 12: 897548.
69. Behel V, Noronha V, Choughule A, et al. Impact of molecular tumor board on the clinical management of patients with cancer. *JCO Glob Oncol* 2022; 8: e2200030.

Loss of aquaporin-1 expression is associated with worse clinical outcomes in clear cell renal cell carcinoma: an immunohistochemical study

Seokhyeon Lee¹, Bohyun Kim², Minsun Jung³, Kyung Chul Moon^{1,4}

¹Department of Pathology, Seoul National University College of Medicine, Seoul;

²Department of Pathology, Konkuk University Medical Center, Konkuk University School of Medicine, Seoul;

³Department of Pathology, Yonsei University College of Medicine, Seoul;

⁴Kidney Research Institute, Medical Research Center, Seoul National University College of Medicine, Seoul, Korea

Background: Aquaporin (AQP) expression has been investigated in various malignant neoplasms, and the overexpression of AQP is related to poor prognosis in some malignancies. However, the expression of AQP protein in clear cell renal cell carcinoma (ccRCC) has not been extensively investigated by immunohistochemistry with large sample size. **Methods:** We evaluated the AQP expression in 827 ccRCC with immunohistochemical staining in tissue microarray blocks and classified the cases into two categories, high and low expression. **Results:** High expression of aquaporin-1 (AQP1) was found in 320 cases (38.7%), but aquaporin-3 was not expressed in ccRCC. High AQP1 expression was significantly related to younger age, low TNM stage, low World Health Organization/International Society of Urologic Pathology nuclear grade, and absence of distant metastasis. Furthermore, high AQP1 expression was also significantly associated with longer overall survival (OS; $p < .001$) and progression-specific survival (PFS; $p < .001$) and was an independent predictor of OS and PFS in ccRCC. **Conclusions:** Our study revealed the prognostic significance of AQP1 protein expression in ccRCC. These findings could be applied to predict the prognosis of ccRCC.

Key Words: Aquaporin; Clear cell renal cell carcinoma; Immunohistochemistry; Prognosis

Received: March 27, 2023 **Revised:** May 22, 2023 **Accepted:** June 16, 2023

Corresponding Author: Kyung Chul Moon, MD, PhD, Department of Pathology, Kidney Research Institute, Medical Research Center, Seoul National University College of Medicine, 103 Daehak-ro, Jongno-gu, Seoul, Korea

Tel: +82-2-740-8380, Fax: +82-2-743-5530, E-mail: blue7270@snu.ac.kr

Renal cell carcinoma (RCC) is one of the most common and clinically important malignant neoplasms of the urinary tract. Its prognosis is favorable when found early and completely resected, but it could be potentially aggressive and fatal with advanced stage, high World Health Organization (WHO)/International Society of Urologic Pathology (ISUP) nuclear grade, and/or distant metastasis. Clear cell renal cell carcinoma (ccRCC) is the most common histologic subtype of RCC and is known to have an unfavorable prognosis compared with other common subtypes. Therefore, ccRCC has been the main topic in several genitourinary oncologic and pathologic studies.

Aquaporins (AQPs) are cell membrane proteins that act as water transporters, facilitating the permeation of water through the plasma membrane [1]. Twelve members of the AQP family are expressed in different types of normal tissue and cells. Earlier studies have shown that AQPs are associated with several character-

istics of malignancies, such as cellular motility, migration, angiogenesis, and metastasis, and may be potential targets for anticancer therapies [2-4]. The overexpression of AQP has been observed in several malignancies. For instance, Kang et al. [5] investigated the relationship between the levels of AQP1, AQP3, and AQP5 expression by immunohistochemistry and several clinical variables in colorectal carcinoma and concluded that lymph node metastasis is positively related to a high level of AQP expression. In a systematic review regarding the relationship of AQP1, AQP3, and AQP5 expressions with different tumors reported by Moosavi and Elham [6], overexpression of AQPs contributed to the pathogenesis of malignant neoplasms and was associated with unfavorable clinical outcomes in malignancies, e.g., gastric, breast, pancreatic, lung, and colorectal carcinomas.

Notably, AQPs may have an unusual relationship with tumorigenesis in genitourinary tumors compared to malignancies of

other origins. This may be explained by the expression of AQPs in the normal renal parenchyma and urothelium. Ticozzi-Valerio et al. [7] showed that the proteomic level of AQP1 expression was significantly lower in ccRCC cells than in adjacent normal proximal tubular epithelial cells using electrophoresis and immunoblotting in small number of ccRCC specimen. Huang et al. [8] reported that the high AQP1 mRNA expression is related to less aggressive characteristics, such as lower grade, smaller tumor size, lower pathological stage, absence of microvascular invasion and symptomatic disease, as well as more favorable outcomes, such as better cancer-specific and cancer-free survival using quantitative real time polymerase chain reaction in ccRCC. Otto et al. [9] demonstrated that the loss of AQP3 expression by immunohistochemistry is significantly associated with worse prognosis-free survival in non-muscle invasive (stage pT1) urothelial carcinoma of the urinary bladder. Therefore, one could hypothesize that AQP expression is related to the degree of aggressiveness in urinary tract neoplasms. However, there has not yet been a study that evaluated the AQP protein expression in ccRCC by immunohistochemistry in a large number of samples.

In this study, we conducted immunohistochemical staining of AQP1 and AQP3 in ccRCC tissue microarrays (TMAs) from nephrectomy specimens and evaluated the expression of AQP and its clinical significance.

MATERIALS AND METHODS

The subjects of this study were 827 primary sporadic ccRCC patients who underwent partial or radical nephrectomy from 2006 to 2011 at Seoul National University Hospital. The clinical data corresponding to tissue specimens were collected from electronic medical records of the hospital. Clinical stage and nuclear grade of carcinomas were assigned according to the American Joint of Committee on Cancer 8th TNM staging and World Health Organization/International Society of Urologic Pathology (WHO/ISUP) nuclear grade, respectively. The representative tumor portions of ccRCC specimen blocks were selected in each case. Two representative cores with 2 mm-diameter was taken from tumor blocks and embedded to new recipient blocks using trephine apparatus (Superbiochips Laboratories, Seoul, Korea).

Tissue microarray (TMA) blocks were cut to make several unstained slides for histopathological and immunohistochemical analyses. Hematoxylin and eosin slides were made for histopathological assessment of TMAs. Immunohistochemical staining was performed using Ventana Benchmark XT automated staining system (Ventana Medical Systems, Tucson, AZ, USA). The

4- μ m-thick slides were stained with anti-AQP1 mouse monoclonal IgG1 antibody (1:100, Santa Cruz Biotechnology, Santa Cruz, CA, USA) and anti-AQP3 IgG1 antibody (1:100, Abcam, Cambridge, UK). The intensity of AQP expression in each slide was scored semi-quantitatively, incorporating the intensity and percentage of RCC cells with membranous stain positivity. The intensity was evaluated with scores of 0–3: 0 for negative staining; 1 for faint positivity; 2 for weak to moderate positivity; and 3 for strong positivity. The percentage of positive tumor cells was scored on a 0–4-point basis: 0 for 0%; 1 for 1 to 25%; 2 for 26 to 50%; 3 for 51–75%; and 4 for more than 75%. Next, the total AQP expression score was produced by the sum of two points and allocated to three categories: AQP-negative for 0–2; weakly AQP-positive for 3–5; and strongly AQP-positive for 6–7 [5]. Finally, both AQP-negative and weakly AQP-positive categories were considered as losing AQP1 expression significantly and allocated to “low” AQP1 expression group, and strongly AQP-positive category was allocated to “high” AQP1 expression group.

Clinical data and immunohistochemical AQP expression scores of TMAs were integrated and statistically analyzed using the R programming language (ver. 4.2.2) with the packages ‘survival’, ‘survminer’ and ‘dplyr’. The overall survival (OS) duration was defined as the interval from the date of surgical resection to death or the last follow-up. The progression-free survival (PFS) duration was defined as the interval from the date of surgical resection to the event of progression, such as death; local recurrence; distant metastasis; or disease progression after chemotherapy, immunotherapy, or radiotherapy. Kaplan-Meier analysis and log-rank tests were conducted to evaluate and compare OS and PFS between patients divided by binominal or dichotomized continuous clinicopathological variables, i.e., low (1, 2) and high (3, 4) TNM stage and/or WHO/ISUP nuclear grade, as well as with weakly and strongly AQP-positive ccRCC. Multivariate Cox regression model was established by statistically significant variables in univariate analyses, and the multivariate analysis was applied to assess the potential clinical significance of AQP expression by immunohistochemistry. A p-value less than .05 was interpreted as statistically significant.

RESULTS

Patient characteristics

Clinicopathological characteristics of the patients are shown in Table 1. The group showed prominent male predominance, and the mean age was 56.5 years. The average size of the tumor was 4.2 cm. TNM stage 1 was the most common of the four stages.

Table 1. Summary of clinicopathological characteristics of the patients

Characteristic	Value
Age (yr)	56.5 ± 12.3
Sex (%)	
Male	619 (74.9)
Female	207 (25.1)
Tumor size (cm)	4.2 ± 2.7
TNM stage (%)	
Stage I	637 (77.0)
Stage II	34 (4.1)
Stage III	96 (11.6)
Stage IV	60 (7.3)
Nuclear grade (%)	
Grade 1	33 (4.0)
Grade 2	424 (51.3)
Grade 3	322 (38.9)
Grade 4	48 (5.8)
Survival (month)	
Overall survival	91.8 ± 40.3
Progression-free survival	79.5 ± 42.4
AQP1 expression (%)	
High	320 (38.7)
Low	507 (61.3)

Values are presented as mean ± standard deviation or number (%). AQP, aquaporin.

The WHO/ISUP nuclear grades 2 and 3 accounted for major proportion in the group. The mean OS interval and PFS interval were 91.8 and 79.5 months, respectively.

Aquaporin expression in ccRCC

AQP immunohistochemical staining was mainly present in the membrane. After evaluation, AQP1 expression was high in 320 cases (38.7%), and low in 507 cases (61.3%) (Fig. 1). On the other hand, the AQP3 expression level was exceptionally low in all cases compared to AQP1 expression, preventing it from being investigated statistically (Fig. 2).

Relationships of aquaporin expression and clinicopathological characteristics

Next, we examined whether there were statistically significant correlations between clinicopathological characteristics and AQP1 expression levels. First, we assigned the patient population to each of the four characteristics. The cutoff for patient age was 55 years. TNM stage and nuclear grade were grouped as “low” for stage/grade 1 to 2 and “high” for stage/grade 3 to 4. The state of distant metastasis (M category) was incorporated for the analysis. Consequently, Fisher’s exact test demonstrated that lower AQP1 expression presented statistically significant correlation with

higher (55 or more) age of the patient, “high” TNM stage (3 or 4) and nuclear grade (3 or 4), the presence of distant metastasis (M1), and presence of microvascular invasion (Table 2).

Impact of aquaporin expressions on survival

Next, we investigated the impact of AQP1 expression level on OS and PFS periods. The survival curves corresponding to OS and PFS, derived from the Kaplan-Meier method are shown in Fig. 3. Survival rates according to AQP1 expression level demonstrated significant difference in both curves, inferring that decreased expression level of AQP1 in clear cell RCC is associated with undesirable clinical outcomes and shorter survival periods. This finding is in accordance with prior statistical analyses showing the relationship of low AQP1 expression level with worse clinicopathological features.

We also conducted multivariate Cox proportional hazards regression analysis corresponding to both OS and PFS to investigate the ability of AQP1 expression to be an independent risk factor in ccRCC. First, univariate analyses were conducted for several clinicopathological factors (Table 3). In univariate analyses, TNM stage, WHO/ISUP nuclear grade, and AQP1 expression level were selected as basic components of the multivariate Cox proportional hazards model (Tables 3, 4). As a result, lower AQP1 expression level showed statistical significance to be an independent predictor of worse OS and PFS in the model.

DISCUSSION

In this study, we demonstrated that lower expression of AQP1 is related to more advanced clinical stage, higher WHO/ISUP nuclear grade, microvascular invasion, and shorter OS and PFS. To our knowledge, this study provides the first evidence that AQP expression level as evaluated by immunohistochemistry has a similar relationship to ccRCC, compared with prior proteomic [7] and transcriptomic [8] studies of AQP1.

AQPs are expressed in normal kidney parenchyma, especially in tubules and the collecting duct system [10]. AQP1 is known to be differentially expressed in proximal tubular epithelial cells, whereas AQP2, AQP3, and AQP4 are mainly located in distal tubules and collecting ducts. Considering that ccRCCs arise from proximal tubular epithelial cells and that a higher WHO/ISUP nuclear grade is significantly associated with a low AQP1 expression level in ccRCC, we can speculate that the loss of AQP1 in ccRCC reflects the loss of differentiation, which is commonly observed in carcinogenesis. As stated in previous publications covering non-urogenital malignancies, aberrant expression of

AQPs could occur [5,11] and may have different correlations with RCCs. In this study, AQP3 was the candidate for such aberrant expression in ccRCC, not showing evidence of expression by im-

munohistochemistry. This point is worth investigating in additional studies.

Some previous studies showed that higher AQP1 expression

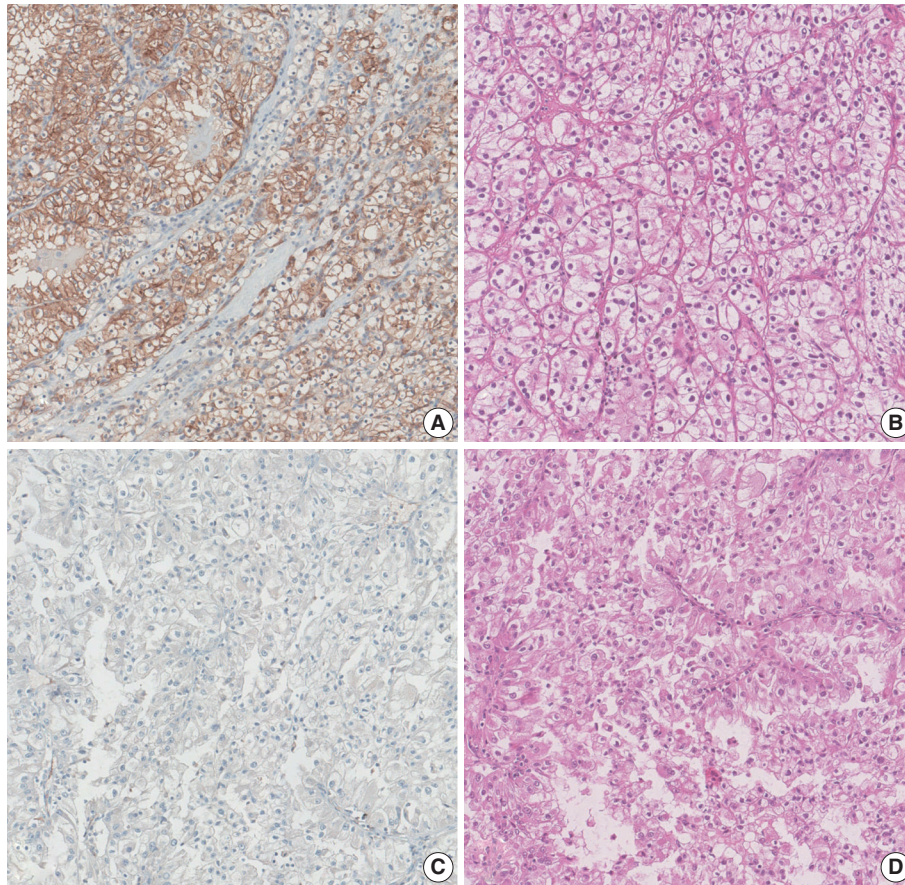


Fig. 1. Representative photographs of the expression levels of aquaporin 1 (AQP1) by immunohistochemistry and corresponding hematoxylin and eosin-stained slides. High expression of AQP1 (A) is associated with favorable histopathology and lower pathological stage (B), and low expression of AQP1 (C) is associated with unfavorable histological features and higher pathological stage (D).

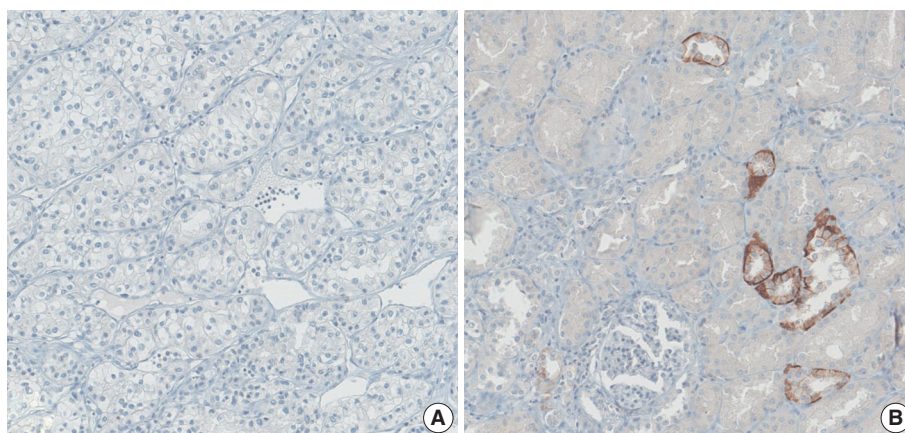


Fig. 2. Representative photographs of the expression levels of aquaporin 3 (AQP3) by immunohistochemistry slides. In contrast to aquaporin 1, the staining intensity of AQP3 was too low in every clear cell renal cell carcinoma tissue (A) to evaluate and analyze statistically. Distal tubular epithelial cells, which normally express the AQP3 protein, are positive for AQP3 immunostaining (B).

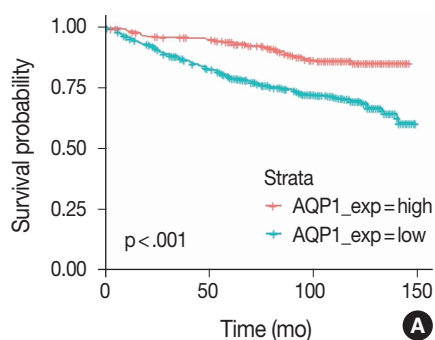
is associated with aggressive clinicopathological characteristics in some malignancies, such as pancreatic ductal adenocarcinoma [12] and cholangiocarcinoma [13]. On the contrary, the results of this study showed that lower AQP1 expression is associated with aggressive clinicopathological characteristics in ccRCC. The mechanisms for the opposite effect in different carcinomas are not well investigated and additional studies are needed to demonstrate the underlying mechanism of this difference.

Further research on the correlation between AQPs and other common and clinically significant subtypes of RCC, e.g., papillary and chromophobe RCC, is anticipated. Other subtypes of AQP might show different relationships between aggressive clinicopathological parameters of RCC. Xu et al. [14] reported elevated AQP9 mRNA expression in ccRCCs of advanced clinical stages with shorter OS and PFS, suggesting that AQP9 could act as an oncogene in ccRCC. This could be a possible topic for later

Table 2. Correlations between clinicopathological characteristics and AQP expression

Characteristics	No. (%)	Low AQP1 expression (%)	p-value
Age (yr)			
≥55	471 (57.0)	67.3	<.001
<55	356 (43.0)	53.4	
pTNM stage			
I, II	671 (81.1)	55.4	<.001
III, IV	156 (18.9)	86.5	
Nuclear grade			
1, 2	457 (55.3)	50.5	<.001
3, 4	370 (44.7)	74.6	
Distant metastasis			
Present	58 (7.0)	86.2	<.001
Absent	769 (93.0)	59.4	
Microvascular invasion			
Present	43 (5.2)	0.9	<.001
Absent	784 (94.8)	7.9	

AQP, aquaporin; pTNM, pathological tumor–node–metastasis.



studies about AQPs and malignancies.

Several previous studies have utilized interventional agents to investigate the potential of AQP as a target of anticancer therapies. AqB013, a small molecule AQP1 inhibitor, demonstrated the potential to prevent cancer cell migration and angiogenesis in colorectal carcinoma cell lines [15]. The microRNA miR-874 showed the ability to inhibit *AQP3* gene transcription and down-regulate the level of AQP3 protein expression, impeding gastric carcinoma cell lines to form tumors, migrate, and metastasize [16]. These results propose the possibility that loss of AQP expression

Table 3. Univariate analysis of overall and progression-free survival (Cox proportional hazard model)

Prognostic factor	Overall survival		Progression-free survival	
	Hazard ratio (95% CI)	p-value	Hazard ratio (95% CI)	p-value
pTNM stage				
III, IV vs. I, II	5.94 (4.45–7.94)	<.001	12.11 (8.45–17.36)	<.001
Nuclear grade				
3, 4 vs. 1, 2	2.95 (1.96–3.60)	<.001	5.02 (3.32–7.58)	<.001
AQP1 expression				
Low vs. High	2.58 (1.80–3.67)	<.001	3.65 (2.29–5.82)	<.001

CI, confidence interval; pTNM, pathological tumor–node–metastasis; AQP, aquaporin.

Table 4. Multivariate analysis of overall and progression-free survival (Cox proportional hazard model)

Prognostic factor	Overall survival		Progression-free survival	
	Hazard ratio (95% CI)	p-value	Hazard ratio (95% CI)	p-value
pTNM stage				
III, IV vs. I, II	7.86 (5.25–11.78)	<.001	4.56 (3.27–6.34)	<.001
Nuclear grade				
3, 4 vs. 1, 2	1.98 (1.24–3.15)	.004	1.36 (0.96–1.92)	.086
AQP1 expression				
Low vs. High	1.85 (1.24–3.15)	.013	1.74 (1.20–2.50)	.003

CI, confidence interval; pTNM, pathological tumor–node–metastasis; AQP, aquaporin.

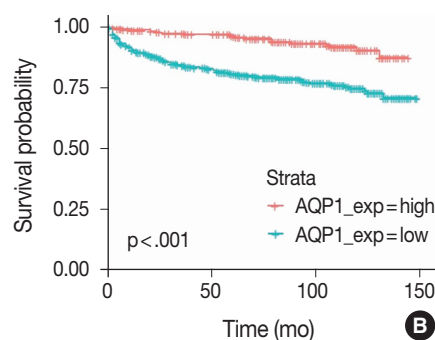


Fig. 3. Overall (A) and progression-free (B) survival curves showing Kaplan-Meier survival probability by time. The difference in overall and progression-free survival rates between higher and lower aquaporin 1 (AQP1) expression was statistically significant in both respects of survival.

in ccRCC could be an exploitable characteristic to be utilized for targeted anticancer therapies.

The study may have some potential limitations, which might have impacted the results and are worth discussing. For instance, only ccRCC cases were incorporated in the study, leaving other common or clinically important subtypes of renal cell carcinomas uninvestigated, such as papillary RCC, chromophobe RCC, collecting duct carcinoma, and medullary carcinoma. Further research is required to investigate the association of AQP expression and these renal malignancies. Despite this, we demonstrated the potential utility of aquaporin family proteins in ccRCC as tools to predict the clinical behavior and prognosis of this clinically important malignancy.

In conclusion, loss of AQP1 expression, evaluated by immunohistochemistry, is related to worse clinicopathological parameters and shorter survival in ccRCC. It would be potentially applied to predict prognosis and develop target anticancer agents.

Ethics Statement

All procedures performed in the current study were approved by the Institutional Review Board of Seoul National University Hospital (IRB No. H-2112-120-1284) in accordance with the 1964 Helsinki Declaration and its later amendments. Informed consent was waived due to the minimal risk and the retrospective nature of this study by the Institutional Review Board.

Availability of Data and Material

The data of this study are available from the corresponding author on reasonable request.

Code Availability

Not applicable.

ORCID

Seokhyeon Lee <https://orcid.org/0000-0001-8945-2238>
Bohyun Kim <https://orcid.org/0000-0002-4097-4710>
Minsun Jung <https://orcid.org/0000-0002-8701-4282>
Kyung Chul Moon <https://orcid.org/0000-0002-1969-8360>

Author Contributions

Conceptualization: SL, KCM. Data curation: SL, BK, MJ. Methodology: SL, BK, MJ. Project administration: KCM. Resources: SL, BK, MJ, KCM. Supervision: KCM. Validation: BK, MJ. Visualization: SL. Writing—original draft: SL. Writing—review & editing: SL, KCM. Approval of final manuscript: all authors.

Conflicts of Interest

The authors declare that they have no potential conflicts of interest.

Funding Statement

This research was supported by Research Program 2021 (Kim Hun Research Fund) funded by Seoul National University College of Medicine Research Foundation.

References

1. Agre P, King LS, Yasui M, et al. Aquaporin water channels: from atomic structure to clinical medicine. *J Physiol* 2002; 542: 3-16.
2. Chen J, Wang Z, Xu D, Liu Y, Gao Y. Aquaporin 3 promotes prostate cancer cell motility and invasion via extracellular signal-regulated kinase 1/2-mediated matrix metalloproteinase-3 secretion. *Mol Med Rep* 2015; 11: 2882-8.
3. Kusayama M, Wada K, Nagata M, et al. Critical role of aquaporin 3 on growth of human esophageal and oral squamous cell carcinoma. *Cancer Sci* 2011; 102: 1128-36.
4. Yang J, Zhang JN, Chen WL, et al. Effects of AQP5 gene silencing on proliferation, migration and apoptosis of human glioma cells through regulating EGFR/ERK/p38 MAPK signaling pathway. *Oncotarget* 2017; 8: 38444-55.
5. Kang BW, Kim JG, Lee SJ, et al. Expression of aquaporin-1, aquaporin-3, and aquaporin-5 correlates with nodal metastasis in colon cancer. *Oncology* 2015; 88: 369-76.
6. Moosavi MS, Elham Y. Aquaporins 1, 3 and 5 in different tumors, their expression, prognosis value and role as new therapeutic targets. *Pathol Oncol Res* 2020; 26: 615-25.
7. Ticozzi-Valerio D, Raimondo F, Pitto M, et al. Differential expression of AQP1 in microdomain-enriched membranes of renal cell carcinoma. *Proteomics Clin Appl* 2007; 1: 588-97.
8. Huang Y, Murakami T, Sano F, et al. Expression of aquaporin 1 in primary renal tumors: a prognostic indicator for clear-cell renal cell carcinoma. *Eur Urol* 2009; 56: 690-8.
9. Otto W, Rubenwolf PC, Burger M, et al. Loss of aquaporin 3 protein expression constitutes an independent prognostic factor for progression-free survival: an immunohistochemical study on stage pT1 urothelial bladder cancer. *BMC Cancer* 2012; 12: 459.
10. Bedford JJ, Leader JP, Walker RJ. Aquaporin expression in normal human kidney and in renal disease. *J Am Soc Nephrol* 2003; 14: 2581-7.
11. Sato K, Miyamoto M, Takano M, Furuya K, Tsuda H. Different prognostic implications of aquaporin-1 and aquaporin-5 expression among different histological types of ovarian carcinoma. *Pathol Oncol Res* 2020; 26: 263-71.
12. Zou W, Yang Z, Li D, Liu Z, Zou Q, Yuan Y. AQP1 and AQP3 expression are associated with severe symptoms and poor-prognosis of the pancreatic ductal adenocarcinoma. *Appl Immunohistochem Mol Morphol* 2019; 27: 40-7.
13. Li C, Li X, Wu L, Jiang Z. Elevated AQP1 expression is associated with unfavorable oncologic outcome in patients with hilar cholangiocarcinoma. *Technol Cancer Res Treat* 2017; 16: 421-7.
14. Xu WH, Shi SN, Xu Y, et al. Prognostic implications of aquaporin 9 expression in clear cell renal cell carcinoma. *J Transl Med* 2019; 17: 363.
15. Dorward HS, Du A, Bruhn MA, et al. Pharmacological blockade of aquaporin-1 water channel by AqB013 restricts migration and invasiveness of colon cancer cells and prevents endothelial tube formation in vitro. *J Exp Clin Cancer Res* 2016; 35: 36.
16. Jiang B, Li Z, Zhang W, et al. miR-874 Inhibits cell proliferation, migration and invasion through targeting aquaporin-3 in gastric cancer. *J Gastroenterol* 2014; 49: 1011-25.

Metastatic choroidal melanoma in the breast: a case report and review of the literature

Loay Abudalu¹, Vinisha Malhotra¹, Nabila Nasir², Sami Titi¹

¹Diagnostics and Pharmacy Group, Northern Care Alliance NHS Group, Oldham Care Organization, Cellular Pathology Department, Oldham, UK;

²Department of Surgery, North Manchester General Hospital Manchester, Manchester University NHS Foundation Trust, Manchester, UK

The breast is an unusual site for metastases, accounting for less than 2% of malignant breast lesions but include those from malignant melanomas, carcinomas, sarcomas, and lymphomas from various organs. We diagnosed a very rare case of metastatic choroidal melanoma for a 67-year-old female who presented with a right breast lump and who had been previously diagnosed with choroidal melanoma-monosomy 3 in 2017. To the best of our knowledge, only five such cases have been published so far, with one in a male patient.

Key Words: Breast neoplasms; Uveal melanoma; Metastasis

Received: February 14, 2023 **Revised:** May 25, 2023 **Accepted:** June 7, 2023

Corresponding Author: Loay Abudalu, MD, MSc, Northern Care Alliance NHS Group, Oldham Care Organization, Cellular Pathology Department, Rochdale Road, Oldham, O11 2JH, UK

Tel: +44-1616561878, E-mail: Loay.Abudalu@nca.nhs.uk

The breast is an unusual site for metastases, which represent less than 2% of malignant breast lesions but include those from malignant melanomas, carcinomas, sarcomas, and lymphomas from various organs [1]. Due to their scarcity, metastatic lesions in the breast are often misdiagnosed as primary breast cancers, which can result in inappropriate treatment.

The most common sites of uveal melanoma (UM) are the choroidal melanocytes (85%–90%), the ciliary body (5%–8%), and the iris (3%–5%) [2]. UM affects approximately 500–600 patients every year in the United Kingdom, and age at presentation is approximately 60 years, except for iris melanomas which usually present at a younger age [3]. Outcomes for uveal melanomas are poor once metastasis occurs; median survival from the time of development of distant metastatic disease is 2–12 months and 1-year survival is 10%–15% [3]. A UM spreads exclusively hematogenously, unless it becomes large enough to infiltrate the conjunctival lymphatics. As per the Collaborative Ocular Melanoma Study, the most frequent sites of metastases at time of death are liver (93%), lung (24%), and bone (16%). More than 80% of cases had multiple sites of metastasis [4].

Here, we present a case of metastatic choroidal melanoma in the breast.

CASE REPORT

A 67-year-old female presented in 2017 with reduced vision in the left eye. A transscleral biopsy was performed, and a diagnosis of choroidal melanoma-monosomy 3 was made. The patient was treated by Ruthenium plaque brachytherapy, which was later complicated by retinal detachment. Almost a year later in follow-up, the patient underwent a computerized tomography scan of the thorax, abdomen, and pelvis and was found to have multiple lung and liver metastatic deposits. Unfortunately, the patient was lost to follow-up at this stage.

In 2021, the patient presented with right breast lump, and ultrasound of the right breast revealed an irregular hyperechoic mass measuring 21 × 18 × 19 mm at the 12 o'clock position with features suggestive of a malignant lesion (Fig. 1). A needle core biopsy was performed and revealed an invasive tumor with some spindle cell differentiation and areas of necrosis, as shown in Figs. 2 and 3. No normal breast tissue was seen in the biopsy sample received. A provisional diagnosis of invasive ductal carcinoma with spindle cell differentiation was made, and further immunohistochemistry was requested to confirm the breast primary. The tumor cells were weakly positive for hormone receptors estrogen



Fig. 1. Ultrasound of the right breast showing an irregular hypoechoic mass.

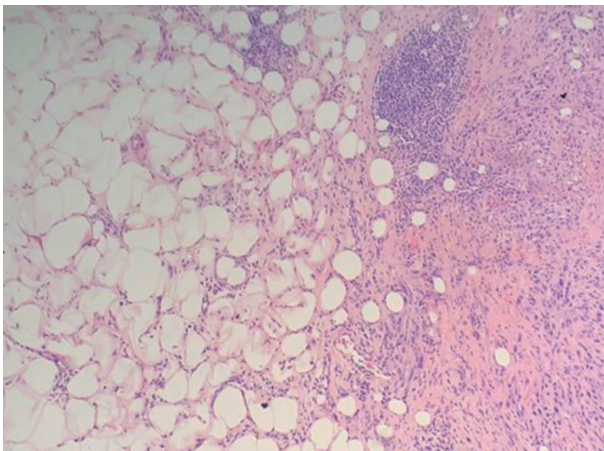


Fig. 2. Core needle biopsy of the breast showed tumor with adjacent benign fibrofatty tissue.

receptor and progesterone receptor and negative for human epidermal growth factor receptor 2.

The case was discussed at a multidisciplinary team (MDT) meeting where more clinical information was provided. It was here revealed that the patient had a previous history of choroidal melanoma, and further immunohistochemistry was therefore performed to rule out a metastatic tumor.

As shown in Fig. 4, the tumor cells showed positive reaction for SOX10 (patchy), Melan-A, human melanoma black 45, and S100 (focal) and negative reaction for CK-AE1/AE3, CK5/6, CK-MNF16, thyroid transcription factor 1, CD31, p63, CD34, smooth muscle actin, desmin, and BCL2 immunostains. The overall findings were in keeping with metastatic malignant mel-

anoma. *BRAF* codon 600 mutation testing was performed, and no mutation was identified. Later, head magnetic resonance imaging showed left posterior meningeal metastasis and a small enhancing lesion in the right occipital lobe, which were likely to be intracranial metastasis. The patient was referred to a specialist tumor center but refused further treatment.

DISCUSSION

Metastatic tumors of the breast are rare, but metastatic malignant melanomas comprise approximately 38.5% of metastatic tumors [5]. The histological features of the metastatic neoplasms may be non-specific or deceiving, particularly in cases of metastatic carcinoma and melanoma. The morphological diversity of melanomas and their presence at unusual sites make diagnosis even more difficult. Even with a history of non-mammary cancer, a breast lesion is most likely to represent a primary breast cancer [6]. Breast metastasis is generally a sign of disseminated disease, and systematic screening is needed to identify metastatic deposits elsewhere.

Malignant melanomas can be divided into primary or secondary. Primary malignant melanoma of the breast (PMMB) is a rare disease, accounting for 3%–5% of all melanomas and for less than 0.5% of malignant breast tumors. So far, 187 cases of PMMB have been reported in the literature [7].

A study by Zhou et al. [8] found that five out of nine cases of metastatic melanoma in the breast were misdiagnosed as primary poorly differentiated invasive breast carcinoma. Of these cases, four had a history of melanoma, one had none, and this history was not known to the reporting histopathologist in all five cases. In our case, a provisional diagnosis of primary breast tumor was made due to a lack of clinical information about the patient's history of choroidal melanoma and the rarity of metastatic tumors in the breast.

The first case of breast metastasis from choroidal melanoma was reported by Chopra and Chandar in 1972 [9]. To the best of our knowledge, only five cases [9–13] have been published since, with one presenting in a male patient [11]. Most of the cases report breast metastasis as the first sign of metastatic disease, appearing between 50 and 60 months. In the present case, the patient presented with metastatic disease in the liver within 12 months and breast metastasis at 50 months, as in Table 1.

As per the literature, monosomy 3 is commonly found in most cases of uveal melanomas that metastasize to the liver [13], as seen in the current case. Breast metastasis from choroidal melanoma is extremely rare. Nevertheless, clinicians should be aware

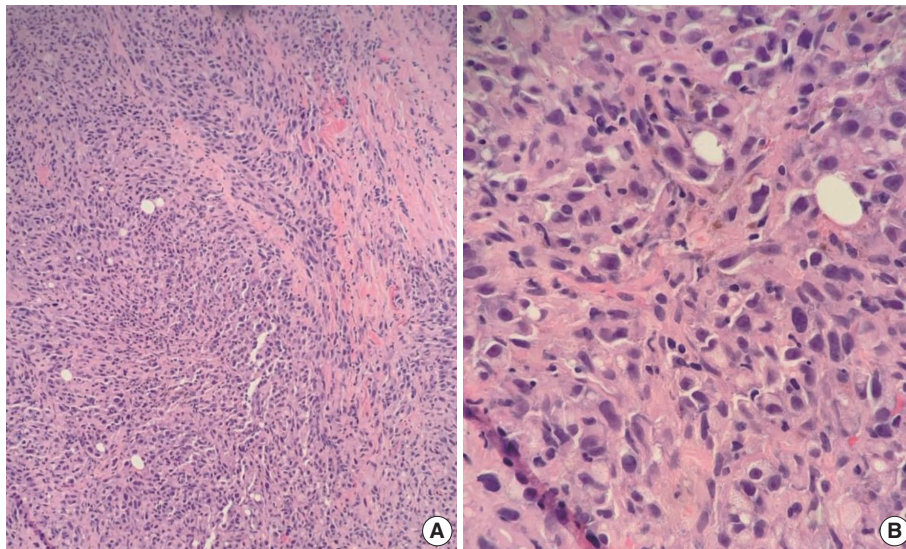


Fig. 3. Core needle biopsy of the breast showed infiltrating tumor with spindle cell differentiation: (A) low power and (B) high power.

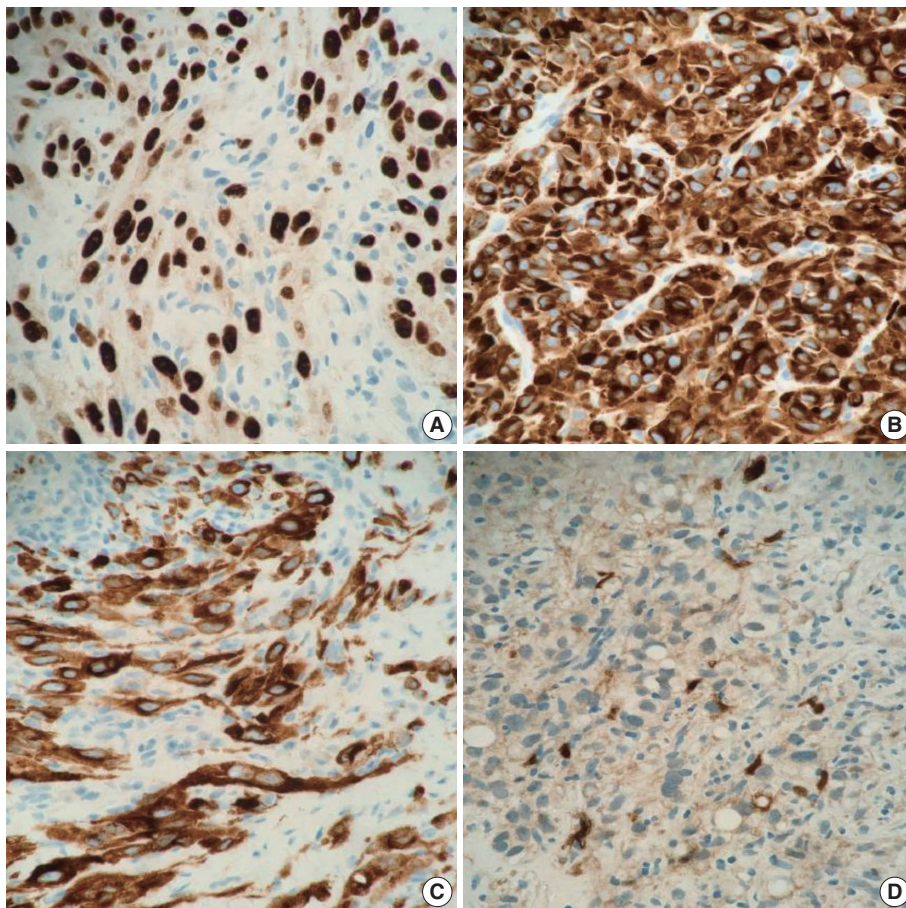


Fig. 4. Tumors cells showed positive reaction for (A) SOX10 (Patchy), (B) Melan-A, (C) human melanoma black 45, and (D) S100 (focal) immunostains.

Table 1. Comparison of all published cases of uveal melanoma including (age of patient, the sex, the age of the patient, the first presentation site of metastasis and the duration time in months between the primary site and breast metastasis) between period the 1972 till 2023

Case	Year of publication	Sex	Age (yr)	First presentation of metastasis	Time interval between primary and breast metastasis in months
1 Our case	2022	Female	67	Liver	50
2 Zhou et al. [8]	2022			7 cases/no details	
3 Taran-Munteanu et al. [5]	2016	Female	61	Breast	50
4 Demirci et al. [10]	2001	Female	48	Breast	37
5 McCormick and Rennie [12]	2001	Female	50	Breast	60
6 Esposito et al. [11]	1994	Male	72	Breast	-
7 Chopra and Chandar [9]	1972	Female	33	Liver and spine bilateral breast	96

of this form of metastasis when treating patients with suspicious breast lesions and a history of choroidal melanoma. This case also emphasizes the importance of relevant clinical information being available to the reporting pathologist and further supports the vital role of MDT meetings and discussions in providing high quality patient care and avoiding erroneous diagnoses.

Ethics Statement

No patient consent was needed for publication as patient details were completely anonymised (neither the patient nor anyone else could identify the published information).

Availability of Data and Material

The datasets generated during and/or analysed during the current study are available from the corresponding author on reasonable request.

Code Availability

Not applicable.

ORCID

Loay Abudalu <https://orcid.org/0000-0002-8935-4133>
 Vinisha Malhotra <https://orcid.org/0000-0003-2018-9587>
 Nabila Nasir <https://orcid.org/0000-0002-3238-7292>
 Sami Titi <https://orcid.org/0000-0002-4892-2878>

Author Contributions

Conceptualization: LA, ST. Data curation: LA, VM, ST. Formal analysis: LA, VM, ST. Investigation: LA, VM, NN, ST. Methodology: LA, VM, ST. Project administration: LA. Resources: LA. Supervision: LA, VM, ST. Validation: LA, VM, ST. Visualization: LA, VM, ST. Writing—original draft: LA, VM, ST. Writing—review & editing: LA, VM, NN, ST. Approval of final manuscript: all authors.

Conflicts of Interest

The authors declare that they have no potential conflicts of interest.

Funding Statement

No funding to declare.

References

- Lee AH, Hodi Z, Soomro I, et al. Histological clues to the diagnosis of metastasis to the breast from extramammary malignancies. *Histopathology* 2020; 77: 303-13.
- Krantz BA, Dave N, Komatsubara KM, Marr BP, Carvajal RD. Uveal melanoma: epidemiology, etiology, and treatment of primary disease. *Clin Ophthalmol* 2017; 11: 279-89.
- Nathan P, Cohen V, Coupland S, et al. Uveal melanoma UK national guidelines. *Eur J Cancer* 2015; 51: 2404-12.
- Sato T. Locoregional management of hepatic metastasis from primary uveal melanoma. *Semin Oncol* 2010; 37: 127-38.
- Taran-Munteanu L, Hartkopf A, Eigentler TK, Vogel U, Brucker S, Taran FA. A case of choroidal melanoma metastatic to the breast. *Geburtshilfe Frauenheilkd* 2016; 76: 579-81.
- DeLair DF, Corben AD, Catalano JP, Vallejo CE, Brogi E, Tan LK. Non-mammary metastases to the breast and axilla: a study of 85 cases. *Mod Pathol* 2013; 26: 343-9.
- Drueppel D, Schultheis B, Solass W, Ergonenc H, Tempfer CB. Primary malignant melanoma of the breast: case report and review of the literature. *Anticancer Res* 2015; 35: 1709-13.
- Zhou P, Chang N, Abraham SC, et al. Metastatic nonhematopoietic neoplasms to the breast: a study of 238 cases. *Hum Pathol* 2022; 125: 59-67.
- Chopra JS, Chandar K. Bilateral breast metastases from malignant melanoma of the eye. *Aust N Z J Surg* 1972; 42: 183-5.
- Demirci H, Shields CL, Shields JA, Eagle RC Jr, Honavar SG. Bilateral breast metastases from choroidal melanoma. *Am J Ophthalmol* 2001; 131: 521-3.
- Esposito A, Gentile D, Ghidotti I, Allegri M. A rare case of metastasis of choroidal melanoma in male breast: mammographic and ultrasonographic diagnosis. *Radiol Med* 1994; 88: 487-8.
- McCormick A, Rennie I. Bilateral breast metastases from choroidal melanoma. *Am J Ophthalmol* 2001; 132: 951-2.
- McCarthy C, Kalirai H, Lake SL, Dodson A, Damato BE, Coupland SE. Insights into genetic alterations of liver metastases from uveal melanoma. *Pigment Cell Melanoma Res* 2016; 29: 60-7.

Intrathyroidal metastasis of tonsillar squamous cell carcinoma masquerading as a primary thyroid tumor

Jai-Hyang Go

Department of Pathology, Dankook University College of Medicine, Cheonan, Korea

Intrathyroidal metastasis of tonsillar squamous cell carcinoma is rare. To date, only six cases have been reported in the literature. This case was unusual and presented with thyromegaly before the diagnosis of the primary tumor. A 55-year-old male patient was suspected to have a primary thyroid tumor with nodal metastasis. The thyroid gland was diffusely enlarged, with no discernible mass. Histologically, the thyroid parenchyma revealed extensive endolymphatic tumor emboli, which were positive for p40 and p16 in a background of chronic lymphocytic thyroiditis. Positron emission tomography-computed tomography revealed hypermetabolic activity in the right tonsillar region. Tonsillar biopsy revealed human papillomavirus-positive squamous cell carcinoma. The present case is the first reported case of intrathyroidal metastasis of tonsillar squamous cell carcinoma with an initial clinical presentation of thyroid enlargement before the primary tumor of tonsillar cancer was diagnosed.

Key Words: Intrathyroidal metastasis; Tonsil; Goiter; Squamous cell carcinoma; Position emission tomography

Received: May 26, 2023 **Revised:** June 15, 2023 **Accepted:** June 16, 2023

Corresponding Author: Jai-Hyang Go, MD, Department of Pathology, Dankook University College of Medicine, 119 Dandae-ro, Dongnam-gu, Cheonan 31116, Korea
Tel: +82-41-550-6974, Fax: +82-41-550-6034, E-mail: cyjy555@daum.net

Metastasis of head and neck carcinoma to the thyroid gland is rare. Intrathyroidal metastasis of tonsillar squamous cell carcinoma (SCC) is even more unusual, with only six previously documented cases [1-5]. All published cases of intrathyroidal metastasis of tonsillar SCC involved a history of tonsillar squamous cell carcinoma. In these cases, metastatic tumors were identified during the staging work-up or follow-up period. Herein, we describe the first reported case of intrathyroidal metastasis of tonsillar human papillomavirus (HPV)-positive SCC with an initial clinical presentation of thyroid enlargement. This case is important because of the unusual clinical presentation of thyromegaly prior to primary tumor diagnosis.

CASE REPORT

A 55-year-old male patient was admitted for right neck swelling for 1 month. Neck computed tomography (CT) showed diffuse heterogeneous parenchymal density without focal nodular lesions in either thyroid gland and multiple lymph node enlargements in the right neck at levels II-V, the supraclavicular area,

and the posterior neck, which suggested a primary thyroid tumor with nodal metastasis. Thyroid function test results were normal. Total thyroidectomy with radical neck node dissection was performed. Grossly, the thyroid gland was diffusely enlarged and had a white-gray solid appearance with no discernible mass (Fig. 1). Histologically, the thyroid parenchyma revealed extensive endolymphatic tumor emboli in a background of chronic lymphocytic thyroiditis (Fig. 2A). The tumor was composed of solid nests of atypical cells (Fig. 2B). The tumor cells were block-positive for p16 (Fig. 2C), positive for p40 (Fig. 2D) and p63 but negative for thyroglobulin and thyroid transcription factors, confirming SCC. Positron emission tomography-CT (PET-CT) revealed symmetrical hypermetabolic activity in and around the right tonsillar region. Tonsillar biopsy revealed HPV-positive SCC (Fig. 3A, B), with tumor cells showing the same immunohistochemical results as those of the thyroid tumor (Fig. 3C, D). Postoperative follow-up PET-CT revealed no residual mass. Because of the advanced stage (stage IVC), nine cycles of palliative chemotherapy with docetaxel plus cisplatin were postoperatively administered. However, PET-CT showed new metastatic lymph nodes in the right

cervical, left supraclavicular, and right upper paratracheal areas 1 year after operation. A second round of chemotherapy with nivolumab was administered. The patient remained alive but with disease at the latest follow-up (15 months).

DISCUSSION

The overall rate of distant metastasis of head and neck tumors

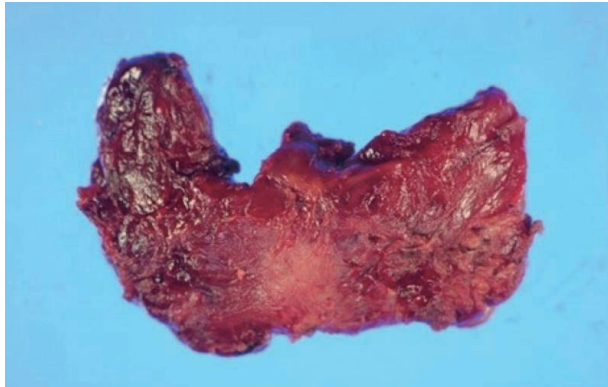


Fig. 1. The thyroid gland is diffusely enlarged with no discernible mass.

is approximately 12% [6]. Head and neck SCC commonly metastasizes primarily to the lung and also bone and liver [5]. Distant metastases of head and neck tumors generally present within 2 years of definitive treatment, usually in the context of poor locoregional control of the primary lesion [6].

Tonsillar cancer may spread locally to the surrounding tissues of the oropharynx, including the base of the tongue, soft palate, and posterior wall of the throat [5,7]. Alternatively, they can access the lymphatic system, which usually involves cervical lymph nodes, because tonsils have a rich vascular supply, providing an easy path for metastases to reach the regional lymph nodes [4,5,7]. However, distant metastases are extremely uncommon [7]. The incidence of distant metastases varies extensively in the literature, ranging from 3%–30% [6,7]. The most common sites include the liver, lungs, bones, mediastinal sites, skin, and, rarely, bone marrow [7]. Tumor stage determines the likelihood of metastasis, with advanced stages associated with approximately 15%–20% chance of metastasis in tonsillar cancer. Early-stage cancers rarely have distant metastases; however, advanced-stage cancers can metastasize beyond the cervical lymph nodes and spread through the lymphatic or vascular channels [5].

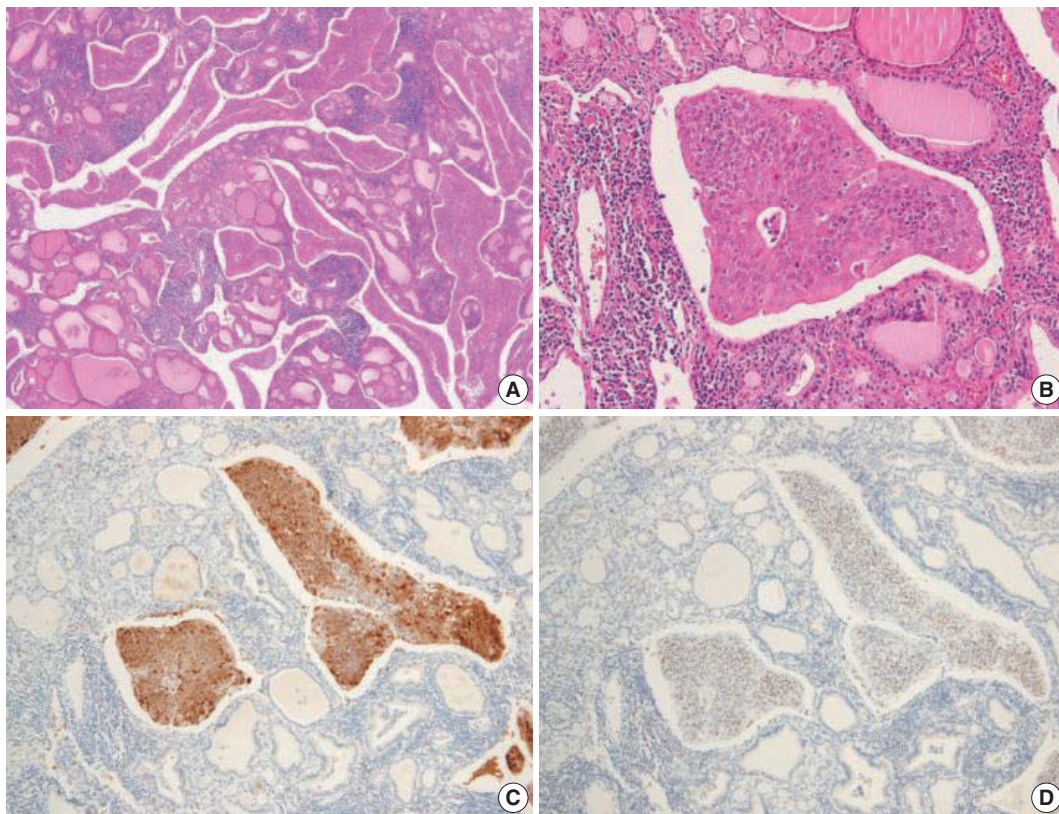


Fig. 2. Histologic findings of thyroid gland. (A) The thyroid parenchyma reveals extensive endolymphatic tumor emboli in the background of chronic lymphocytic thyroiditis. (B) The tumor is composed of solid nests of atypical cells. The tumor cells are positive for p16 (C) and p40 (D).

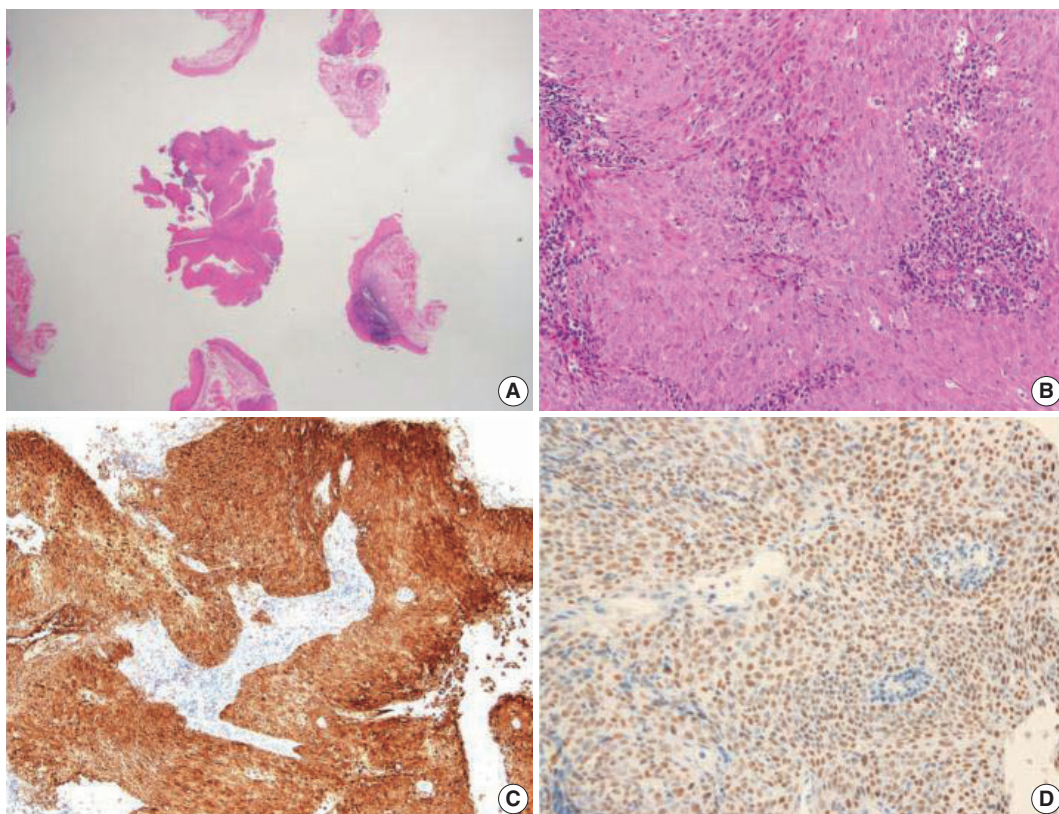


Fig. 3. Histologic findings of tonsil. (A, B) Tonsillar biopsy shows squamous cell carcinoma. The tumor cells are positive for p16 (C) and p40 (D).

Intrathyroidal metastases are rare, ranging from 0.6%–2.2% [1]. The primary sites most commonly identified in autopsy series are the breast and lung. However, in clinical series, renal cell carcinoma is the most frequent source of metastasis, often presenting many years after the original diagnosis [1,3]. Patients with metastatic thyroid cancer usually present with symptoms similar to those of primary thyroid cancer, particularly palpable neck masses. Dysphagia or dysphonia may develop if the metastatic cancer is advanced [1,4]. The time interval between the original primary cancer diagnosis and metastasis to the thyroid gland varies from a few months to years [4]. Thyroid function is usually normal [1,4].

Metastasis of head and neck SCC to the thyroid gland is rare. Intrathyroidal metastasis of tonsillar SCC is even more unusual [1]. To date, only six cases of intrathyroidal metastasis of tonsillar SCC have been documented [1-5]. All published cases involved a history of tonsillar SCC. Metastatic tumors were identified during the staging workup for tonsillar cancer in two patients [3]. In two patients, a whole-body PET scan performed as part of the screening process showed an enlarging nodule in the thyroid gland 18 months and 4 years after the diagnosis of tonsillar

cancer, respectively [4,5]. One patient presented with a neck mass 3 years after diagnosis of the primary tumor [1], and another patient complained of dysphonia and dysphagia 6 months after initial diagnosis [2]. HPV status was described in only one case and was positive. Clinical characteristics are summarized in Table 1. In this case, the patient first presented with thyromegaly, which was clinically suggestive of a primary thyroid tumor. HPV-positive tonsillar SCC was unexpectedly identified during systemic workup.

The oropharynx, especially the tonsils and base of the tongue, represents the most common anatomical site of SCC of unknown primary origin of the head and neck, with an incidence ranging from 74%–89% [8]. HPV-positive oropharyngeal SCCs may distantly metastasize in unexpected sites [9] and frequently metastasize early in the course of disease when the primary tumor is small [10]. It is not uncommon for a patient to present with a neck metastasis and a small occult primary tumor that is HPV-related and located deep in the oropharyngeal tonsillar crypts [10]. Therefore, a thorough oropharyngeal examination is necessary if metastatic SCC of the thyroid gland is suspected, although this is a rare event.

Table 1. Clinical characteristics of patients with intrathyroidal metastasis of tonsillar cancer

Case No.	Tonsillar cancer	Time interval	Clinical symptom	Thyroid gland	HPV	Treatment	Reference
1	T2N2b	3 yr	Neck mass	Nodules	N/A	Chemotherapy	[1]
2	N/A	6 mo	Dysphonia	Mass	N/A	Thyroidectomy	[2]
3	T1N2cM0	N/A	Staging	N/A	N/A	N/A	[3]
4	T2N2bM0	N/A	Staging	N/A	N/A	N/A	[3]
5	T3N0	18 mo	Screening	Nodule	N/A	N/A	[4]
6	T2N2M0	4 yr	Screening	Mass	Positive	N/A	[5]
Present case	T1N2cM1	0 mo	Neck mass	Thyromegaly	Positive	Chemotherapy	

HPV, human papilloma virus; N/A, not available.

Ethics Statement

The Institutional Review Board of Dankook University Hospital (2023-01-015) approved this case report and informed consent was waived.

Availability of Data and Material

All data generated or analyzed during this study are included in this published article and available from the corresponding author.

Code Availability

Not applicable.

ORCID

Jai-Hyang Go <https://orcid.org/0000-0002-2105-7837>

Conflicts of Interest

The author declares that I have no potential conflicts of interest.

Funding Statement

No funding to declare.

References

- Jankowska P, Teoh EM, Fisher C, Rhys Evans P, Nutting CM, Harrington KJ. Case report: isolated intrathyroid metastasis from undifferentiated and squamous carcinoma of the head and neck: the case for surgery and re-irradiation. *Br J Radiol* 2008; 81: e154-61.
- Scanelli G, Aimoni C, Marchetti E, Geminiani M, Pastore A. Thyroid's metastasis of tonsillar squamous cell carcinoma. *Recenti Prog Med* 2005; 96: 428-30.
- Millare GG, Kwon M, Edeiken-Monroe BS, Debnam JM. (18)F-PET/CT imaging of metastasis to the thyroid gland: Imaging findings and effect on patient management. *J Solid Tumors* 2017; 7: 7-13.
- Gumaa D, Christakis I, Mihai R. Metastasis to the thyroid gland from a tonsil squamous cell carcinoma. *AME Case Rep* 2018; 2: 7.
- Aparici CM, Win AZ. Two cases of thyroid metastasis from head and neck squamous cell carcinoma detected by FDG-PET/CT. *J Clin Imaging Sci* 2014; 4: 62.
- LeRose CC, Ramirez CA. Atypical metastasis of p16-positive tonsillar squamous cell carcinoma to the pleura: a case report. *J Oral Maxillofac Surg* 2018; 76: 2577-81.
- Khan S, Anichini G, Mian A, Kareem H, Syed N, O'Neill K. Tonsillar carcinoma spreading metastases to central nervous system: case report and literature review. *J Neurol Surg Rep* 2021; 82: e11-6.
- Di Maio P, Iocca O, De Virgilio A, et al. Role of palatine tonsillectomy in the diagnostic workup of head and neck squamous cell carcinoma of unknown primary origin: a systematic review and meta-analysis. *Head Neck* 2019; 41: 1112-21.
- Sacks R, Law JY, Zhu H, et al. Unique patterns of distant metastases in HPV-positive head and neck cancer. *Oncology* 2020; 98: 179-85.
- Chernock RD, Lewis JS. Approach to metastatic carcinoma of unknown primary in the head and neck: squamous cell carcinoma and beyond. *Head Neck Pathol* 2015; 9: 6-15.



PathologyOutlines.com

What's new in hematopathology 2023: updates on mature T-cell neoplasms in the 5th edition of the WHO classification

Mario L. Marques-Piubelli, MD¹, Roberto N. Miranda, MD²

¹Department of Translational Molecular Pathology, The University of Texas MD Anderson Cancer Center, Houston, TX, USA

²Department of Hematopathology, The University of Texas MD Anderson Cancer Center, Houston, TX, USA

Received: February 23, 2023

Accepted: June 15, 2023

Corresponding Author: Roberto N. Miranda, MD
 Department of Hematopathology, The University of Texas MD Anderson Cancer Center, Houston, TX, USA
 E-mail: roberto.miranda@mdanderson.org

ORCID

Mario L. Marques-Piubelli
<https://orcid.org/0000-0002-6324-2096>
 Roberto N. Miranda
<https://orcid.org/0000-0002-8467-5464>

This article has been published jointly, with consent, in both Journal of Pathology and Translational Medicine and PathologyOutlines.com.

Abstract

The overview of the upcoming Blue Book of the 5th edition of the World Health Organization Classification of Hematolymphoid Tumors was published in Leukemia in June 2022. The updates on mature T-/NK-cell lymphomas and leukemias are organized in nine groups based on cell of origin, morphology, clinical scenario, and localization, and are highlighted in this newsletter.

MATURE T-CELL AND NK-CELL LEUKEMIAS

- T-prolymphocytic leukemia (T-PLL)
- T-large granular lymphocytic leukemia (T-LGLL)
- Adult T-cell leukemia/lymphoma (ATLL)
- Aggressive NK-cell leukemia (ANKL)
- Sezary syndrome

This group includes entities that mostly present in a leukemic phase. T-PLL requires monoclonal T-cell lymphocytosis ($> 5 \times 10^9/L$), T-cell monoclonality and aberrations in *TCL1A* or *MTCP1*. T-LGLL with *STAT3* mutations is associated with cytopenias, splenomegaly and autoimmune diseases. ATLL has shown new immune evasion mechanisms: *CTLA4::CD28*, *ICOS::CD28*, *REL* truncations, variations of *CD274*, and alterations in *HLA-A* and *HLA-B*. *ANKL* is associated with mutations in the JAK/STAT pathway, epigenetic modifiers and immune checkpoints. Although Sezary syndrome is much closer to mycosis fungoides, it is discussed here because of its leukemic presentation, mimicking the other leukemic processes.

PRIMARY CUTANEOUS T-CELL LYMPHOID PROLIFERATIONS AND LYMPHOMAS (CTCL)

- Primary cutaneous CD4+ small or medium T-cell lymphoproliferative disorder
- Primary cutaneous acral CD8+ lymphoproliferative disorder
- Mycosis fungoides
- Primary cutaneous CD30-positive T-cell lymphoproliferative disorder: lymphomatoid papulosis
- Primary cutaneous CD30-positive T-cell lymphoproliferative disorder: primary cutaneous anaplastic large cell lymphoma
- Subcutaneous panniculitis-like T-cell lymphoma
- Primary cutaneous gamma/delta T-cell lymphoma
- Primary cutaneous CD8-positive aggressive epidermotropic cytotoxic T-cell lymphoma
- Primary cutaneous peripheral T-cell lymphoma (PTCL), NOS

These are well-known disorders as noted in previous WHO editions, 9 in total.

The most significant change is the removal of the umbrella term of PTCL from which 4 different entities have been derived, including PTCL, NOS to emphasize that the CTCL are still difficult to classify [1]. It is expected that the publication of the 5th edition will abound with underlying molecular mechanisms for each of the disorders in this group. The diagnostic criteria for each entity are well defined from previous editions. It is acknowledged that mycosis fungoides has a range of clinical and histologic subtypes, and it is of interest that its folliculotropic subtype has divergent outcomes when comparing early with advanced stage cases. Because of overlapping clinical, pathologic and immunophenotypic features of these 9 entities, clinical correlation is more valid than ever for achieving the most accurate diagnosis.

INTESTINAL T-CELL AND NK-CELL LYMPHOID PROLIFERATION AND LYMPHOMAS

- Indolent T-cell lymphoma of the gastrointestinal tract
- Indolent NK-cell lymphoproliferative disorder (LPD) of the gastrointestinal tract
- Enteropathy-associated T-cell lymphoma
- Monomorphic epitheliotropic intestinal T-cell lymphoma
- Intestinal T-cell lymphoma, NOS

There may be an increased frequency of reported intestinal lymphoma, likely due to its recognition as a distinct group. The category of intestinal LPD and lymphomas includes 2 indolent disorders. The indolent T-cell lymphoma (Fig. 1) has been observed to have significant morbidity over time, including dissemina-

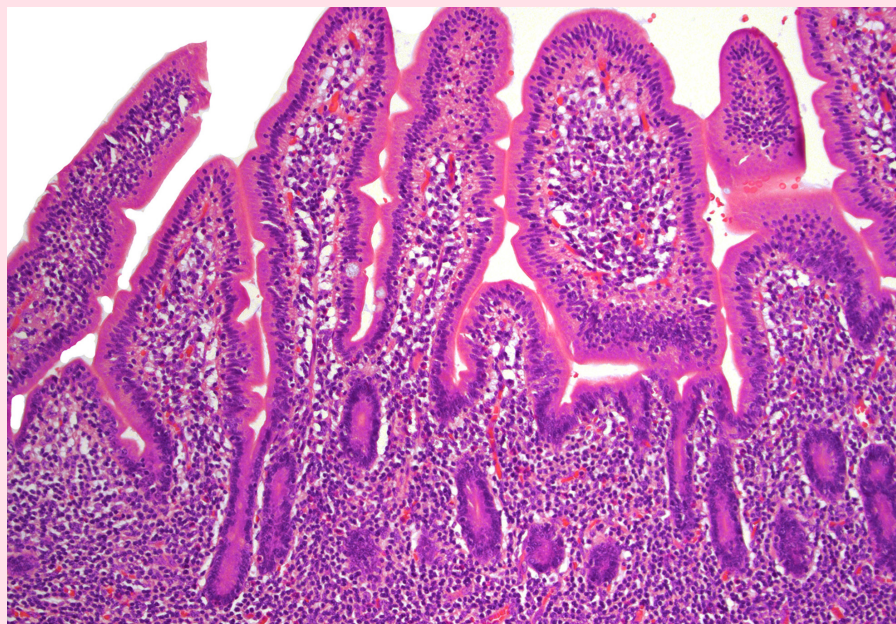


Fig. 1. Expansion of the lamina propria by small-sized and mature-appearing lymphocytes in indolent T-cell lymphoma of the gastrointestinal tract.

tion. Alterations in the JAK/STAT pathway and mutations of epigenetic modifiers are more common in CD4+, CD4+/CD8+, and CD4-/CD8- subsets. The indolent NK-cell LPD seems to behave more as an enteropathy, have no aggressive behavior and carry *JAK3* mutations. Lesions are well circumscribed and small, but cells show moderate atypia, therefore NK-cell LPD can be confused with extranodal NK/T-cell lymphoma which is associated with EBV. The other entities in the group of intestinal lymphomas remain unchanged.

HEPATOSPLENIC T-CELL LYMPHOMA (HSTCL)

This rare lymphoma is difficult to diagnose due to its well-known protean presentation, histopathology (Fig. 2, 3), phenotype and clinical aggressiveness; it is also a diagnosis that may portend allogeneic stem cell transplant as the only means of achieving cure. Not only young, but also adult patients can be affected. HSTCL usually presents at stage

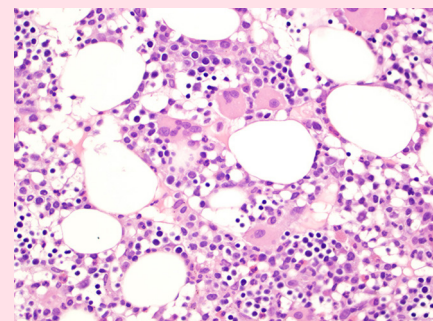


Fig. 2. Bone marrow core biopsy involved with HSTCL shows hypercellularity displaying small and hypoblasted megakaryocytes, morphologically consistent with dysmegakaryopoiesis, raising the possibility of underlying myelodysplastic syndrome.

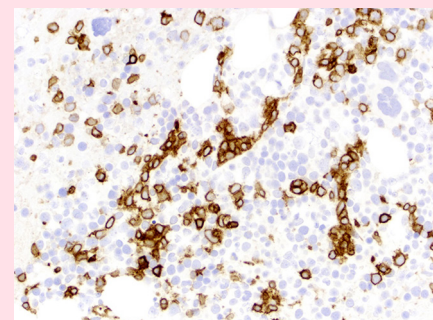


Fig. 3. CD3 immunostaining shows that the lymphocytes have a sinusoidal pattern characterized by clusters of lymphocytes in a cord-like pattern in HSTCL.

IV. The diagnosis can be missed in a bone marrow that mimics a myelodysplastic syndrome, and the spectrum of tumor cells may resemble blasts of acute leuke-

nia. TCR $\gamma\delta$ is expressed in ~75% of cases, TCR $\alpha\beta$ is expressed in ~20% and TCR is silent in 5% of cases.

ANAPLASTIC LARGE CELL LYMPHOMAS (ALCL)

- ALK+ ALCL
- ALK- ALCL
- Primary cutaneous CD30-positive T-cell lymphoproliferative disorder: primary cutaneous ALCL (see also CTCL)
- Breast implant-associated ALCL

These lymphomas have in common a pleomorphic cytomorphology, uniform and strong expression of CD30 and conspicuous absence of T-cell lineage markers. Four entities are recognized, 2 systemic and 2 site-specific forms. The systemic entities are divided by the presence of *ALK* gene rearrangement, as ALK+ and ALK- ALCL. Patients with ALK+ ALCL are usually young, while ALK- ALCL (Fig. 4) patients are adults and elders. Patients with ALK+ have better outcomes than patients with ALK- ALCL. ALK- ALCL can have *DUSP22* or *TP63* rearrangements, with the latter conveying the worst outcomes. Of interest, cases with *DUSP22* rearrangements show a uniform cytomorphology, with doughnut-like cells and LEF1

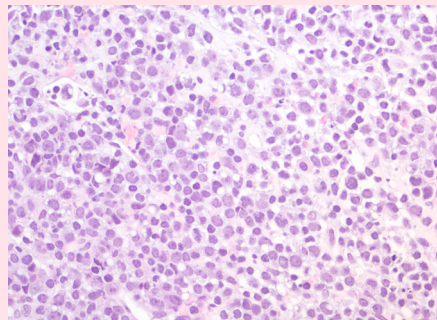


Fig. 4. Lymph node involved by ALK- ALCL shows diffuse replacement of normal architecture by large and anaplastic lymphocytes with no distinct nucleoli; some of them have a doughnut-like shape.

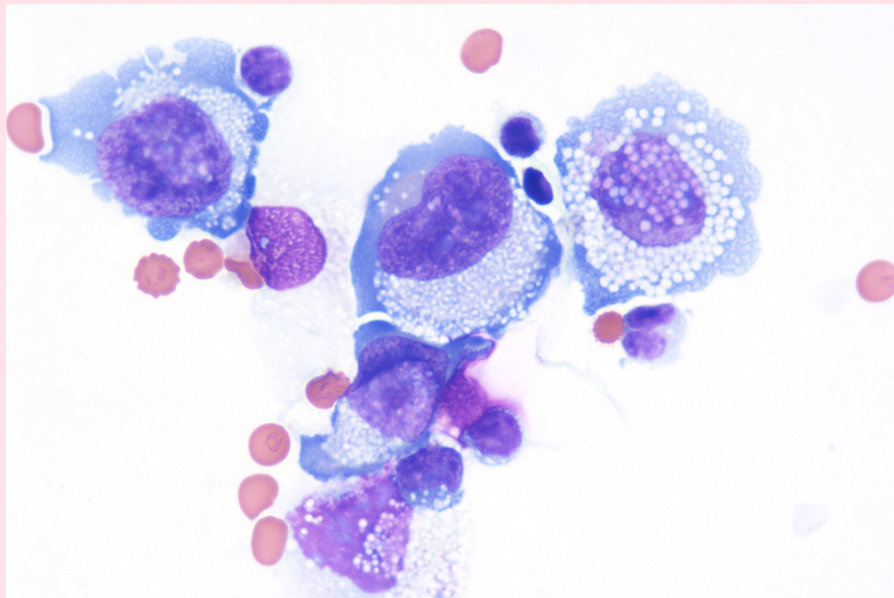


Fig. 5. Cytologic preparation of an effusion around a breast implant in a case of BIA-ALCL shows large and atypical cells with irregular nuclear contours, inconspicuous nuclei and abundant cytoplasm with small inclusions.

expression.

The site-specific forms of ALCL include the primary cutaneous ALCL that is grouped together with primary cutaneous T-cell LPD and lymphomas, and breast implant-associated ALCL (BIA-ALCL). BIA-ALCL (Fig. 5–7) is associated with textured implants and has an excellent outcome if surgically excised with negative margins. Patients with non-resectable disease require chemo- or immunotherapy.

NODAL T-FOLLICULAR HELPER CELL LYMPHOMAS (NTFHL)

- Nodal T-follicular helper cell lymphoma angioimmunoblastic-type (nTFHL-AI): formerly angioimmunoblastic T-cell lymphoma
- Nodal T-follicular helper cell lymphoma follicular-type (nTFHL-F): formerly follicular T-cell lymphoma
- Nodal T-follicular helper cell lymphoma, NOS (nTFHL-NOS); formerly PTCL with TFH phenotype that does not meet criteria for nTFHL-AI or

nTFHL-F

This group includes 3 nodal TCL with T-follicular helper phenotype (≥ 2 markers are required for diagnosis: PD1, ICOS, CXCL13, CD10, BCL6, CXCR5, SAP, c-MAF and CD200), derived from gene expression signature of CD4+ lympho-

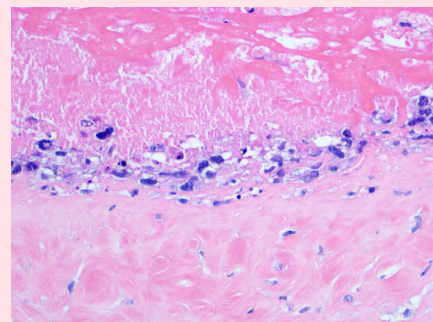


Fig. 6. Breast capsule with BIA-ALCL shows large and neoplastic cells confined to the luminal space in a necrotic background.



Fig. 7. CD30 immunostaining shows diffuse and strong cytoplasmic and nuclear positivity in the BIA-ALCL cells.

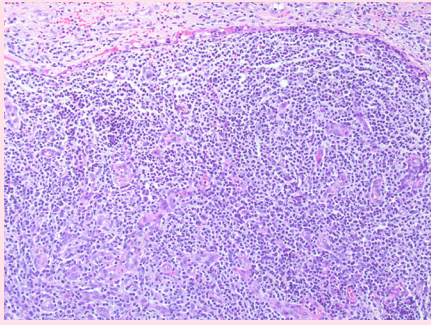


Fig. 8. nTFHL-AI with effacement of the nodal architecture and infiltration of the capsule and subcapsular sinus.

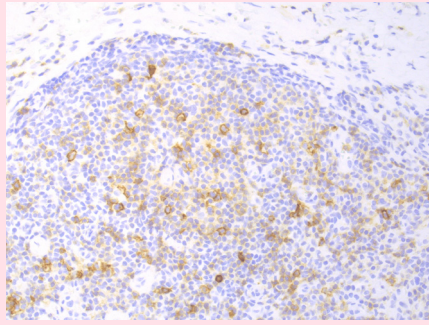


Fig. 9. Positivity for the checkpoint molecule PD-1 in scattered lymphoma cells supports a T follicular helper phenotype in a case of nTFHL-AI.

cytes. There is morphologic overlap between these entities, and the prototype is nTFHL-AI (Fig. 8, 9). While the 3 entities have mutations of *RHOA* and *IDH2*, nTFHL-AI has also recurrent mutations of *TET2* and *DNMT3A* in hematopoietic precursors. The diagnosis of nTFHL is recommended for small samples and to avoid misclassification.

OTHER PERIPHERAL T-CELL AND NK-CELL LYMPHOMAS

• PTCL, NOS

This entity remains as a heterogeneous group of neoplasms and the diagnosis is performed based on the exclusion of other described entities. Two distinct biological groups can be identified using T-cell markers by immunohistochemistry: PTCL-TBX21 (PTCL-TH1) and PTCL-GATA3 (PTCL-TH2). The PTCL-TH1 group is usually associated with a cytotoxic phenotype, while the PTCL-TH2 group is a more heterogeneous group and is associated with poorer outcomes. Although these important biological mechanisms have been described, the experts concluded that there is still insufficient data to perform systematic classification in subtypes [1].

EBV-POSITIVE NK/T-CELL LYMPHOMAS

- EBV-positive nodal T- and NK-cell lymphoma (EBV+ NTNKL)
- Extranodal NK-T-cell lymphoma (ENKTL)

This is a group of mature lymphomas with NK/T phenotype that are associated with EBV infection. The EBV+ NTNKL is a distinct entity that was under the PTCL, NOS umbrella in the previous WHO classification. The disease is more common in East Asians and presents with extensive lymphadenopathy and sometimes extranodal involvement. Angioinvasion and coagulative necrosis are usually absent and there is no clear cut-off for EBV positivity. The ENKTL is an updated denomination where the qualifier “nasal-type” is dropped, following primary tumors found in diverse extranodal sites. Importantly, the use of L-asparaginase-based regimens has resulted in improved outcomes in affected patients.

EBV-POSITIVE T- AND NK-CELL LYMPHOID PROLIFERATIONS AND LYMPHOMAS OF CHILDHOOD

- Chronic active EBV disease (CAEBVD)
- Severe mosquito bite allergy (SMBA)

- Hydroa vacciniforme lymphoproliferative disorder (HVLPD) classic form
- Hydroa vacciniforme lymphoproliferative disorder (HVLPD) systemic form
- Systemic CAEBVD

- Systemic EBV-positive T-cell lymphoma of childhood

EBV+ NK/T-cell LPD and lymphomas of childhood comprise an uncommon group of disorders that mostly affect children of Asian and native American ethnic ancestry. CAEBVD has a broad clinical spectrum, which ranges from localized, mostly cutaneous forms to systemic disease with fever, hepatosplenomegaly and lymphadenopathy. The systemic form of HVLPD should be distinguished from systemic CAEBVD, which has a more aggressive behavior.

Reference

1. Alaggio R, Amador C, Anagnostopoulos I, et al. The 5th edition of the World Health Organization Classification of Haematolymphoid Tumours: Lymphoid Neoplasms. *Leukemia* 2022; 36: 1720-48.

Meet the Authors

Dr. Marques-Piubelli has been part of the PathologyOutlines.com hematopathology editorial board since 2021. He is an Assistant Professor in the Department of Translational Molecular Pathology, at The University of Texas MD Anderson Cancer Center.

Dr. Miranda has been part of the PathologyOutlines.com hematopathology editorial board since 2021. He is a Professor in the Department of Hematopathology, The University of Texas MD Anderson Cancer Center.

